INFORMATION TO USERS

This manuscript has been reproduced from the microfilm master. UMI films the text directly from the original or copy submitted. Thus, some thesis and dissertation copies are in typewriter face, while others may be from any type of computer printer.

The quality of this reproduction is dependent upon the quality of the copy submitted. Broken or indistinct print, colored or poor quality illustrations and photographs, print bleedthrough, substandard margins, and improper alignment can adversely affect reproduction.

In the unlikely event that the author did not send UMI a complete manuscript and there are missing pages, these will be noted. Also, if unauthorized copyright material had to be removed, a note will indicate the deletion.

Oversize materials (e.g., maps, drawings, charts) are reproduced by sectioning the original, beginning at the upper left-hand corner and continuing from left to right in equal sections with small overlaps. Each original is also photographed in one exposure and is included in reduced form at the back of the book.

Photographs included in the original manuscript have been reproduced xerographically in this copy. Higher quality 6" x 9" black and white photographic prints are available for any photographs or illustrations appearing in this copy for an additional charge. Contact UMI directly to order.

UMI

A Bell & Howell Information Company
300 North Zeeb Road, Ann Arbor MI 48106-1346 USA
313/761-4700 800/521-0600

UNIVERSITÉ D'OTTAWA
UNIVERSITY OF OTTAWA

PROBING PROTEIN SECONDARY STRUCTURE

&

CONFORMATIONAL HETEROGENEITY

Tanya E. S. Dahms

Those who first shape your mind

are your true teachers...

To Fred, Ruth & John Dahms

Today i SEE the moon

In childhood's eye,
it was the outer edge
of world and space,
beyond the painted sky
akin to gods of night.

Today i see the Moon
anew in time,
as real as rock,
smashed surface
scarred and smeared,
besieged with light below.

Floating lone,
the hollow glow recedes.
Moon shadow arcs to
quickened silver,
looming through mystique.

moon's image is not lost,
(perception broadens)
and i do prosper,
having known them both.

February 12/1994

ABSTRACT

Time-resolved and steady-state fluorescence spectroscopy in conjunction with circular dichroism were employed to investigate secondary and tertiary structural features of proteins. Several single tryptophan (Trp) proteins with known crystal structures were examined both in solution and in the crystalline state.

The three neurotoxins, α-bungarotoxin, α-cobratoxin and erabutoxin b, consist primarily of antiparallel β-sheet and contain a number of structurally important disulphide bridges. In each case, the Trp residue is situated approximately in the centre of a β-sheet. Complete random coil secondary structure for these proteins could be facilitated via the reduction and carboxymethylation or amidocarboxymethylation of the disulphide residues. Concurrent studies, by time-resolved fluorescence and circular dichroism, of these proteins at varied denaturant concentrations showed time-resolved fluorescence provides a highly sensitive probe of local secondary structure.

Time-resolved fluorescence measurements for erabutoxin b single crystals exhibited multiexponential decay kinetics (single Trp residue). The relative proportion of each decay time component was found to be dependent upon the angular orientation of the protein crystal, with respect to the vertical polarization of the incident laser beam. These experimental data provide evidence for Trp side chain rotamers in the protein crystal. Model functions, which simulated the orientational dependence of the decay component relative

proportions, were consistent with this rationalization. These results are the first direct experimental evidence obtained by fluorescence, to confirm the "rotamer" model for the interpretation of Trp fluorescence decay in solution. The measurement of crotonase, apoazurin and holoazurin crystals which display a range of exponential decay kinetics, provide further evidence for Trp rotamers in single protein crystals.

ACKNOWLEDGEMENTS

As a graduate student at the University of Ottawa, I was given the unique opportunity to conduct the research required for this dissertation, at the National Research Council of Canada (NRC) in the "Protein, Structure and Function" group. The abundance of expertise from the members of that group was a source of inspiration, and ironically this section of NRC no longer exists. I was able to work with many world-class scientists during my tenure at NRC, including my supervisor, Dr. Arthur G. Szabo.

Art has acquired the rare talent of adapting to each group member's personality. His students, as a result, are granted both explorative freedom and steady guidance. Art has allowed my independence to flourish and has helped me to optimize my research productivity. Above all, I wish to thank Art for his unwavering support.

I owe a special thanks to Kevin Willis who held a senior postdoctoral position in Art's laboratory when I first arrived. During the first two years of my research, Kevin had a keen interest in my project and I considered him to be a second supervisor. As well as becoming a good friend, Kevin was a superb mentor and role model.

The technical assistance which I received in Art's laboratory was second to none, and for this I owe Don Krajcarski. Don, having set up the wet laboratory and laser system during his many years with Art, was well versed in the technical aspects of experimental fluorescence and was often "the voice of reason" when no other voice was heard... After

our section at NRC was declared "surplus", Don was not able to relocate to Art's new facilities at the University of Windsor - his cheerful personality (hi-hi) and technical expertise were sorely missed!

I became aware of the NRC's quality reputation during my undergraduate years as a University of Waterloo co-operative student. I have never been disappointed by any of the scientists with whom I have worked, and my opinion of their excellence has been strengthened by my experience. There are a number of people whom I would like to acknowledge for their technical input, intellectual discussions and friendship: Xavier Lee, Peter Tonge, Lise Bramall, Joanne Ridgeway, Svetlana Borisova, Makoto Yaguchi, Dave Watson, Doug Griffith, Perry Fleming, Robert Campbell, Heather Gordon, Steven Evans, Carol Huber and Rebecca To.

John Baezinger, Marianna Sikorska-Walker and Martin Young accepted the responsibility of forming my advisory committee. I thank them for their continual interest and constructive criticism.

As an "off-campus" graduate student, I relied on the small core of students at NRC for advice and companionship. I have enjoyed the company of Christopher Hogue, John Doran, Fang Huang and Jamshid Davoodi. I would like to extend a special thanks to BeAtrice Winsborrow, who became a very close friend and confident. Through our exchange of ideas and activities, she was able to teach me that it is better to climb rocks than "climb walls".

During my tenure at the University Windsor, I befriended many people in the

Department of Chemistry and Biochemistry. I specifically wish to thank John Brennan (the wonky 1), Natalie Labbé, Sonya Cyr and Bob Berno for making my stay in Windsor bearable... Natalie was also my rowing mentor/partner (scull and sweep) and for this I give her my deepest gratitude. Rowing has been an invaluable outlet during the creation of this dissertation and without Natalie's patient guidance last fall, I would not have had the opportunity to row competitively this year. I wish to commend Andromeda Bruckman for maintaining her gleeful personality while working very hard on several difficult aspects of my project (I maintain that protein crystallization IS witchcraft!).

There are so many administrative assistants who have helped keep me organized that I am unable to list them all. I specifically thank those at the NRC, University of Ottawa Department of Biochemistry (Smyth Road), and the University of Windsor Chemistry and Biochemistry Department.

My acknowledgements would not be complete without mentioning the emotional support and intellectual stimulation that my family has provided over the years. My grandmother, Eileen; my parents, Ruth and Fred; and my brother and sister-in-law, John and Tammy; have all supplied me with various forms of encouragement. Most importantly my family has never discouraged my "unusual qualities" which have lead to creativity in my research. To my heart of hearts and new husband, Michael Riem, I owe this dissertation. Michael has acted as friend, partner, husband and most recently, editor, during my doctoral pursuit and has offered me unconditional support (second to none). I would enjoy no success without Michael by my side...

TABLE OF CONTENTS

PART III: Conformational Heterogeneity & Fluorescence

Part IV: Future Directions

Part V: Bibliographic and Supplemental Information

List of Appendices

List of Figures

List of Tables

Abbreviations

aa	amino acid
A	absorbance (= OD)
ACM	amidocarboxymethylation
ADC	analogue-to-digital converter
"c" value	relative proportion of fluorescing species
CM	carboxymethyl cellulose cation exchange resin; carboxy methylation
DAS	decay-associated spectra
ex	excitation
em	emission
EF	calcium binding site formed by the arrangement of the "E" and "F" α-helices
ESIMS	(nebulization-assisted) electro-spray ionization mass spectrometry
FWHM	full width at half maximum
HD	helical dimer
IRF	instrument response function
ISC	intersystem crossing
L_a', L_b'	electronic transitions of Trp
MCA	multichannel analyzer
MCP	microchannel plate
nr	nonradiative
NATA	N-acetyl tryptophan amide
Pfl	*Pseudomonas fluorescens*
PMT	photomultiplier tube
q, Q	quenching, quenching species
R6G	rhodamine-6-G (dye)
SVR	serial variance ratio
T	thermal deactivation
TAC	time-to-amplitude converter
TCSPC	time-correlated single photon counting
WSSR	weighted sum of squares residual

PART I: Theoretical Particulars

Proteins & Spectroscopy: An Introduction

It is necessary to present sufficient theory and background information, such that the reader is able to fully appreciate the studies presented herein. The research area is first introduced through a basic biochemical review of proteins, followed by an overview of spectroscopic theory. Finally, previous studies related to this work are reviewed and the goals of this research are stated.

1.1 Molecular Architecture of Proteins

Without the elegant design and function of proteins, there would be no complex organisms. Proteins have been described as the "molecular machinery" of the cell and are synthesized according to the genetic information (DNA) stored within the cell's nucleus. The proteins observed in nature have evolved via selection pressure to perform specific functions: such as enzymatic catalysis, transport and storage, coordinated motion, mechanical support, immune protection, generation and transmission of nerve impulses, and genetic control which mediates growth and differentiation (Stryer, 1989).

Proteins are synthesized, both *in vivo* and *in vitro*, from single amino acids. These monomeric subunits consist of a central carbon atom (C^{α}) to which are attached a hydrogen atom, an amino group (NH_2), a carboxyl group (COOH), and a variable "R" group. The exception to this rule is proline which has an imino (-NH-) group instead of the amino group.

The "R" group or side chain is the distinguishing feature for each amino acid (Branden & Tooze, 1991).

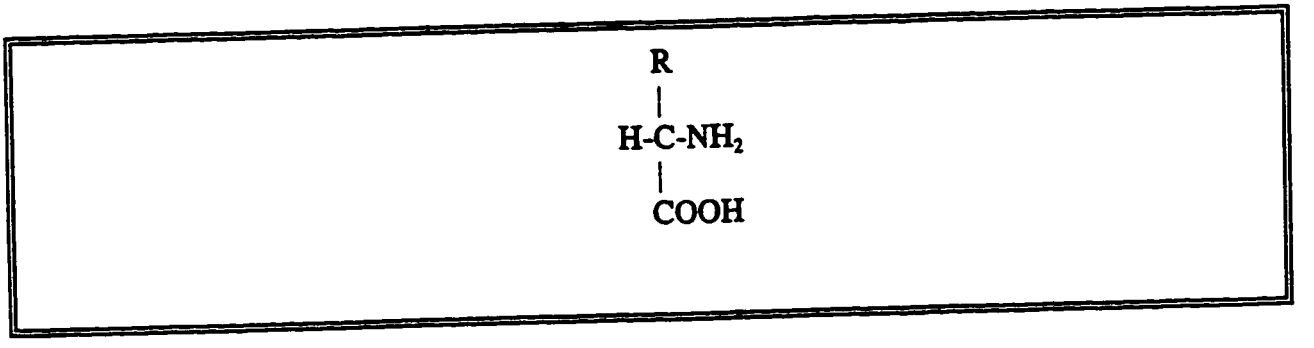

The four groups attached to the C^{α} atom are chemically different for all the amino acids, except glycine which has two H atoms bound to alpha carbon. Therefore all other amino acids are chiral molecules (no symmetry) and can exist as either L- or D-enantiomers (Lehninger, 1981).

There are 20 naturally occurring amino acids (Figure 1.1) which can combine to produce a vast number of protein sequences resulting in macromolecules with various structures and functions. Side chains other than those specified by the genetic code are rare and are products of post-translational enzymatic modification (Wold, 1981). During protein synthesis, amino acids (aa) are joined via condensation of the carboxyl group of aa_1 and the amino group of aa_2, resulting in the loss of one water molecule and the formation of a peptide bond. As the process continues the peptide elongates to generate a main chain or backbone $(-NH-C^{\alpha}-C=O)_n$ with various side chains (Figure 1.2). The translational

machinery necessary for protein synthesis has evolved to utilize only the L-enantiomer of amino acids. The primary sequence of a protein can be defined as being governed by covalent bonds. Thus disulphide bridges, which are formed by the oxidation of two cysteine residues, can be included in the primary structural classification. Proteins may also contain prosthetic groups (which are either covalently attached or strongly associated with the protein) or coenzymes which are comprised of other organic or inorganic elements.

The specific sequence of amino acids dictates the overall secondary and tertiary structure of a protein through side chain interactions. However, the rules which govern protein folding are largely unknown despite an intense research effort in this area. Creation of an hydrophobic core, by packing of the hydrophobic side chains, is the main driving force for the folding of water-soluble globular proteins. To accomplish this, a portion of the hydrophilic backbone must also be folded into the hydrophobic protein interior. The hydrophilicity of the protein backbone originates from the hydrogen bond donor (NH) and the hydrogen bond acceptor (C=O) which are spaced at regular intervals along the backbone (Figure 1.2). These main chain polar groups can form hydrogen bonds, thereby reducing their polarity in the hydrophobic environment. This hydrogen bonding structure is achieved by the formation of a regular secondary structure within the interior of the protein molecule (Goldberg, 1985). Different secondary structural motifs have been identified and are most accurately characterized by a unique set of phi (ϕ), psi (ψ) angles (Figure 1.2).

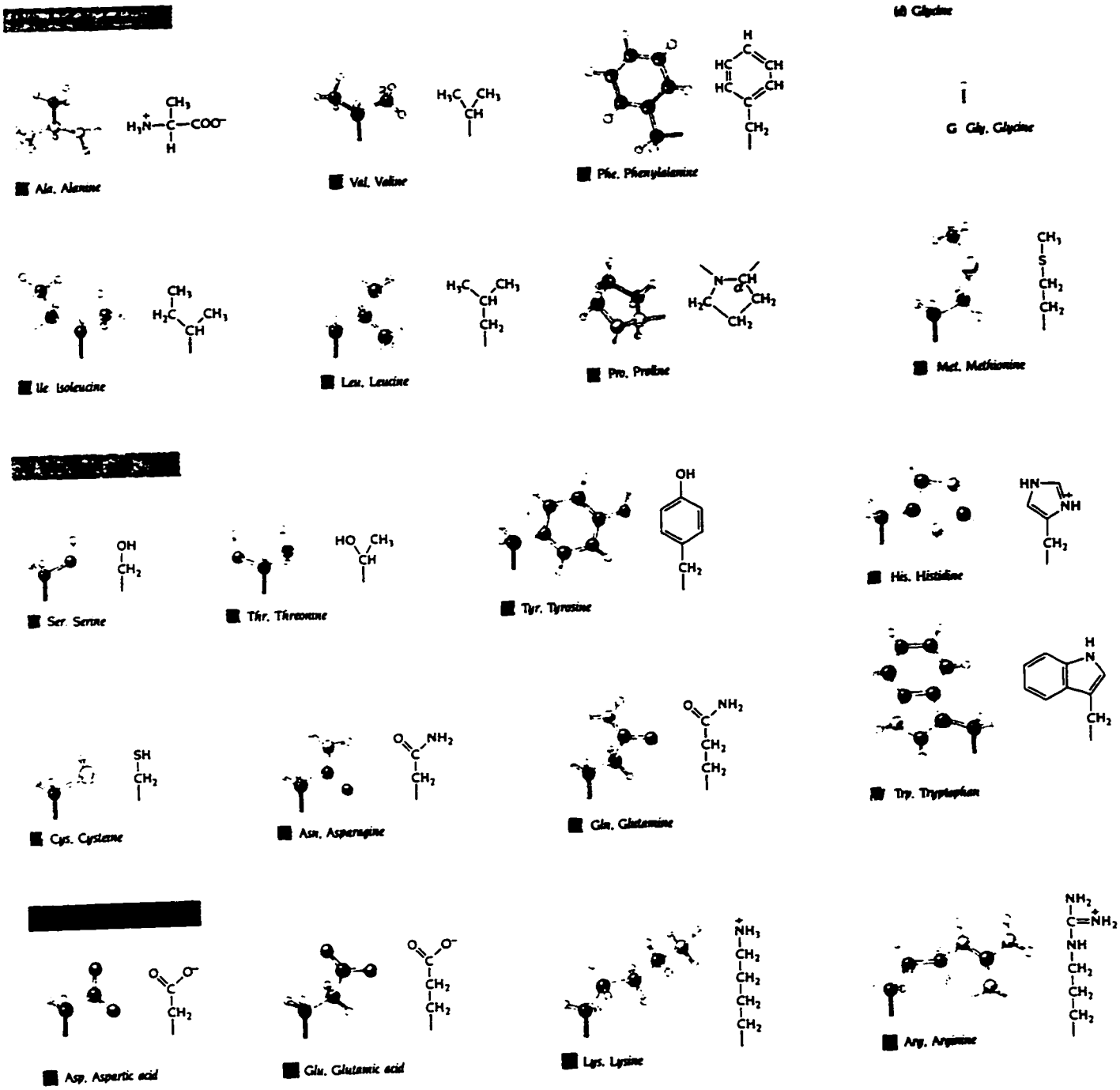

Figure 1.1 The 20 different naturally occurring amino acids are depicted using a ball-and-stick model and the chemical formula. All atoms are shown for alanine and only side chain atoms are displayed for the other nineteen amino acids. The amino acids are classified according to common properties: hydrophobicity, charge, and polarity. The names of amino acids are given in full, three-letter and one-letter codes (Branden & Tooze, 1991).

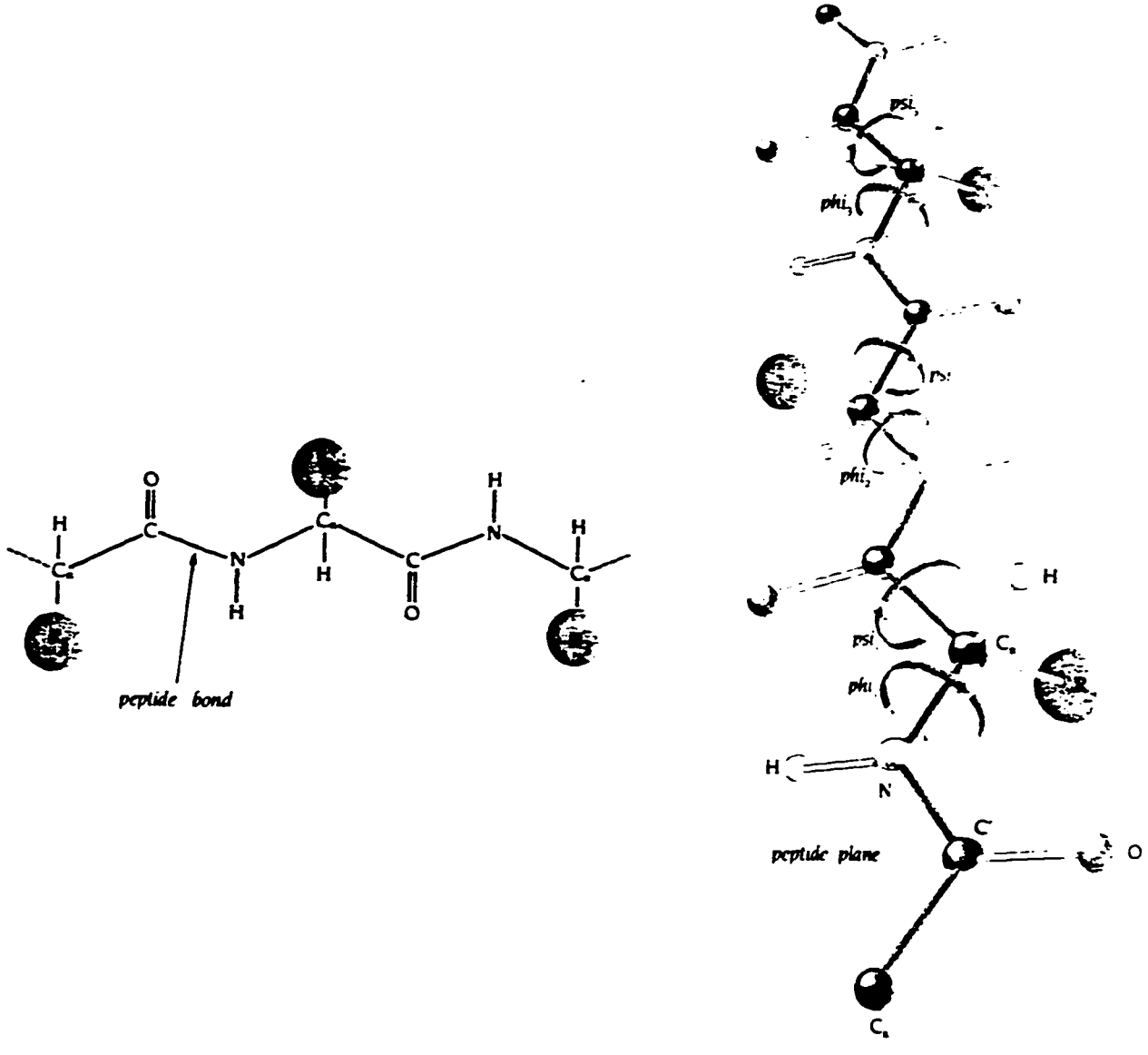

Figure 1.2 Repeating main chain subunit: a peptide bond is created when the carboxy group of one amino acid is condensed (elimination of H_2O) with the amino group of another amino acid. The main chain consists of the (-NH-C^{α}-C=O) repeating subunit and the side chain is considered the variable 'R' group. The secondary structure of a protein is classified based on the phi (ϕ) and psi (ψ) angles which represent the only degrees of freedom for the main chain. Both angles are dihedral and describe rotation about the N-C^{α} (ϕ is C_{i-1}-N_i-C_i^{α}-C_i) and C^{α}-C' (ψ is N_i-C_i^{α}-C_i-N_{i+1}) bonds, respectively (Branden & Tooze, 1991).

The two most commonly recognized types of secondary structures are the α-helix and the β-sheet (Figure 1.3 A). The associations which form secondary structural motifs are noncovalent in nature, although disulphide bridges (cysteine residues) are often found to stabilize secondary structure (Freedman et al., 1984).

The most common α-helical structure is characterized by a stretch of consecutive residues all having the ϕ, ψ angle pair of approximately -60° and -50° with 3.6 residues per turn, and hydrogen bonds between the C=O of residue n and the NH of residue n+4 (Stryer, 1989). In this way, all NH and C=O groups participate in hydrogen bonding except the first NH groups and the last C=O groups at either end of the helix. Consequently, the ends of the α-helices are often found at the protein surface. Theoretically, the α-helix may be either "right-handed" or "left-handed" depending upon the direction in which the chain forms the helix. Due to the close approach of the side chains to the C=O group, a left-handed helix is rare (ie. gramicidin) for L amino acids, whereas, right-handed α-helices are almost always observed in proteins. The alignment of the NH and C=O groups in an α-helix results in a significant net dipole for which the amino end displays a partial positive charge and the carboxy end exhibits a partial negative charge (Branden and Tooze, 1991).

A

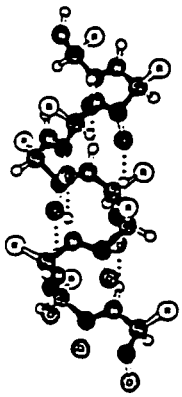

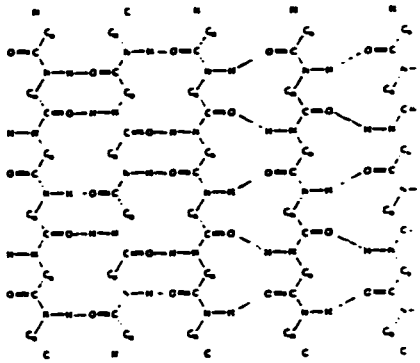

α-helix

"Mixed" β-sheet

random coil

B

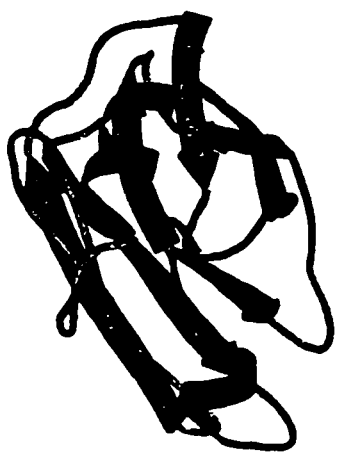

C

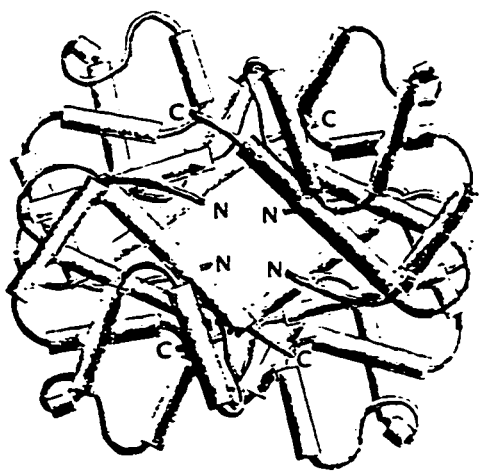

Figure 1.3 a) Common secondary structural motifs i) α-helix ii) β-sheet and iii) random coil (Branden & Tooze, 1991). b) Tertiary structure of *Pseudomonas fluorescens* azurin formed by the packing of secondary structural motifs into one or several compact units. c) Association of more than one haemoglobin molecule to form a quaternary structure (Branden & Tooze, 1991).

The α-helix is formed by a continuous set of residues, whereas the β-sheet is comprised of several distinct regions of the polypeptide chain. These regions exhibit an almost fully extended conformation with a broad range of phi (-40° to -180°), psi (30° to 180°) angles. The separate β strands are adjacently aligned such that the C=O from one strand and the NH from another may hydrogen bond. The β-sheets are pleated with alternating amino acid side chains above and below the sheet. There are two classes of β-sheets: parallel, where the amino acids of all β strands are aligned in the same direction (amino to carboxy terminal), and antiparallel, where the amino acids of each successive strand are aligned in the opposite direction (1. amino to carboxy 2. carboxy to amino 3. amino to carboxy etc.). Each type of β-sheet has a distinct hydrogen bonding pattern. Antiparallel and parallel β strand pairs may also combine to form mixed β-sheet structures and in known protein structures, β-sheets occur with a right-handed twist (Richardson, 1981). Loop regions serve to connect different combinations of secondary structural elements. These regions are generally found on the surface of a protein and are stabilized by hydrogen bonding of their NH and C=O groups to water molecules. Loops adjoining antiparallel β strands are termed hairpin loops or β turns (Richardson, 1981).

There are many possible combinations of simple secondary structural elements, those occurring frequently in proteins have been classified. These patterns of secondary structure are termed either supersecondary structure or motifs. Such structures include the EF hand, leucine zipper, β hairpin, greek key and the Rossman fold (Richardson, 1981).

Larger proteins often adopt more than one type of secondary structure within different

regions of the macromolecule. The term tertiary structure refers to the way in which these secondary structural subunits are arranged in three dimensional space to create a more compact overall structure (Figure 1.3 B). Often, the arrangement of tertiary structure is driven not only by hydrogen bonding, but hydrophobic interactions. Further structural complexity (quaternary structure) is determined by the non-covalent association of more than one protein molecule to form a multimeric network (Figure 1.3 C).

After protein purification, the order of amino acids in the peptide chain can be determined via well established protein sequencing methods. In a number of instances, secondary and tertiary structural details may be obtained by X-ray crystallography or 2-D NMR,. X-ray crystallography requires a crystallized protein and provides a static representation of the protein molecule. Unlike protein crystallographic techniques, NMR can provide dynamic information and structure when the molecule is less than 10 kDa. For each method, the samples used are highly concentrated and are not necessarily representative of a protein under *in vivo* conditions. Since modern biochemistry is often concerned with the interrelationships between protein structure, function and dynamics, other methods are required to probe different aspects of protein properties. Chemical modification, kinetics, site-directed mutagenesis, optical and NMR spectroscopy are all important contributors to our current understanding of proteins (Stryer, 1989). The majority of the research to follow describes data which were obtained utilizing various types of optical spectroscopy such as absorbance, circular dichroism (CD), and fluorescence.

1.2 Spectroscopic Methods: Photons and Proteins

The discipline of spectroscopy is concerned with the interaction of electromagnetic radiation with matter. Figure 1.4 displays wavelength regions of the electromagnetic spectrum which can be used as spectroscopic tools (adapted from Tinoco et al., 1995).

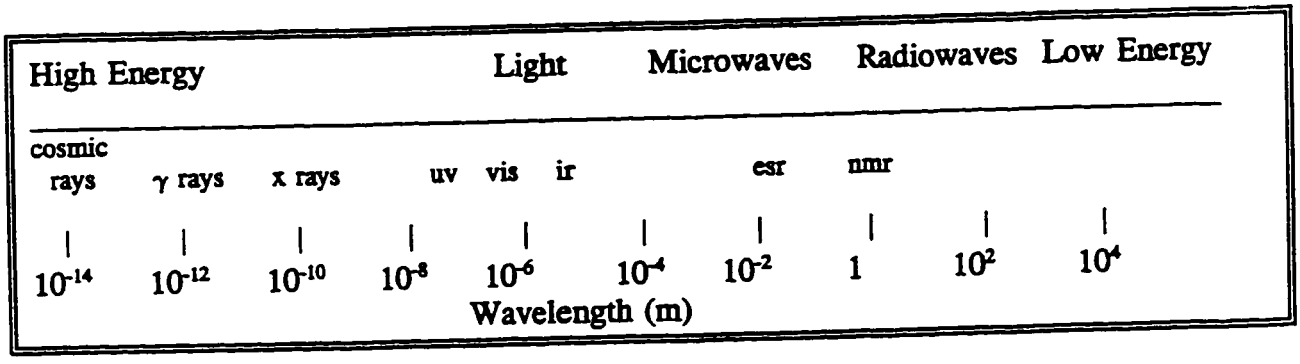

Figure 1.4 Wavelength regions of the electromagnetic spectrum adapted from Tinoco et al. (1985).

The electromagnetic spectrum is characterized in terms of wavelength, frequency (which are measures of the energy) or energy of the radiative field. The wavelength (λ) of radiation is inversely related to its frequency, ν, through the velocity of light, c:

$$\lambda = c/\nu \tag{1.1}$$

Electromagnetic radiation has both wave-like and corpuscular properties (Rabek, 1982). Wave theory describes a beam of light as orthogonal electric and magnetic fields moving through space in wave motion where both fields are mutually perpendicular to the direction of wave propagation. The particle theory depicts a beam of light as a stream of particles called photons. The energy of a photon is related to the frequency of the electromagnetic wave by:

$$E = h\nu \text{ or } E = hc/\lambda \tag{1.2}$$

where h is Plank's constant (6.626×10^{-34} Js). Thus for an electromagnetic oscillator of frequency ν, its quantum-mechanically permitted energies are multiples of $h\nu$.

1.2.1 Absorption Events (Excitation)

When electromagnetic radiation (ER) interacts with a molecule upon which it is incident, the radiation may be absorbed by the molecule according to a set of quantum mechanical selection rules (Turro, 1978). The molecules able to absorb the radiation are termed chromophores. Electromagnetic interactions are responsible for the absorption of light, hence the electrons in a molecule experience a force generated by the electromagnetic field by association with the incoming photon (Becker, 1969). If the electromagnetic force is large enough ($h\nu$) to promote an electron from an occupied orbital to an unoccupied orbital

within a molecule, there is a transition to a new electronic state. The probability of a transition occurring between two stationary electronic states also depends upon whether the incident radiation can change the electronic distribution of the ground state to that necessary for the excited state (change of dipole moment). The resultant transition can be spin, space, orbital or symmetry forbidden. Spin forbidden identifies a transition with no electron spin inversion and is the most rigorous rule. Space forbidden involves cases where the electron density in the region of space that orbitals overlap is low. Orbitally forbidden cases exist when there are large changes in the angular momentum about an axis and symmetry forbidden character relates to those cases allowed or forbidden depending upon a symmetry consideration (Becker, 1959). Molecule excitation involves the promotion of an electron from the highest occupied molecular orbital (HOMO) to the higher energy lowest unoccupied molecular orbital (LUMO). Since molecules absorb or emit energy in discrete packets termed quanta, the measurement of the radiative absorption or emission will provide information about the molecular energy levels. The energy of the quantum radiation is equal to the energy difference between two energy levels within the molecule ($\Delta E = E_2 - E_1 = h\nu$). Molecules possess, in addition to electronic energy, vibrational and rotational energy. Therefore, the radiative absorption by a molecule over a series of wavelengths (absorption spectrum) will often reflect the distribution of vibrational levels in the electronically excited states (Figure 1.5). Notably, this is observed for aromatic molecules such as pyrene, anthracene and naphthalene in 95% ethanol. The balance of this dissertation considers primarily electronic transitions.

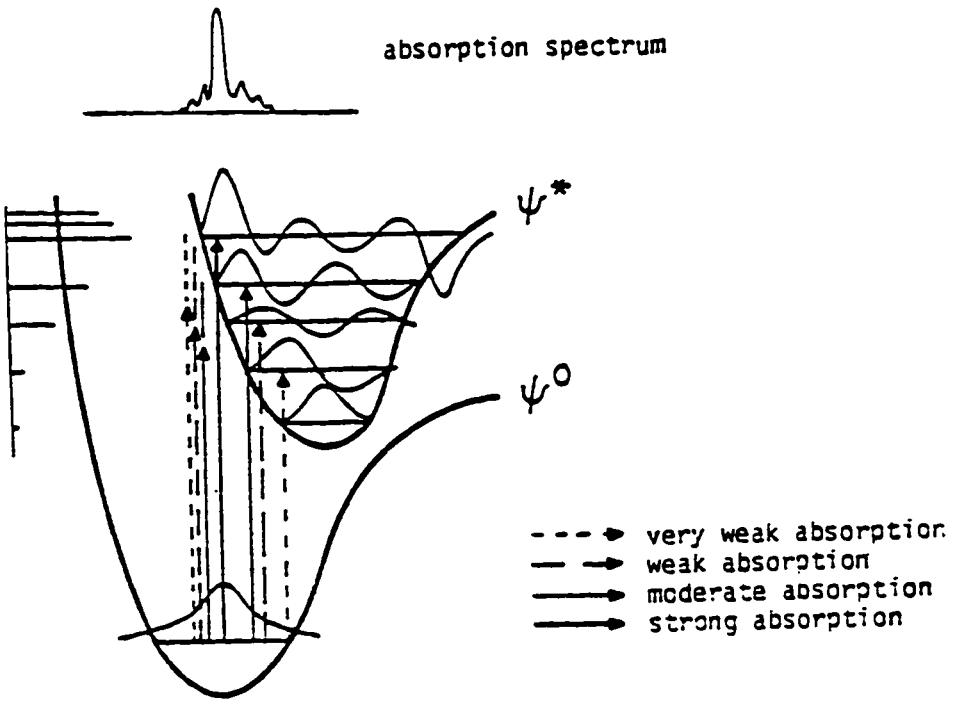

Figure 1.5 Energy level (horizontal lines) diagram illustrating transitions (vertical lines) between the ground state and vibronic states associated with the first electronic excited singlet state (Turro, 1978).

For saturated molecules, the σ molecular orbital is the highest energy orbital containing electrons, whereas molecules having double bonds contain electrons in π molecular orbitals. The π molecular orbital has a higher energy than that of the σ molecular orbital since the electrons are further from the nucleus. Therefore, a $\pi \rightarrow \pi^*$ transition of a solute molecule will require less energy than a $\sigma \rightarrow \sigma^*$ transition of the solvent molecule (Becker, 1969) providing the basis for optical spectroscopy in solutions.

1.2.1.a Absorption Spectroscopy

Consider a solution of absorbing species in a container which transmits light, as the light passes through the sample, the decrease in light intensity (I) will be dependent upon the concentration of the absorbing species (c):

$$- dI/I = \alpha c \, dx \tag{1.3}$$

where dI/I is the fractional decrease in light intensity, α is a constant of proportionality and dx is a small interval across the container. If the container has a fixed length (l), equation 1.1 can be integrated between its limits I_0 (intensity of incident light) at x = 0 and I_t (intensity of light transmitted) at x = l. Since neither α nor c are dependent upon x, these values are considered constant and integration yields:

$$\ln (I_0 / I_t) = \alpha c l \tag{1.4}$$

$$\text{and} \quad I_t = I_0 e^{-\alpha c l} \tag{1.5}$$

When expressed in $\log_{10}$ and not natural logarithms, the equation can be written in terms of the absorbance (A) or optical density (OD) as follows:

$$A = \log(I_0 / I_t) = \epsilon c l \tag{1.6}$$

where ϵ (α/2.303 ($M^{-1}cm^{-1}$)) is termed the molar extinction coefficient and is an intrinsic property of the absorbing species. The above equation (Beer-Lambert Law) demonstrates that absorbance is linearly related to both the concentration of the absorbing molecule and the cell path length (Tinoco et al., 1995). The value ϵ, and therefore A, is wavelength dependent for all compounds. Measuring the absorbance of a species over a range of wavelengths produces an absorption spectrum (Figure 1.6).

The extent of double bond conjugation affects the energy of $\pi \rightarrow \pi^*$ transitions (Jaffé & Orchin, 1962). Proteins absorb in two main regions of the ultraviolet (UV) spectrum with an absorption maximum between 240 nm and 300 nm (low energy) and a much stronger maximum between 205 nm and 220 nm (high energy). The absorption of low energy radiation can be attributed to the $\pi \rightarrow \pi^*$ transitions of the highly conjugated aromatic amino acids and the high energy absorption accounts for the $\pi \rightarrow \pi^*$ transitions of the amide group. The UV spectra of the aromatic amino acids; Trp, Tyr and Phe are displayed in Figure 1.6. The molar extinction coefficients have been determined for each of the aromatic amino acids in solution. At 280 nm the values of ϵ were: $\epsilon_{Phe,\ 280nm} = 0.7 \pm 0.3\ M^{-1}cm^{-1}$, $\epsilon_{Tyr,\ 280nm} = 1197 \pm 0\ M^{-1}cm^{-1}$, $\epsilon_{Trp,\ 280nm} = 5559 \pm 12\ M^{-1}cm^{-1}$ (Sober, 1970) and these values can be used as good approximations ($\pm$ 5%) of ϵ for aromatic amino acids in a protein. If the number of aromatic amino acids is known, the molar extinction coefficients may be summed and used to calculate protein concentration given the measured absorbance at a certain wavelength (see equation 1.4: $c = A/\epsilon l$).

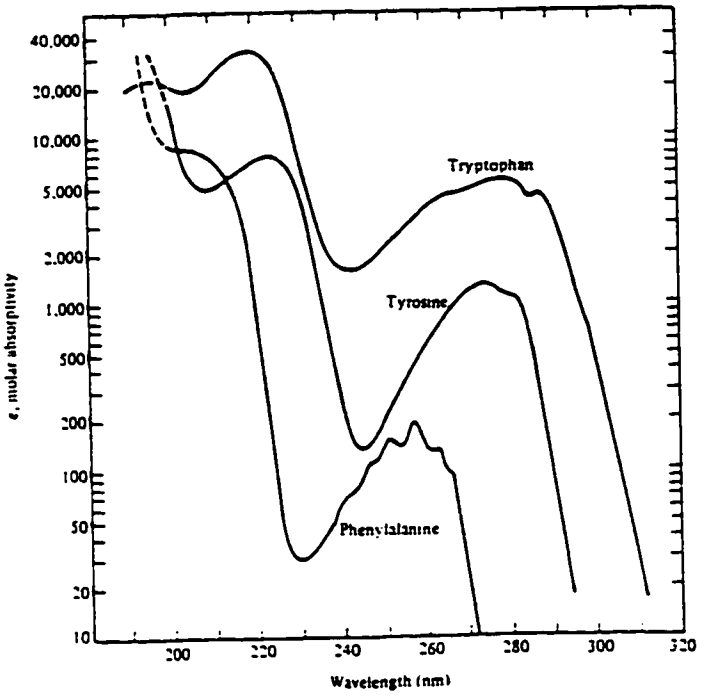

Figure 1.6 Ultraviolet absorption spectra of the aromatic amino acids (tryptophan, tyrosine and phenylalanine) adapted from Tinoco et al. (1995).

1.2.1.b Circular Dichroism

Molecules which have an asymmetric centre are not identical to their mirror image and are described as chiral. Mirror images of chiral molecules (enantiomers) in solution interact differently with circularly polarized light. Therefore, chiral structures can be distinguished and characterized using polarized light. Circular dichroism (CD) is a measure of the difference in absorption of left and right circularly polarized light (Freifelder, 1982) of

a molecular solution. This unequal absorption (CD) and unequal velocity of transmission (optical rotation) of left and right circularly polarized light, in the region of optically active absorption bands, is termed the Cotton effect (Crabbé, 1965).

Electromagnetic radiation can be depicted as an electric field vector which oscillates with a certain frequency in time and space. The propagation of circularly polarized light can be described as an electric vector in which the tip sweeps out a helix (Figure 1.7).

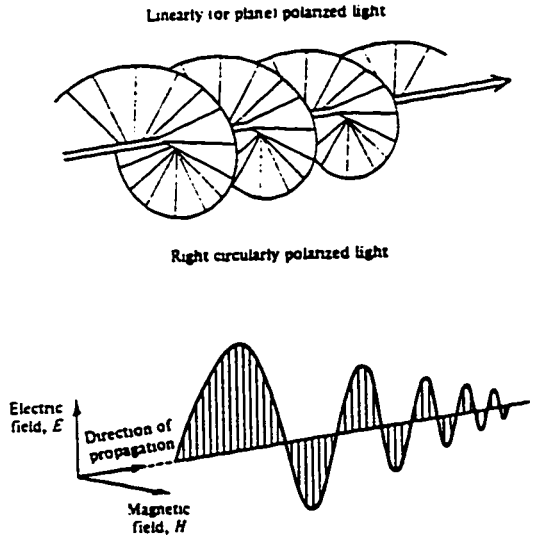

Figure 1.7 Comparison of linearly (plane) polarized light (top) with right circularly polarized light (bottom). The right circularly polarized light sweeps out a helix in the direction of polarization to produce a right-handed helix (Tinoco et al., 1995).

The electric vector can be resolved in terms of its components (Tinoco et al., 1995). For circularly polarized light propagating in the z-direction, the x and y components of the electric vector are expressed as:

Left Circularly Polarized Light:

$$E_x (z, t) = E_0 \sin 2\pi(z/\lambda - ct/\lambda) \quad (1.7)$$

$$E_y (z, t) = E_0 \sin 2\pi(z/\lambda - ct/\lambda + 1/4) \quad (1.8)$$

Right Circularly Polarized Light:

$$E_x (z, t) = E_0 \sin 2\pi(z/\lambda - ct/\lambda) \quad (1.9)$$

$$E_y (z, t) = -E_0 \sin 2\pi(z/\lambda - ct/\lambda + 1/4) \quad (1.10)$$

where λ and c are respectively the wavelength and speed of light in a vacuum and t is time. The x and y components of the oscillating electric vector are E_x (z, t) and E_y (z, t) and E_0 is the maximum amplitude of the vector. Change in absorbance for a sample which displays molecular asymmetry can be expressed as:

$$\Delta A = A_L - A_R \quad (1.11)$$

Therefore, CD can only occur in a region of the spectrum in which the sample absorbs. Proteins which absorb light from approximately 190 nm up to 310 nm can be scanned in these regions by CD. The passage of plane-polarized light (E_0) through a circularly dichroic sample produces a decrease in the magnitude of the left and right circularly polarized electric vector components due to selective absorbance. As a result, the emerging beam (E) is elliptically polarized and the ellipticity is given by:

$$\theta \text{ (rad cm-1)} = 2.303 (A_L - A_R)/4l \quad (1.12)$$

where θ represents ellipticity and l is the path length through the sample.

As previously described, polypeptides and proteins are polymers of amino acids joined though a peptide linkage. Apart from glycine, all amino acids are optically active since they contain one or more optical centres. Peptide bonds absorb between 190 nm and 240 nm and it has been shown that measurements of aqueous proteins in this region will report on secondary structural features (Fasman, 1967) such as the α-helix, β-sheet (parallel and antiparallel) and random coil (Figure 1.8). A characteristic ellipticity pattern is observed for each type of structural motif at different wavelengths. Each type of secondary structure is associated with a characteristic set of ϕ,ψ angles (Section 1.1), giving rise to the overall circular optical activity.

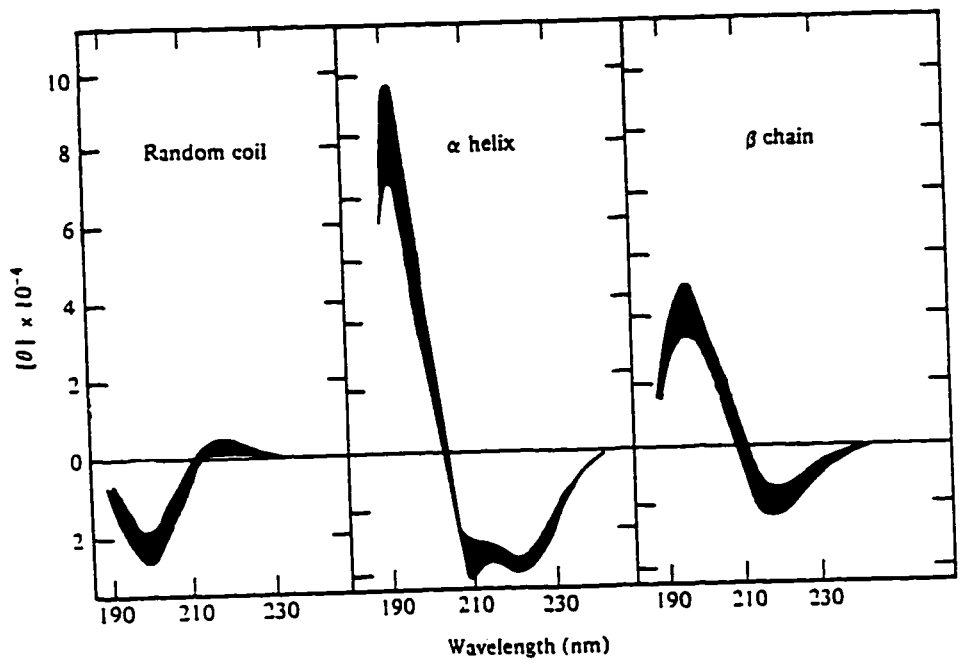

Figure 1.8 Typical CD spectra of secondary structural features in proteins (Cantor & Schimmel, 1980).

1.2.2 Relaxation from the Excited State

Once a photon has been absorbed ($S_0 \rightarrow S_n$), resulting in the promotion of an electron from the HOMO to LUMO, there are several possible routes by which the molecule may return to its original ground state (Figure 1.9). If the absorption process results in the excited molecule being in an upper vibrational level of the first S_1 state, the molecule will undergo a rapid conversion to the lowest vibrational level of the excited state. This radiationless process, termed internal conversion, occurs within 10^{-11} s. Internal conversion can also occur from the lowest vibrational level of the first excited state S_1 (0-0) to the ground state S_0 but this process is usually much slower, on the order of 10^{-5} - 10^{-7} seconds. Energy may also be lost as rotational or translational motion (Becker et al., 1969).

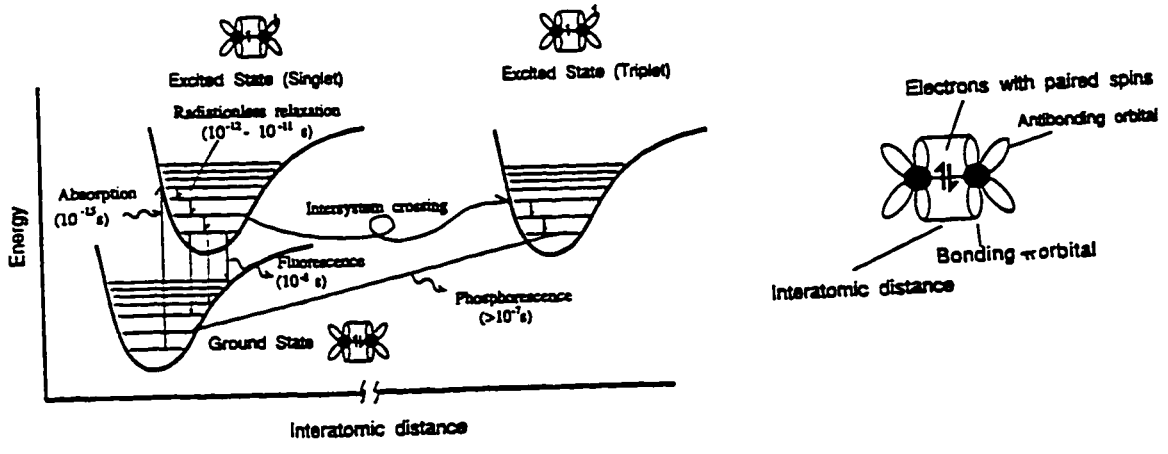

Figure 1.9 Modified Jablonski diagram: the schematic state energy level diagram shows how the absorption of one photon results in the promotion to an excited electronic state and the processes responsible for relaxation to the ground state (Hogue, 1994).

Radiative processes which allow relaxation to the ground state are termed luminescence. If the states from which the emission originates and terminates have the same multiplicity, the emission is called fluorescence. Multiplicity (J) is defined as 2S + 1 where S is the resultant spin of all the electrons in a molecule (Becker et al., 1969). This means the electron which is promoted to the excited state (vacant, antibonding orbital) retains its original spin, such that all spins sum to zero (J = 1; S = 0). However, if the spin of one of the unpaired electrons is inverted, the molecule has undergone a process known as intersystem crossing (typically 10^{-8} s) and enters the triplet state (J = 3; S = 1). Radiative relaxation to the ground state from the triplet state by another spin inversion is termed phosphorescence. There is a low probability of phosphorescent transitions and the rates are relatively slow with a low intensity, long wavelength emission (Turro, 1978). Although triplet-triplet absorption can occur, direct absorption from the ground state to the first excited triplet state is spin forbidden and normally does not occur or does so with a very low probability (Figure 1.9).

The time between which a molecule absorbs and emits, molecular processes may occur and compete with the fluorescence process (10^{-7} - 10^{-9}). Such processes include: molecular rotation, collisional deactivation, complexation, solvent motion and photochemistry.

There are four characteristics that can be associated with a molecular emission. These are a) energy, b) quantum yield, c) lifetime and d) polarization (Becker, 1969). The way in which these parameters can be measured will be discussed in Chapter 2.

1.2.2.a Emission and Excitation Spectra (Energy)

A useful fluorescence emission spectrum is produced by exciting a molecule with radiation from a constant-wavelength external energy source within the molecule's absorption band, followed by measurement of the emission from the excited molecule over a range of wavelengths. Radiative relaxation may result in a ground state molecule which is in a vibrational level higher than the lowest vibrational level (S_0 (0-0)). Therefore, the absorption and emission spectra will be mirror images of one another if the ground and excited state nuclear coordinates remain the same (Franck-Condon factor; Turro, 1978; Figure 1.10).

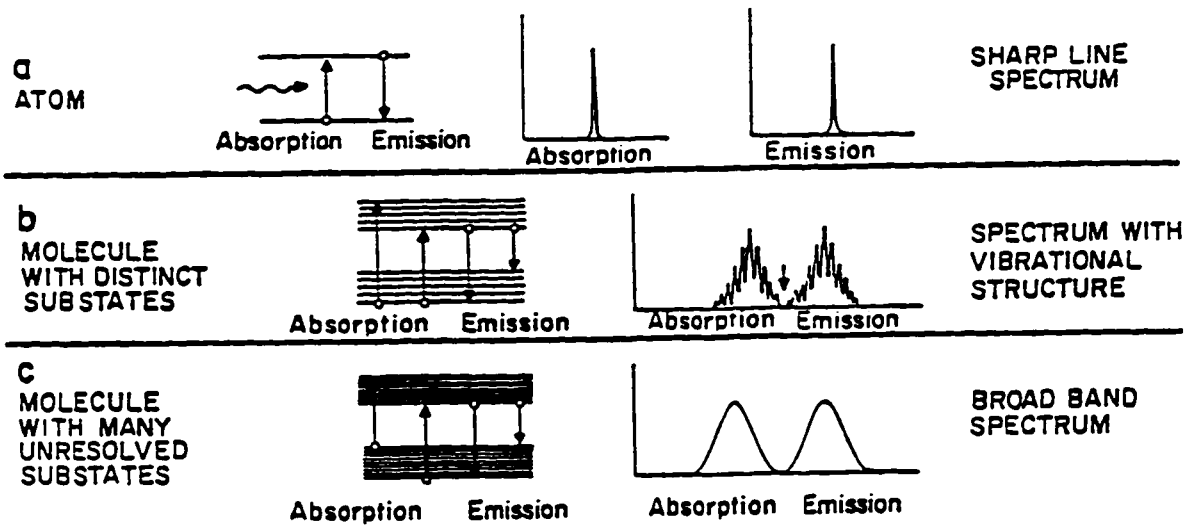

Figure 1.10 a) Sharp-line absorption and emission spectrum typical of atoms at low vapour pressures. b) Broad-band absorption and emission spectrum typical of rigid molecules at low pressure in the vapour phase. c) Structureless broad absorption and emission spectrum typical of molecules in solvents. Each absorption and emission corresponds to a single electronic transition (Turro, 1978).

The emission from the excited state will be of lower energy (red-shifted; Figure 1.10) than the absorption spectra due to a phenomena termed Stokes' shift (Stokes, 1852). This effect is caused by the rapid relaxation (10^{-14}) of the molecule to the lowest vibrational level of the first excited singlet state (internal conversion) which is lower in energy. Subsequent relaxation to an upper vibrational level of the ground state results in the emitted radiation having lower energy and a longer wavelength. The relaxation from higher energy excited states (S_2, S_3, S_4...) to the lowest vibrational energy of the first excited singlet state (S_1) is very efficient. Internal conversion efficiency also explains why in most cases emission spectra are independent of excitation wavelength (Vavilov's Law).

The Stokes' shift can also be the result of solvent relaxation, where the interaction of the excited molecule with solvent results in the loss of energy of the excited state. The Franck-Condon principle implies that the time required for absorption (10^{-15}) is insufficient for nuclear displacement, however, electron redistribution can occur during this time (Turro, 1978). In most cases, the excited state dipole moment of a fluorophore is different from the ground state and in some cases there is a full charge separation. In the case of polar solvents, the fluorophore's solvent cage (surrounding solvent molecules) can reorient about the excited state dipole. This rearrangement is termed dielectric relaxation and serves to minimize the total excited state energy attributed to the new excited state dipole (Lakowicz, 1983). The magnitude of Stokes' shift is due to changes in the transition energies. Vibronic energies of the ground state may also be affected by solvation in polar solvents and the resultant blurring of fine vibrational structure is observable in nonpolar solvents (Becker,

1969; Figure 1.10). The effect of solvent is directly related to the degree of interaction of solvent and solute, which is greater the more polar the solvent. Due to the largely random arrangement of molecules in the liquid state, the solvent environment of no two molecules is identical, therefore, spectra in solution generally appear as broad bands with or without a certain amount of vibrational structure (Jaffé & Orchin, 1962).

An excitation spectrum measures the dependence of emission intensity as a function of excitation wavelength. Most often, a molecule's excitation spectrum is similar to its absorption spectrum. This phenomena can be explained by reasons given above, where emission will always occur from the lowest vibronic level of the first excited singlet state. Hence, the first excited singlet state will be induced at a rate proportional to absorbance at the excitation wavelength, regardless of absorption wavelength, and the fluorescence emission intensity will be proportional to the absorption magnitude at excitation wavelength. The excitation spectrum reflects only that absorbance which leads to fluorescent emission, therefore, differences between the absorption and excitation spectra can be ascribed to the presence of more than one emitting species.

The sensitivity of fluorescence emission maxima to environmental factors has several important uses in studying proteins. The emission maximum can distinguish whether or not the Trp is solvent exposed or buried, based on the Stokes' effect for Trp in a protein. This makes Trp a sensitive probe for protein unfolding studies where the Trp becomes more and more solvent exposed with denaturation. For proteins, the binding of ligands or reaction with substrates may alter the collisional deactivation pathway sufficiently to result in a

change in fluorescence intensity in either the ligand or protein. This allows the fluorescent determination of ligand association constants and enzyme kinetics, respectively (Eftink, 1990).

1.2.2.b Fluorescence Quantum Yields

The fluorescence quantum yield of a species can be defined as the number of quanta emitted per exciting quantum absorbed:

$$\Phi = \frac{\text{number of emitted fluorescence quanta}}{\text{number of quanta absorbed to a singlet excited state}} \qquad (1.13)$$

Nonradiative relaxation processes (see Figure 1.9) affect the quantum yield and these are associated with specific rate constants (Becker, 1969). Nonradiative relaxation can occur by internal conversion (k_{IC}), intersystem crossing (k_{ISC}), thermal deactivation (k_T), photochemical reaction (k_p), concentration dependent collisional quenching ($k_q[Q]$; where Q is the quencher) and static quenching (k_{sq}). The total nonradiative rate constant is a sum of the individual rate constants:

$$k_{nr} = k_{IC} + k_{ISC} + k_t + k_p + k_q[Q] + k_{sq} \qquad (1.14)$$

The quantum yield may be expressed in terms of the rate constants of the competing processes (radiative and nonradiative) responsible for excited state deactivation:

$$\Phi = k_f/(k_f + k_{nr}) \tag{1.15}$$

where k_f is the rate of fluorescence decay. Nonradiative deactivation processes are sensitive to temperature and solvent characteristics. Thus, fluorescence quantum yield measurements are sensitive to fluorophore interactions and its surroundings. For proteins, the quantum yield of an intrinsic fluorophore can report on the local environment of the fluorophore.

The singlet lifetime is defined according to the rate constants which were introduced above:

$$\tau = 1/(k_f + k_{nr}) \tag{1.16}$$

Since the rate of fluorescence decay from a molecule (k_f) is related to the molecule's radiative lifetime (τ_r);

$$\tau_r = 1/k_f \tag{1.17}$$

the fluorescence quantum yield can be written as a function of the singlet (τ) and radiative lifetimes:

$$\Phi = \tau / \tau_r \tag{1.18}$$

Both the τ and Φ values can be measured for a given compound, facilitating the calculation of the radiative lifetime (τ_r) and the sum of the nonradiative rates (k_{nr}).

Furthermore, quantum yields can be used to calculate fluorophore sensitivity (S):

$$S = \Phi \times \epsilon\lambda \tag{1.19}$$

Fluorescence quantum yields are routinely measured by comparing the sample compound's integrated fluorescence with that of standard compounds for which the quantum yield is known.

1.2.2.c Fluorescence Lifetimes and "c" Values

A fluorescence lifetime can be described as the average time for which a molecule remains in the first excited singlet state (Birch and Imhof, 1991). For a population of fluorophores in the excited state, [F*], fluorescence emission to the ground state is random and only a fraction of the molecules will emit their photons at time τ. Fluorescence intensity decays exponentially with time, according to a first-order rate equation (Tinoco et al., 1995):

$$\frac{d[F^*]}{dt} = (k_f + k_{nr})[F^*] \tag{1.20}$$

Integration of this expression with respect to time yields the exponential function:

$$[F^*] = [F_0^*]e^{-t(k_f + k_{nr})} \tag{1.21}$$

where $[F_0^*]$ is the concentration of excited singlet state molecules at $t = 0$.

Equation 1.19 can be substituted into the above equation to give:

$$[F^*] = [F_0^*]e^{-t/\tau} \tag{1.22}$$

When t is equal to τ, the emission has decreased to 1/e of its initial value. The fluorescence intensity (I) observed for a given wavelength at time t is directly proportional to the rate of excited state depopulation, giving:

$$I(\lambda,t) = \alpha(\lambda)e^{-t/\tau} \tag{1.23}$$

where $\alpha(\lambda)$ is the preexponential term at wavelength (λ). Consider the case in solution where there is more than one fluorophore or several populations of one fluorophore due to conformational heterogeneity where k_{nr} is different for each. Then the fluorescence decay

becomes multi-exponential and can be adequately described by the following multiexponential decay function:

$$I(\lambda,t) = \sum_{i=1}^{n} \alpha_i(\lambda)e^{-t/n} \tag{1.24}$$

where n is the number of components, $\alpha_i(\lambda)$ is the preexponential term of the i^{th} component at wavelength λ and τ_i is the singlet lifetime of the i^{th} component. The preexponential terms are considered to be proportional to the excitation probabilities of each ground state species and estimate the relative proportions of ground state fluorophores (Donzel et al., 1974).

The average fluorescence lifetime ($<\tau>$) can be calculated as a sum of the weighted lifetime values:

$$<\tau> = \sum_{i=1}^{n} \alpha_i\tau_i \tag{1.25}$$

or the intensity-weighted mean lifetime τ_m can be calculated from the decay data by the following equation:

$$\tau_m = \sum_{i=1}^{n} \alpha_i\tau_i^{\,2} \Big/ \sum_{i=1}^{n} \alpha_i\tau_i \tag{1.26}$$

which can be derived from equation 1.27. The average fluorescence lifetime is used to compare lifetime and intensity data, whereas, the intensity-weighted mean lifetime provides a comparison between lifetimes and quantum yield data.

The steady state emission spectra (section 1.2.2.1) can be time-resolved into i emission spectra associated with each decay component (Knutson et al., 1982). The resulting spectra are termed decay associated spectra (DAS) and can be formulated using the following equation:

$$I_i(\lambda) = I_{ss}(\lambda)\,[\alpha_i(\lambda)\tau_i \,/\, \sum_{i=1}^{n} \alpha_i(\lambda)\tau_i\,] \qquad (1.26)$$

where $I_i(\lambda)$ is the spectral intensity of the i^{th} component, $I_{ss}(\lambda)$ is the steady-state spectral intensity and $\alpha_i(\lambda)$ is determined from equation 1.21 where $\Sigma\,\alpha_i$ is unity. In practice, the DAS is calculated from $I_{ss}(\lambda)$ multiplied by the fractional fluorescence ($f_i(\lambda)$) which is defined as follows:

$$f_i(\lambda) = \alpha_i(\lambda)\tau_i \,/\, \sum_{i=1}^{n} \alpha_i(\lambda)\tau_i\,] \qquad (1.27)$$

The spectral maximum of each decay component reports on its relative solvent exposure for reasons given in section 1.2.2.a. The fluorescence decay time values of

proteins are thought to reflect the local electronic environment of the Trp (made up of neighbouring amino acid side chains), however, structural correlations with τ values have not yet been definitively established.

The quantum yield from a mixture of fluorophores in solution (Φ_t) is merely the sum of the fractional contribution from each individual quantum yield (Φ_i):

$$\Phi_t = \sum_{i=1}^{n} \Phi_i c_i \tag{1.28}$$

where c_i is the concentration of fluorophore in solution. The concentration (c_i) of each component can be resolved from the DAS, if the multiexponential decay arises from one fluorophore. The area (A) of the DAS is directly proportional to both the sensitivity ($S = \epsilon\Phi$) of the fluorophore and its relative concentration (c):

$$A_i \propto \epsilon_i(\lambda)\Phi_i c_i \tag{1.29}$$

Since each decay component arises from a single fluorophore, albeit in different environments, the sensitivity ($\epsilon_i(\lambda)$) and the radiative lifetime (τ_r) are considered to be the same for each emitting species. Applying these conditions and considering equation 1.17, the DAS area is now only dependent upon fluorophore concentration and lifetime:

$$A_i \propto c_i \tau_i \tag{1.30}$$

and fluorophore concentration can be calculated by the following equation:

$$c_i = (A_i / \tau_i) / \sum_{i=1}^{n} (A_i / \tau_i)$$

This parameter will be evaluated in Chapter 3 as a sensitive probe of local secondary structure in proteins.

1.2.2.d Fluorescence Anisotropy

Certain protein motions, such as segmental flexibility and whole body rotation, occur on the picosecond and nanosecond timescales and can be measured by fluorescence anisotropy decay (Weber, 1952). Any molecule in solution (ambient temperature) will undergo Brownian rotational diffusion and at any given moment the molecule and hence the molecule's dipole will be oriented in a certain direction. Excitation of a sample with a plane polarized excitation beam provides an anisotropic distribution via the selection of a population of oriented molecules, from a set of randomly oriented molecules. Only those molecules having their $S_0 \rightarrow S_1$ absorption transition moment parallel to the plane of polarization will be maximally excited, since absorption is proportional to the resultant of the

absorption transition moment into the plane of polarization. Several processes such as electronic, motional and energy transfer effects can result in depolarization of the emitted light. Monitoring the change in polarized emission with time is the basis for measuring fluorescence anisotropy decay (Steiner, 1991). Given the proper experimental arrangement, vertically polarized light can be used to excite the sample and both vertical ($I_{\parallel}$) and horizontal ($I_{\perp}$) emission components can be monitored. The anisotropy (r) is defined by the following:

$$r = (I_{\parallel} - I_{\perp})/(I_{\parallel} + 2I_{\perp}) \tag{1.32}$$

where ($I_{\parallel} + 2I_{\perp}$) is proportional to the total isotropic fluorescence intensity.

A molecule's steady-state emission anisotropy is dependent upon the average angle (θ) between vectors, which represent orientations of the absorption and emission oscillators for a number of fluorophores:

$$r = (3\overline{\cos 2\theta} - 1)/5 \tag{1.33}$$

In solution, if there is no change in orientation of the absorption and emission transitions during the excited state lifetime, where $\theta = 0$, and, there are no other depolarizing processes, then the anisotropy will be 0.4. This value is the theoretical limit and is referred to as the fundamental anisotropy (r_0). Those processes (see above), which

result in a different orientation of the emission transition with respect to the absorption transition, will lead to a non-zero value for θ. Electronic effects can be described as a situation where the absorption moment ($S_0 \rightarrow S_1$ or $S_0 \rightarrow S_2$) and emission moment ($S_1 \rightarrow S_0$) are not parallel in the plane of the chromophore. Motional effects are the result of reorientation of the molecule during the excited state lifetime. Resonance energy transfer may occur between the initially excited donor molecule and the acceptor molecule, which has a different transition moment orientation. In each case, the emission will be depolarized to some extent. If the rate of rotation of the excited molecule is very swift, the anisotropy will rapidly decay to zero and integration over the lifetime of the excited state results in a steady state anisotropy of zero.

The modified Perrin equation relates the anisotropy to the fluorescence lifetime (τ) and the rotational correlation time (ϕ) for a rigidly attached fluorophore in an isotopically rotating sphere (ie. protein):

$$r = (r_0(app))/(1 + \tau/\phi) \qquad (1.34)$$

In the case of Trp in a protein, there may be side chain or peptide fragment flexibility, in addition to tumbling of the entire molecule during the excited state lifetime. For a spherical molecule there are generally two anisotropy decay times, the longer time is associated with whole body rotation and the short correlation time is related to the flexibility of the Trp side chain or peptide fragment containing the Trp.

1.3 General Protein Fluorescence

Protein fluorescence generally results from the emission of the three aromatic amino acids, Phe, Tyr and Trp (see Figure 1.1). These fluorescence probes are naturally occurring in proteins, and are termed intrinsic fluorophores. The fluorescence emissions of zwitterionic Trp, Tyr and Phe, free in solution, are depicted in Figure 1.11.

Of the three aromatic amino acids, Trp normally makes the largest contribution to protein fluorescence. Trp has the largest molar extinction coefficient of the three aromatic amino acids (recall from section 1.2.1.a) and displays the lowest energy absorption and emission spectra (Figures 1.3 & 1.11). Figure 1.3 also illustrates the spectral overlap of Phe, Tyr and Trp and the sequence of singlet energies (Phe, Tyr, Trp). Based on all of these observations, Teale & Weber (1957) proposed that excited state energy transfer from Phe to Tyr to Trp could occur as a result of dipolar resonance coupling, provided the rings were properly aligned. This energy transfer in proteins will enhance the fluorescence emission from Trp while reducing that observed from Tyr and Phe.

Even in the absence of energy transfer effects, it is obvious from inspection of the three molar extinction coefficients (section 1.2.1.1) that the contribution of Phe to protein fluorescence will be negligible at excitation wavelengths > 280 nm. As well, the quantum yield from Tyr is often low in proteins due to quenching caused by the presence of the peptide bond (Cowgill, 1967), nearby charged or neutral carboxy and amino groups (Weber & Rosenheck, 1964), and hydrogen bonding of the Tyr hydroxyl moiety (Cowgill, 1976).

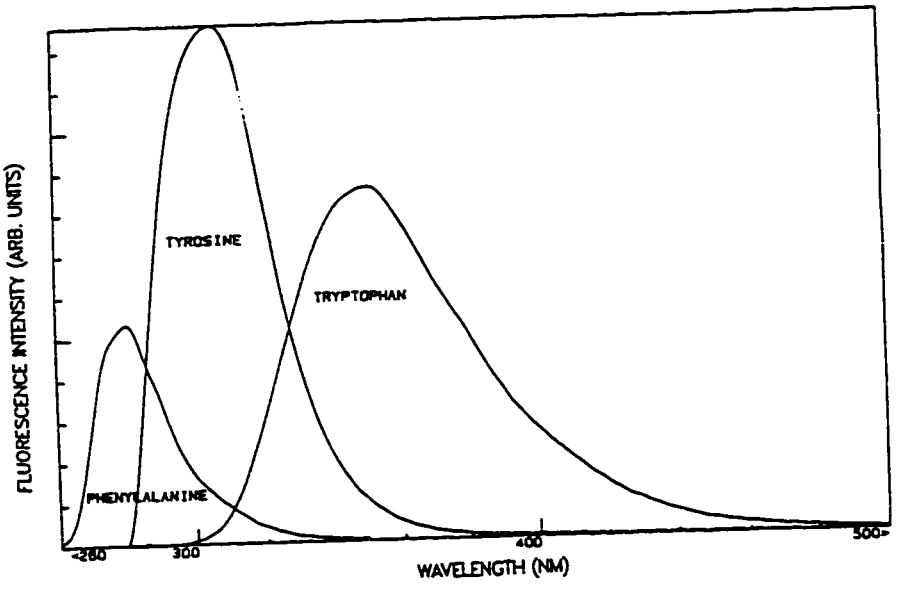

Figure 1.11 Fluorescence emission of the aromatic amino acids: phenylalanine (Phe), tyrosine (Tyr) and tryptophan (Trp) adapted from Hutnik (1989).

1.3.1 Tryptophan as an Intrinsic Probe of Protein Fluorescence

A closer inspection of Figure 1.3 reveals that Trp has an extended UV absorption spectrum compared to Tyr and Phe. Therefore, at wavelengths of 295 nm or longer, Trp may be photoselectively excited in the presence of a large number of Phe and Tyr residues. Furthermore, Trp has been found to be very sensitive to its environment, and in typical proteins Trp is relatively low in abundance. Based on all the concepts put forth, in conjunction with the above observations, Trp is considered to be the preferred intrinsic fluorophore.

Absorption studies of indoles in oriented crystals (Yamamoto & Tanaka, 1972) have demonstrated that two electronic transitions, designated ^1L_a and ^1L_b, occur between 260-300

nm (Figure 1.12). Equilibration between the two states occurs very rapidly (<1 ps), such that emission will occur from the lowest S_1 state. The ^1L_b absorption transition of indole seems to be insensitive to solvent environment, shows vibronic features and has a lower energy level than ^1L_a in nonpolar solvents. In polar solvents, the ^1L_a state becomes the lowest energy singlet state, due to interactions of this dipole with dipoles of the polar solvent molecules (Sun & Song, 1977). The ^1L_a absorption transition is thought to be able to participate in these dipole-dipole interactions due to its magnitude (higher than ^1L_b) and direction through NH (Figure 1.12). It is this interaction that accounts for Trp's sensitivity to its environment and observed Stokes' shifts (Sun & Song, 1977; refer to section 1.2.2.a). For Trp in a protein, the Stokes' shift will be dependent upon both the static polarity of the environment, as well as the dynamic ability of the solvent molecules contained within the local Trp environment to experience dielectric relaxation with the ^1L_a dipole (Eftink, 1990; and references cited therein). The range of Stokes' shift for proteins can be quite dramatic. The buried Trp in both the holo and apoazurins from Pseudomonas fluorescens (Pfl) display spectral maxima at 308 nm, whereas the solvent exposed Trp of small peptides such as parathyroid hormone (PTH) have spectral maxima as long as 350 nm.

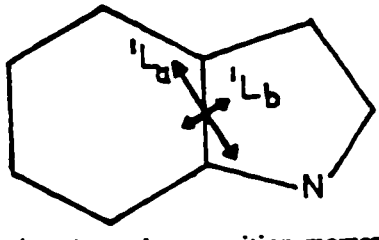

Figure 1.12 Orientations of the ^1L_a and ^1L_b absorption transition moment directions in the molecular reference frame of the tryptophan indole ring.

The fluorescence lifetime and quantum yield of Trp in a protein show significant variation, which corresponds to the many possible quenching contributions from a proteinaceous environment. Certain species have been found to be responsible for quenching of Trp; such as metal ions, heme groups and other cofactors (Lakowicz, 1983), the charged groups of His, Asp and Glu (Cowgill, 1976) or nearby Cys and disulphides (Cowgill, 1970). By analyzing crystallographic structures, Burley and Petsko (1986) observed that the positively charged or $\delta(+)$ amino groups of Lys, Arg, Asn, Gln and His are preferentially located within 6 Å of the ring centroids of Phe, Tyr and Trp, where Van der Waals' contact with the $\delta(-)$ π-electrons and the $\delta(+)$ ring edge is avoided. This geometric pattern is distinct from the expected distribution of random close packing of side chains in a protein and opposite to oxygen- and sulphur-aromatic interactions, which are almost certainly electrostatic in origin. In spite of the identification of potential Trp fluorescence quenching species in proteins, often the interpretation of relative quantum yields and fluorescence lifetime values is unclear. In fact, the original goal of this research was to create a data base by measuring single Trp proteins with known crystal structures. This type of data would aid in identifying the origin of the different fluorescence decay time values often observed for Trp in a protein. The reasoning behind this idea is further explored in Chapter 5.

1.3.2 Trp Multiexponential Decay and the Rotamer Hypothesis

Even as a free amino acid in dilute solution, Trp zwitterion fluorescence decay

behaviour is complicated by two distinct fluorescence decay times (Szabo and Rayner, 1980; Chang et al. (1983)). The biexponential decay of Trp zwitterion was originally proposed to originate from the dual emission of the ^1L_a and ^1L_b excited states (Rayner and Szabo, 1978). If this were the case, then other compounds having both ^1L_a and ^1L_b absorption transitions such as indole, 3-methyl-indole and N-acetyl tryptophan amide (NATA) would also be described by a biexponential decay. However, further investigation revealed monoexponential decay for all the aforementioned compounds. An interaction between the indole ring and the alanyl side chain of Trp was not discounted. This lead to a second hypothesis put forth by Szabo and Rayner (1980) where the biexponential decay was explained by the presence of Trp rotamers. There can be rotation about the C^α - C^β and C^β - C^γ bonds of Trp which would allow for different proximities between the indole ring and the α-amino group. Further study revealed that the biexponential decay of Trp zwitterion likely originates from excited-state reactions (Szabo, 1988; Willis & Szabo, 1991), nonetheless, these earlier ideas are important in understanding Trp fluorescence from proteins.

Single exponential decay kinetics for single Trp proteins in solution is rare and appears to require that the Trp is well buried in a motion-restricted environment of the protein. Single Trp containing proteins have often been shown to exhibit multi-exponential fluorescence decay kinetics in solution (Beechem and Brand, 1985; Eftink, 1991). Grinvald and Steinberg (1976) compiled values from single Trp proteins and found that the long decay times were within the 2 - 5 ns range, with intermediate values between 0.5 - 1.5 ns and the shortest lifetimes in a range of 0.02 - 0.5 ns. In many of these cases, the heterogeneous

decay behaviour observed for single Trp proteins was attributed to different local environments of the indole ring as a result of alternate protein conformations (Beechem & Brand, 1985). Assignment of the decay behaviour is further complicated by a protein containing more than one Trp residue. Often multi-Trp proteins display similar kinetics and decay values as those observed by Grinvald and Steinberg. This phenomena is explained by limitations in the data analysis technique, unable to resolve more than 5 discrete exponential values and values that are separated by less than a factor of two (McKinnon et al., 1977; Szabo, unpublished results), hence only average values from the emission of all Trp residues in the protein are observed. Increasingly, single Trp mutants of selected proteins, where the Trp residue has been specifically incorporated into sites at different segments of the protein, have been investigated by time resolved fluorescence methods (Harris and Hudson, 1990; Hutnik et al. (1991), Kilhofer et al. (1992)). The observation of multiexponential decay from single Trp proteins has more recently been rationalized in terms of Trp conformational heterogeneity originating from different side chain rotamer conformations (Ross et al., 1992; Willis and Szabo, 1992). The "rotamer model" for Trp in a protein proposes that the Trp side chain may adopt low energy conformations, due to rotation about the C^{α} - C^{β} and/or the C^{β} - C^{γ} bonds (Gordon et al. (1992)), with each conformation displaying a distinct decay time. Each decay time would correspond to a distinct protein environment of Trp. This model originated from studies on Trp in a diketopiperazine (Donzel et al. (1974)), and the aforementioned studies utilizing Trp zwitterion (Szabo and Rayner, 1980; Chang et al. (1983)). The rotamer model was shown to be applicable to fluorescence decay studies of

small peptides, where the relative proportions of each decay component corresponded to the individual rotamer populations measured by NMR (Ross et al. (1992)). Potential energy minimization calculations (Gordon et al., 1992) revealed three low energy χ_1 Trp conformers effected by rotation about the C^{α} - C^{β} bond (rotation about the peptide backbone) and two low energy χ_2 Trp conformers which corresponds to rotation about the C^{β} - C^{γ} bond (Trp ring flip). The IUPAC-IUB definitions of the χ_1 , χ_2 dihedral angles (IUPAC-IUB Commission on Biochemical Nomenclature, 1970) are illustrated in Figure 1.13. Newman projections of the six possible Trp conformations are depicted in Figure 1.14. Other factors such as secondary and tertiary structure will restrict the configuration of Trp in a protein, therefore decreasing the number of possible rotamers.

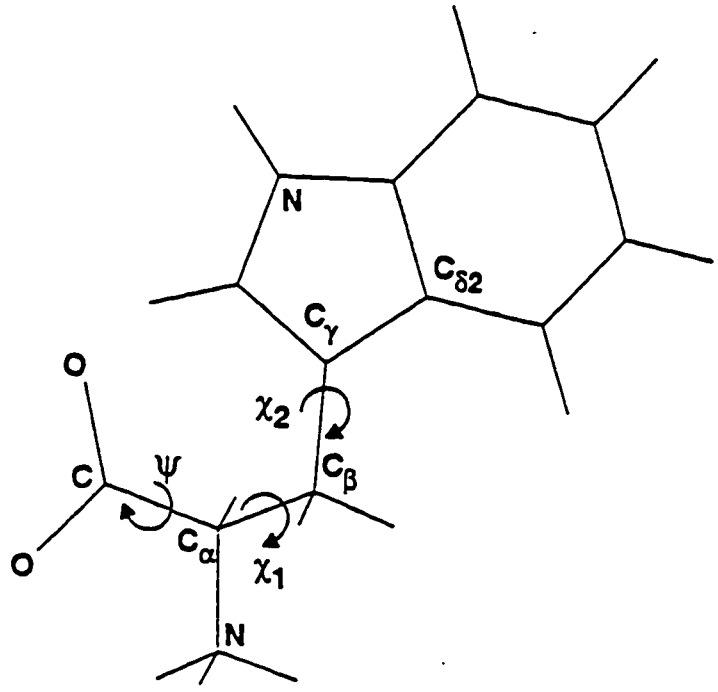

Figure 1.13 χ_1 and χ_2 dihedral angles in tryptophan: χ_1 = N-C^{α}-C^{β}-C^{γ} dihedral angle; χ_2 = C^{α}-C^{β}-C^{γ}-$C^{\delta 2}$ dihedral angle.

Figure 1.14 The six low energy rotameric configurations of tryptophan zwitterion.

1.4 Crystalline Proteins

In 1934, J. D. Bernal and Dorothy Crowfoot marked the dawn of macromolecular structure determination by successfully measuring a diffraction pattern from pepsin crystals (Rhodes, 1993). Since this time, many different structures of protein and DNA have been determined by X-ray crystallography and more recently by NMR. Protein structural determination by X-ray crystallography requires the growth of protein crystals. Methods such as vapour diffusion and microdialysis allow a highly concentrated protein in solution to experience a slow increase in precipitant concentration. Ultimately, the protein crystal is grown from a supersaturated solution since protein molecules diffuse together very slowly.

1.4.1 Properties of Protein Crystals

Due to the nature of globular proteins, the growth of well-ordered protein crystals is often difficult. Factors such as; pH, temperature, protein concentration and purity, the nature of the solvent and precipitate, as well as the presence of added ions or ligands are critical in the crystallization process. Globular proteins are large, spherical or ellipsoid macromolecules with irregular surfaces such that their packing into a crystal is impossible without the formation of large spaces between individual molecules. These channels are filled with solvent molecules and often occupy more than fifty percent of the entire crystal volume (Branden and Tooze, 1991). In some cases, the protein molecules only make contact at a few small regions. Even at sites of protein-protein contact in a crystal, interactions may be indirect, through one or several layers of solvent molecules. It is for this reason, that crystallographic structures are thought to be the same as those found in solution (Rhodes, 1993).

Protein crystals are fragile and unstable in solvents other than those from which they have been grown. Therefore, experimentation involving protein crystals requires gentle techniques, and those pertinent to these studies will be outlined in Chapter 3.

1.4.2 The Rotamer Libraries

X-ray crystallography has produced a large number of unique protein structures which have been conveniently catalogued and stored in computer based archival files; the Brookhaven Data Bank (BDB; Bernstein et al., 1977). The accessibility of protein structural coordinates from the protein data bank, make it possible for researchers to sort through this immense data base in search of structural patterns. The possibility of predicting secondary and tertiary protein structure from primary sequence has been a driving force for many of these searches and has led to the construction of rotamer libraries. The first such study, by Ramachandran and his group (1963), found that the presence of any side chain considerably reduces the conformational possibilities of neighbouring peptide groups, characterized by the ϕ and ψ dihedral angles. Chandrasekaran and Ramachandran (1970) undertook to examine the actual configurations adopted by side chains for three protein structures. By analyzing the distribution of side-chain dihedral angles, the authors attempted to prove that simple geometric considerations could predict side chain conformation. Other early work based on structural surveys (Janin et al., 1978; Bhat et al., 1979) and energy calculations (Gelin & Karplus, 1979) implied that, in general, the side-chain dihedral angles in proteins correspond to the potential energy minima observed for the isolated amino acid. As the resolution of crystal structures has improved, fewer side-chains have been found to significantly deviate from the minima of isolated amino acids (Bhat et al., 1979; James & Sielecki, 1983; Ponder & Richards, 1987). More recent studies have elaborated on this

concept, having found that correlations exist between the side chain χ_1, χ_2 pairs and the local backbone ϕ, ψ dihedral angles (Ponder and Richards, 1987; McGregor et al., 1987). This type of correlation for very small ϕ, ψ ranges has been used to predict amino acid side-chain conformation from main-chain coordinates (Dunbrack & Karplus, 1993). Schrauber et al. (1993) have evaluated the reliability of side-chain prediction and have found that tertiary structural interactions must also be considered.

Although molecular dynamics simulations and spectroscopic techniques have been useful in determining flexible groups in proteins, very few crystallographic studies have been focussed on side-chain conformational heterogeneity. Lack of sufficient resolution is partly the reason that crystallographic studies have not elaborated on such problems. As technological advances have improved the resolution of crystallographic structures, numerous examples of discrete heterogeneity have been observed. Several researchers, who had noted conformational heterogeneity in their high resolution structures, put forth a collaborative effort and developed an approach to modelling heterogeneous protein conformations and multiple solvent sites found to be associated with protein heterogeneity (Smith et al., 1986). From 6% to 13% of the amino acid side chains of the four proteins studied were observed in multiple, discrete conformations and heterogeneity was occasionally noted for buried side chains and the polypeptide backbone. Only a few side chains of the four protein crystals displayed missing or weak electron density, indicating a strong preference for discrete conformational perturbations rather than continuous disorder. Although few cases of heterogeneity have been reported for refined protein models, the results of this study

suggested that conformational heterogeneity in protein crystals is common and should be detectable in structure analyses at 2 Å resolution or better.

Recently, it has been suggested that the relative proportions of the fluorescence decay components may be correlated with protein secondary structure, since rotamer populations appear to be a common link (Willis and Szabo, 1992; Willis et al., 1994). For Trp, the rotamer libraries are almost exclusively based on structures in which the Trp has been modelled into a single conformation. It is reasonable to assume that the ϕ, ψ dihedral angles which characterize protein secondary structure will largely govern the rotameric conformations of the Trp side-chain (Ponder and Richards, 1987; McGregor et al., 1987; Dunbrack & Karplus, 1993; Schrauber et al., 1993). Given the rotamer hypothesis of Trp photophysics (refer to section 1.3.2), where the fluorescence lifetime values are proposed to originate from different rotameric configurations, the relative proportions of those lifetimes should then reflect the rotamer populations. The lifetime relative proportions ("c" values) then have the potential to provide a very local monitor of protein secondary structure. This concept is the basis for the studies presented in Chapter 4.

1.4.3 Spectroscopy of Crystalline Proteins

Although X-ray diffraction studies produce high-resolution structural information from proteins in the crystalline state, there is an ongoing debate as to whether or not this data is an accurate description of protein conformation in solution. In almost all cases, the biological

relevance of protein function is related to proteins associated with lipid membranes or proteins in solution. For this reason, spectroscopic techniques such as NMR (Rothgeb et al., 1981), EPR (Fiamingo et al., 1989), Raman (Sage et al., 1988) and XAFS (Lin et al., 1990) have been employed to probe differences and/or similarities between data from proteins in the crystalline state and those in solution. Unlike crystallography, these techniques generally provide information on the immediate environment of an atom or bond. The first study to examine protein crystals by fluorescence involved the analysis of the ligand chromophore from *Aequorea* green fluorescent protein. The emission wavelengths monitored were long (450-590 nm) and there was no contribution from Trp to the overall fluorescence observed in this region.

In order to compare the fluorescence parameters of intrinsic Trp fluorophores, sperm whale and yellow fin myoglobin were studied both in solution (Willis et al., 1990) and in the crystalline state (Willis et al., 1991). The fluorescence parameters of each myoglobin were found to be quite similar, but the lifetime values were 30% shorter in the crystalline protein. It was found that the fluorescence lifetimes from crystalline myoglobin could be calculated and that the shorter decay times in the crystals could be attributed to the energy transfer, facilitated by the heme groups of neighbouring myoglobin molecules in the crystal lattice. Another important discovery was that the preexponential terms associated with the two lifetimes of sperm whale myoglobin (contains two Trps) were dependent upon crystal orientation. This result was consistent with the crystallographic structure in which the two Trp residues were found to be virtually orthogonal. The most significant aspect of this study

was the conclusion that accurate time-resolved fluorescence measurements could be determined from single protein crystals.

Since Trp is modelled almost exclusively in a single conformation for crystallographic studies (Bernstein et al., 1977), one might think it is possible to selectively excite individual tryptophan residues from multi-Trp protein crystals, facilitating the assignment of decay kinetics. Such a strategy would allow for the creation of a data base of fluorescence decay parameters from single Trp proteins (with known crystal structures) both in solution and in the crystalline state. This data would provide a comparison of the fluorescence parameters to Trp environmental parameters such as; the hydrophobicity of neighbouring amino acid side chains, hydrogen bonding interactions, charge distribution, spacial packing constraints, solvent accessibility, local water structure, fluorophore conformers (interaction with the main chain NH and C=O), neighbouring side chain flexibility and other structural elements. Such an intensive comparison would provide valuable insights into the origin of the complex decay kinetics observed for proteins in solution.

Part II of this thesis will outline the instrumentation and data processing (Chapter 2) as well as the experimental methods (Chapter 3) used for this research. The major goal of this work was the systematic determination of relationships which exist between time-resolved fluorescence parameters and protein structural features. Trp fluorescence is used to probe local secondary structure of aqueous proteins (Chapter 4) and conformational heterogeneity in protein crystals (Chapter 5). Suggestions for future work will be outlined in Chapter 6.

PART II: Methods

Instrumentation & Data Analysis

This chapter will describe the practical details of the spectroscopic instrumentation and data analysis. The reader will become familiar with the complexity of the instrumentation and the statistical criteria which has been utilized to evaluate the data.

2.1 Circular Dichroism

Circular dichroism (CD) measurements were made with a JASCO 6000 (J-600) spectropolarimeter using 0.1 mm or 0.2 mm cylindrical quartz cells. Since temperature can have a dramatic effect on CD measurements (Crabbé, 1965), the instrument includes a special cylindrical cell holder which allows the sample to be thermostated (water jacket). A schematic of the instrument is shown in Figure 2.1. Light from the 450 W xenon lamp is focussed by mirror M_1 onto the entrance slit S_1. The optical system between S_1 and S_2 defines the first monochromator and the system between S_2 and S_3 defines the second monochromator. A double monochromator system is essential for CD measurements in order to minimize stray light. Each prism has a different axial direction, hence, the light passing through each monochromator will be both monochromated and linearly polarized. This linearly polarized light is then modulated by the CD modulator, producing right and left

circularly polarized beams of light. When measuring a fluorescent sample, the CD signal may be distorted depending upon the intensity of the fluorescence at a given excitation wavelength. The concentration of a strongly fluorescent solution should be prepared to give an absorbance of less than 0.5 (λ_{max}).

A standard is required to calibrate the CD instrument: 0.06% (w/v) aqueous ammonium d-10-camphorsulfonic acid was measured in the wavelength region of 350 nm to 210 nm in a 1 cm cell using a 20 m°/cm CD scale. The CD reading in the range from the baseline (~ 350 nm) to the peak value (290.5 nm) was +95.2 mm (Takakuwa et al., 1985).

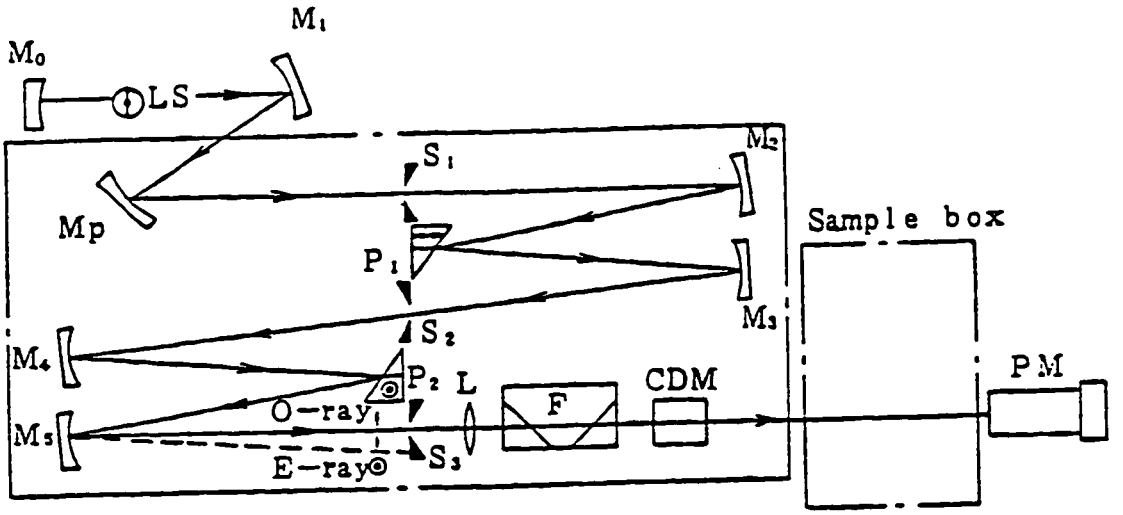

Figure 2.1 Schematic arrangement of the optical system from the J-600 spectropolarimeter. M = mirror; LS = light source; S = slit; P = prism; O-ray = ordinary ray; E-ray = extraordinary ray; L = lens; F = filter; CDM = CD modulator; PM = photomultiplier tube.

2.1.1 Spectral Correction

A blank is measured for each sample using a CD cell containing only buffer solution in the absence of sample. This blank spectrum is subtracted from the CD spectrum of the sample in buffer solution. The instrument measures the ellipticity at a given wavelength, θ_λ, in degrees:

$$\theta_\lambda = \pm H \times S \tag{2.1}$$

where H (cm) is the instrument reading and S (deg/cm) is the CD scale. The raw data is then statistically smoothed in order to minimize noise, resulting in more easily interpretable curves. In order to express the CD values in terms of specific ellipticity (Ψ_λ), the ellipticity values from the instrument must be corrected for both concentration and cell path length:

$$[\Psi]_\lambda = \theta_\lambda / (c \times l) \tag{2.2}$$

where c is concentration (g/ml) and l is cell path length (dm).

Protein concentration is calculated from the measured absorbance according to the equations and procedure outlined in the previous chapter (Section 1.2.1.1).

The molecular ellipticity is the specific ellipticity corrected for the molecular weight of the sample species:

$$[\theta]_\lambda = [\Psi]_\lambda \times M/100 \qquad (2.3)$$

where M is the molecular weight (g/mol) to give units in deg•cm^2•dmol^{-1}.

In order to allow for spectral comparison between different protein molecules, the mean residual molar ellipticity must be calculated. To obtain this value, the molecular ellipticity value is divided by the number of amino acid residues (N) which make up the protein:

$$[\theta]_{m,\lambda} = (\Psi_\lambda \times M/100)/N \qquad (2.4)$$

All of the CD values reported herein have been calculated as mean residue molar ellipticity.

2.2 Absorption & Steady-State Fluorescence

Two different UV-VIS spectrophotometers; Varian (DMS 200) and SLM Aminco (DM 2000), were utilized for the collection of absorption spectra. Fluorescence excitation and emission spectra were measured with an SLM 8000C spectrofluorometer. Details of the instrument are shown diagrammatically in Figure 2.1. Not shown in this figure is the Neslab Endocal RTE-5DD refrigerated circulating bath connected to the sample holders which allowed for temperature control. Such an addition to the fluorometer is desirable, since the fluorescence yield of certain samples can be dramatically affected by even small

temperature fluctuations (Pilulik & Solomakho, 1960).

For the collection of all fluorescence spectra, a depolarizer is placed in the excitation path and a polarizer oriented at 35.3° to the vertical in the emission path (Figure 2.2), thereby, providing equal intensities to both the vertical and horizontal emission components (Spencer & Weber, 1970).

This particular fluorometer operates in a T-format, which provides two emission paths symmetrically arranged on either side of the sample compartment and allows for convenient polarization measurements. Routine collection of fluorescence emission and excitation spectra are collected in the L-format. The SLM 8000C instrument was equipped with three monochromators; two single grating emission monochromators and one double grating excitation monochromator. The light from the 450W xenon lamp passes through the double grating excitation monochromator to a beam splitter. Most of the excitation light continues on its path to the sample, while a portion of the light ($<10\%$) is directed orthogonally towards a triangular reference cell containing the standard Rhodamine-6-G (R6G). The R6G signal is passes through a red filter (620 nm cut off) and the resultant signal is detected by a photomultiplier tube (PMT). This process enables the sample fluorescence to be corrected for excitation light variation (ratio). After having passed through a single grating monochromator, the sample's fluorescent emission is detected by a thermo-electrically cooled PMT at right angles to the excitation beam.

A

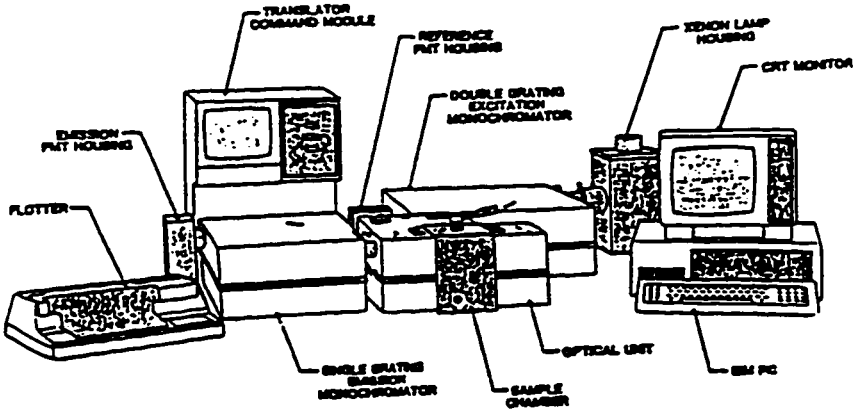

B

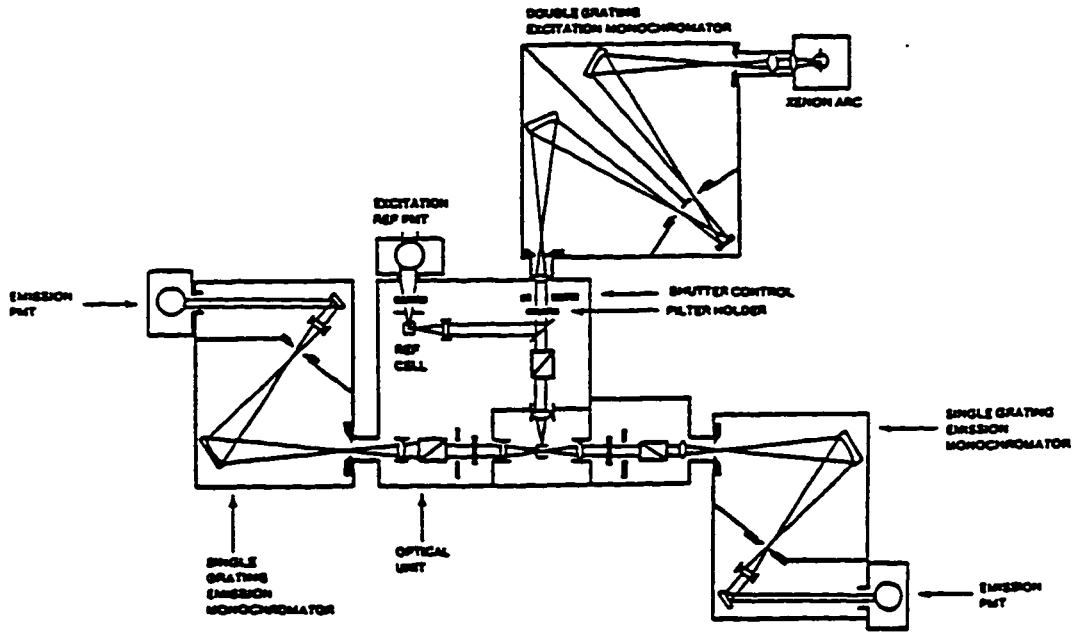

Figure 2.2 Schematic arrangement of the SLM 8000C Aminco fluorometer.
A) This diagram shows all optical and electronic components of the fluorometer as they would appear in the laboratory. Not shown is the second single grating emission monochromater which completes the T-format and the water bath connected to the sample compartment.
B) Schematic of the optical fluorometer components as viewed from above. The continuous thin lines denote the light path which originates at the xenon arc lamp. Mirrors are represented by rectangles with one curved side, small rectangles indicate prisms, small ellipses designate the various lenses, the solid rectangles in the light path symbolize filter holders while those falling on either side of the light path signify shutter control and the larger rectangles split by a diagonal line mark the position of the polarizers. The beam splitter is marked in the diagram by a cross and the sample holder is indicated by an asterisk.

Typically a sample is placed in a·1 cm quartz fluorescence cuvette and its absorbance spectrum measured. For fluorescence measurements, a sample should have an optical density (OD) or absorption (A) of less than 0.05 at the excitation wavelength. At values greater than $A_{ex} = 0.05$, the increase in fluorescence emission may not be linear as a function of sample concentration (Lakowicz, 1983). This behaviour has been termed the inner filter effect and is the result of both the excitation and emission optics being focussed upon the centre of the sample. Therefore, the majority of the detected fluorescence will emanate from this focus (Penzer, 1980). If the sample concentration is too high, then the fluorescence collection efficiency will be reduced for one or both of the following reasons:

1) There is a high probability of absorption by the many chromophores which the excitation beam encounters prior to reaching the part of the sample viewed by the monochrometer emission slit. Thus, the amount of exciting light which reaches the focus will be diminished.

2) The fluorescence which is emitted from the many chromophores may be reabsorbed by other molecules.

In either case, the result is an apparent fluorescence intensity less than expected based on the molecule's intrinsic quantum yield.

2.2.1 Spectral Correction

The process of fluorescence ratio correction (see section 2.2) is accomplished by dividing the sample emission value by the reference signal value from R6G. The resultant

signal is automatically processed by the instrument's software during the spectral scan. This process will account for lamp intensity fluctuations which occur during the time required for data collection (Parker, 1958).

Both the absorption and fluorescence spectra must be corrected for any contribution from the sample solvent. In order to accomplish this, a quartz cell containing only buffer (in the absence of protein) is measured and this spectrum is subtracted from that of the sample. Reagents used as buffering systems will often show an absorbance at shorter wavelengths (<280 nm) and some fluorescence due to small amounts of contaminants.

The most significant contributor to the blank fluorescence spectrum originates from scattered light. Most of the light scattered by the sample is elastic scattering (Rayleigh scatter) at the same wavelength as the exciting light. Most protein fluorescence spectra are shifted with respect to the absorption spectrum (see section 1.2.2.1), therefore, the Rayleigh scatter signal is at a shorter wavelength than the spectral scan (ie. λ_{ex} = 295 nm; λ_{em} = 300 nm - 420 nm). The intensity of scattered light displays a cosine squared dependence on the angle between excitation and emission, exhibiting a minimum at 90 degrees (Kirby, 1971). This is the principal reason that fluorometers are constructed with the emission optics perpendicular to the excitation source. A small portion of the incident irradiation is scattered with a shift in wavelength. This inelastic scattering process, termed the Raman effect, occurs as a result of the dipole moment induced vibrational transition caused by the exciting light. Since the Raman scatter is shifted to wavelengths longer than that of the excitation source, this peak will appear in a fluorescence emission spectrum and is the major

component of the blank spectrum. For example, in aqueous solution a Raman band occurs due to the O-H stretch of water at approximately 3300 cm^{-1} lower energy than the energy of the exciting light.

As well as the above considerations, errors are introduced into the spectrum due to variation in the wavelength efficiency of the excitation monochromator, polarization of the excitation source with wavelength as well as the wavelength dependence of the PMT and emission monochromator sensitivity. The former applies to excitation spectra while the latter needs to be considered for emission spectra, even though this is partially accounted for by the reference R6G signal. R6G is a suitable reference standard since it is photochemically stable and at high concentrations neither its quantum yield nor emission maximum vary with excitation wavelength (Melhuish, 1955). The correction curve used for excitation spectra is simply a R6G (3 mg/mL in ethylene glycol) excitation spectrum (λ_{em} = 640 nm; λ_{ex}= 250 nm - 300 nm) collected in the ratio mode. In order to obtain the corrected spectra of a sample, the sample spectrum is divided by the R6G excitation spectrum. The 250 nm - 300 nm range shows little variation in the correction curve, therefore, correction of protein excitation spectra by this method is optional.

To account for the distortions in emission spectra, a quartz diffuser plate at an angle of 45° to the excitation beam (Kirby, 1971) was utilized during the synchronous scan of the excitation and emission monochromators. Since the diffuser plate scatters light of all wavelengths with equal efficiency, one can obtain a lamp-excitation monochromator spectrum which is distorted by the variation in the emission monochromator and PMT sensitivity with

wavelength. The R6G excitation spectrum is divided by the scatter spectrum to give the emission spectra correction curve. The blank subtracted sample spectrum is then multiplied by the correction curve in order to yield the actual spectrum of the sample.

Finally, the fluorescence spectra are normalized to unity at their maximum to give fluorescence arbitrary units, facilitating a comparison between the spectral shapes and maxima of different samples.

2.2.2 Quantum Yield Calculation

As previously mentioned in section 1.2.2.2, the quantum yield of a protein can be measured using a reference standard such as NATA. No single direct method of determining quantum yield has been found to be exemplary (Miller, 1981), therefore, the reference method is most commonly used due to its ease of measurement. The absorbance and fluorescence of both the sample (s) and reference (r) compound are measured sequentially. The quantum yield can then be calculated from the following equation (Demas & Crosby, 1971):

$$\Phi_f(s) = \frac{1 - 10^{-A\omega}}{1 - 10^{-A\omega}} \times \frac{D_s}{D_r} \times \frac{I(\lambda_s)}{I(\lambda_r)} \times \left[\frac{\eta_d(s)}{\eta_d(r)}\right]^2 \times \Phi f(r) \qquad (2.5)$$

where A is the absorbance at excitation wavelength of either the sample or reference

compound, D is the value of the integral for the corrected fluorescence spectrum, I is the intensity of the light at each excitation wavelength and η_d is the refractive index of the solvent. In practice, the absorbance of both the standard and sample are measured at the same excitation wavelength, and the solvent is the same for sample (protein) and reference (NATA). Therefore equation 2.5 reduces to:

$$\Phi_f(s) = \frac{1 - 10^{-A(r)}}{1 - 10^{-A(s)}} \times \frac{D_s}{D_r} \times \Phi f(r) \qquad (2.6)$$

The quantum yield of NATA is taken to be 0.14 (Eisinger, 1969) and all other parameters can be measured.

2.3 Time-Resolved Fluorescence Spectroscopy (TRFS)

The fluorescence measurements made utilizing the instrumentation described in section 2.2 (continuous excitation source and emission collection) provided a steady state fluorescence spectrum. The fluorescence decay of the excited singlet state can be time-resolved by performing measurements under transient conditions, rendering the lifetime of that state. Two methods which are most widely used to determine fluorescence decay

parameters are "phase and modulation" (reviewed in Lakowicz, 1983) and "time correlated single photon counting" (TCSPC, reviewed in O'Connor & Phillips, 1984). The latter method was exclusively used to obtain the data reported herein. Using this technique, the sample is repetitively excited by a short pulse of light and in turn the sample emits many photons. A single photon is randomly detected by the instrument and its emission time is measured. This process is repeated many times and eventually enough single photon events are recorded to yield an emission decay curve (probability distribution).

Any instrument used for TCSPC must have the following features:

1. A repetitive pulsed excitation source, where each pulse has closely similar characteristics.
2. A means of detecting only single photons.
3. A method of measuring the time difference between sample excitation and single photon emission.
4. Low numbers of correlated dark counts (noise).
5. Data storage.

The above requirements are met by the operating system used for these studies and will be discussed in detail in the following sections.

2.3.1 Time Correlated Single Photon Counting

TCSPC has been applied to the study of a wide variety of molecules having chemical, biochemical and biological significance. The sophisticated methods and instrumentation

currently used for TCSPC measurements are the culmination of more than thirty years of development (O'Connor & Phillips, 1984). The details of determining time-resolved fluorescence parameters for proteins by TCSPC has been reviewed by Szabo (1988). Figure 2.3 displays a detailed schematic diagram of the instrumentation used to collect the data reported herein. To obtain a more detailed description of this system's components refer to Hutnik (1990).

For a typical TCSPC experiment, the sample is repeatedly excited with very short pulses of light. A mode-locked (82 MHz) argon ion laser is used to synchronously pump a dye laser whose output is cavity-dumped to give high peak power (Canonica & Wild, 1985), and frequency doubled. Such an instrument produces vertically polarized pulses with repetition rates selectable from 1 Hz - 4 MHz, a pulse width of 10 ps (FWHM) and an average power of 50 mW at 590 nm. The temperature controlled (30 °C), circulated (100 psi) dye solution used was R6G in ethylene glycol, providing a useful tunable range of 575 - 640 nm. The cavity dumper reduces the pulse repetition rate to within the time capability of the detection electronics; the result is enhanced peak power. The repetition rate (typically 825 kHz) selected at the cavity dumper allows for rapid data collection, but is sufficiently low to permit the fluorescence from one excitation event to decay before the next excitation event occurs (Phillips et al., 1985).

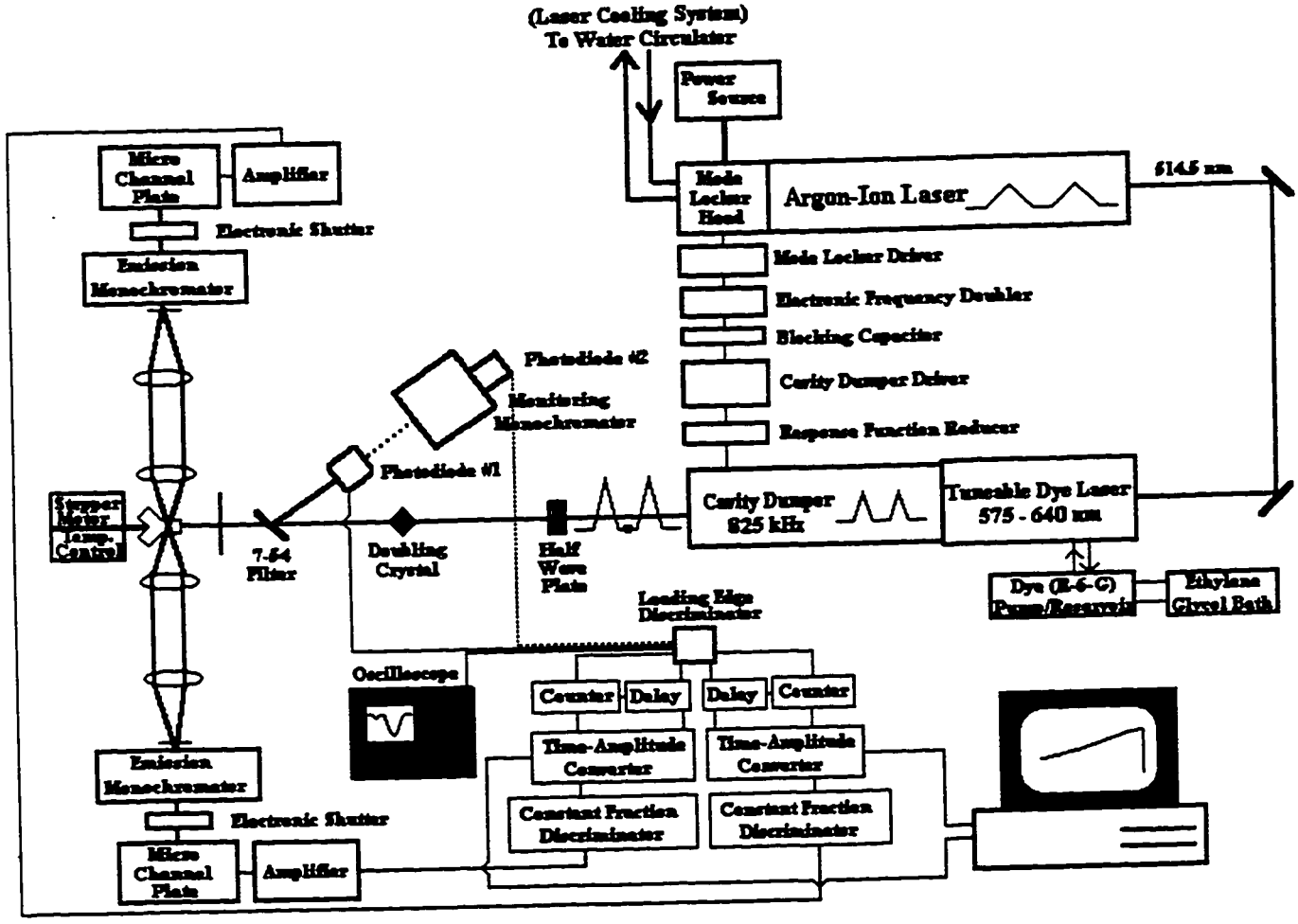

Figure 2.3 Schematic arrangement of time-correlated single photon counting instrumentation utilized for these studies.

The light emerging from the cavity-dumped dye laser is rotated by the half wave plate and frequency doubled by an angle-tuned second harmonic generating KD*P crystal to provide a UV excitation range (284 - 300 nm) appropriate for protein fluorescence and other applications. A Corning 7-54 filter removes any fundamental light which passes through the doubling crystal, and as well, it reflects the visible light pulses onto a monochromator with fast avalanche photodiode. A fraction (10%) of the electronic signal from the photodiode is directed to a cathode ray oscilloscope to monitor the stability of the cavity-dumped laser pulse, while the other 90% is directed to a leading edge discriminator and subsequently to the STOP input of the time-to-amplitude converter (TAC). In order to facilitate laser wavelength adjustment, the photodiode can be removed, allowing the smaller (10%) electronic signal to be detected by the monitoring monochromator.

Prior to reaching the sample, the excitation beam is passed through an adjustable neutral density filter attenuating the incoming light so the ratio of detected photons to excitation pulses is 1:100 (Harris & Selinger, 1979). Such a ratio will restrict the number of observed photons relative to the number of excitation pulses, in order to assure that a single photon is randomly detected from all those emitted (single photon counting). Thus "pile-up" errors, which can arise as a result of detecting several emission photon events and bias the data to shorter decay times, is prevented (Coates, 1968). The light is then allowed to pass through the quartz cuvette containing sample (housed in a rotating thermostated three-cell holder). Prior to detection, the fluorescent photons proceed through a Glan-Taylor polarizer set at 54.7° degrees to the vertical and a wavelength-adjustable JY H10 emission

monochromator (4 nm bandpass; 0.5 mm slits).

The resultant single photon response detected by a microchannel plate (MCP) photomultiplier tube (PMT) detector is amplified and directed through a constant fraction discriminator to the START input of a time-to-amplitude converter (TAC). This process initiates a linear voltage-time ramp, which is terminated by the electrical pulse (STOP pulse) from the fast photodiode. The electrical STOP pulse is generated at a fixed time precisely correlated with the moment at which the excitation event occurred. The voltage which is reached in the TAC ramp is proportional to the time difference between the START and STOP pulses.

The TAC voltage output from a single photon event is converted to a digital value by the analogue-to-digital converter (ADC) and the "count" is output to a computer-controlled (PC) multichannel analyzer (MCA). The accumulating digitized signals are stored in one of 2048 data channels corresponding to different time points. A typical channel width (typically 10 ps) provides a total range (2048 channels $\times$ 10 ps channel = 20.48 ns) at least three times greater than the longest measured lifetime value, hence the sample decay curve is completely represented. A minimum of 1×10^6 counts are collected for a standard decay curve with 10 000 counts in the peak channel. This number of counts renders statistically significant data (McKinnon et al., 1977) and optimizes the signal-to-noise ratio. The data is transferred from the PC to a faster unix-based computer for data analysis.

The negligible fluorescence from a blank solution containing only aqueous buffer is measured for each particular sample, and the resultant intensity-time profile subtracted from

that of the sample, thus reducing contributions from scattered light (Chang et al., 1985) or small amounts of contaminating fluorophores. The finite width of the laser pulse is overcome by measuring the time-intensity profile of the laser pulse using the Stokes' Raman scattering of pure water at the appropriate wavelength (Willis et al., 1990). Two raman signals (instrument response functions) are measured for each sample; one immediately prior to sample data collection and one directly following blank measurement. The raman signal providing the best statistical fit for the data, representing the instrument response function (IRF), is used for subsequent data analysis. Usually both IRFs give satisfactory fits to the data. Figure 2.4 shows the laser pulse profile and a representative fluorescence decay of a single Trp protein.

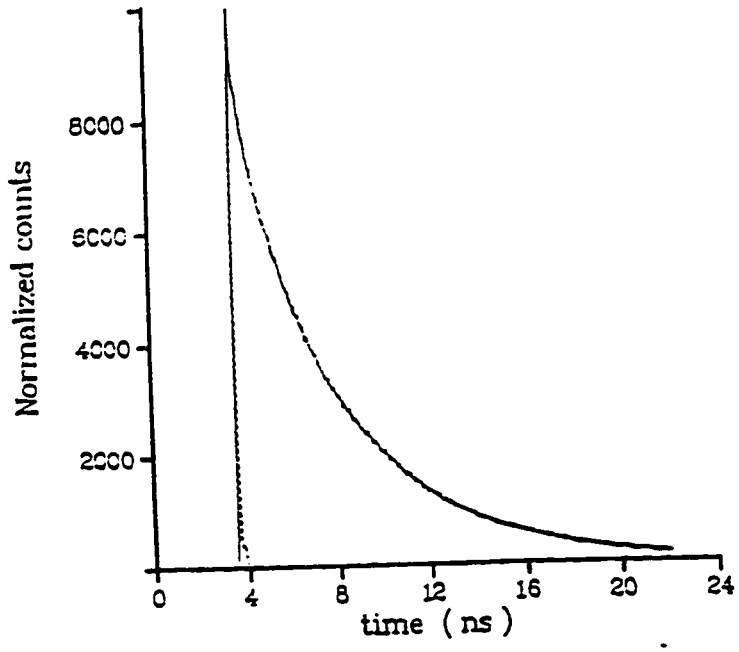

Figure 2.4 Typical fluorescence decay curve from a single Trp protein (solid line) and the instrument response function as measured by the raman scattering of water (dashed line).

2.3.2 Data Analysis & Statistical Parameters

Since the noise associated with this counting procedure is characterized as Poissonian, a number of well-defined statistical parameters can be used to assess the quality of the fitting procedures. The complicated analysis of TCSPC fluorescence data requires the speed and accuracy associated with sophisticated computers, such as the Silicon Graphics Indy (Figure 2.3).

2.3.2.a Fluorescence Decays

If the pulse of light which excites the sample were infinitely narrow and the response of the detection system infinitely fast, the "true" fluorescence decay curve ($F_S(t)$) would be observed (O'Connor & Phillips, 1984). In reality, the observed decay curve ($D_S(t)$) represents a convolution ($\otimes$) of the instrument response function ($D_L(t)$) and the true decay of the sample:

$$D_S(t) = D_L(t) \otimes F_S(t) \tag{2.7}$$

The true decay, $F_S(t)$, can be solved for using the following convolution integral:

$$D_S(t) = \int_0^t D_L(t') F_S(t-t') dt' \tag{2.8}$$

if $D_S(t)$ and $D_L(t)$ are measured with identical instrument distortion. The instrument response function, $D_L(t)$ is measured experimentally as the raman scattering of water and $D_S(t)$ is a measurement of the sample (minus the blank) at each emission wavelength.

The convolution is then solved using non-linear least squares fitting procedures based on the Marquardt (1963) algorithm. This iterative process preferentially weights data points having the most number of counts and yields a trial convolution function, $D_C(t)$:

$$D_C(t) = D_L(t) \otimes F_S'(t) \tag{2.9}$$

where $F_S'(t)$ is a trial function representing the fluorescence decay behaviour of the sample.

The quality of fit between the experimentally measured decay curve, $D_S(t)$ and the mathematically convolved curve, $D_C(t)$, was determined by the minimization of the difference between these curves, which is the weighted sum of squares of residuals (WSSR) between the experimental points ($D_S(t_i)$) and the fitted points ($D_C(t_i)$):

$$WSSR = \sum_{i=1}^{n} \omega_i [D_S(t_i) - D_C(t_i)]^2 \tag{2.10}$$

where n is the number of data points (channels), t_i is the decay time at which the i^{th} interval measurement was made, and ω_i is the weight allocated to the square deviation between the experimental and calculated points in the i^{th} channel. The WSSR value is equivalent to that

of the statistical parameter χ^2 (O'Connor & Phillips, 1984). The greatest weight is given to the points for which the variance of the experimental observation was small such that WSSR is minimized, where the variance is:

$$\omega_i = 1/D_S(t_i) \tag{2.11}$$

Therefore the weighted residual value $r(t_i)$ for all i channels is defined as follows:

$$WSSR = \sum_{i=1}^{n} \left[\frac{[D_S(t_i) - D_C(t_i)]^2}{D_S(t_i)} \right] = \sum_{i=1}^{n} [r(t_i)]^2 \tag{2.12}$$

Three different statistical parameters are used to judge the quality of fit. The first is the residual plot, where residuals from successful fits when plotted against channel number should be randomly distributed about zero, falling in a range of -1 to 1 (reflection of the standard deviation). An example of a residual plot is shown in Figure 2.5. Inspection of this plot for a fit to single, double and triple exponential decay kinetics reveals that this particular decay curve was best fit to a triple exponential function, indicated by the complete randomness of the points about zero. The other two statistical parameters used to evaluate the data are the σ value and the serial variance ratio (SVR).

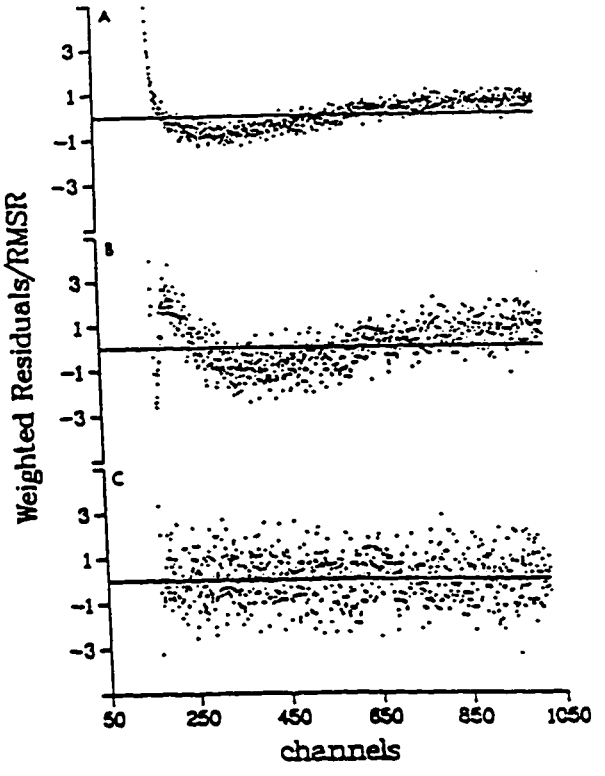

Figure 2.5 Weighted residual plots from the fitting of a decay curve to single, double and triple exponential decay kinetics (from top to bottom).

The σ value is defined as the square root of the reduced chi-square (χ^2_r):

$$\sigma = \left[\frac{\chi^2_r}{n_2 - n_1 + 1 - p} \right]^{1/2} \qquad (2.13)$$

where n_1 and n_2 are the start and end channels, p is the number of variable parameters and χ^2 is the equivalent of the WSSR as previously stated. An optimal fit is indicated when σ is 1, although values between 0.9 and 1.2 are generally accepted when taken in combination with other statistical criteria (Phillips et al., 1985). In our laboratory, a fully random distribution of residuals coincides with a σ value of 1.01 - 1.05.

The serial variance ratio is able to test a series of observations with respect to their independence. The SVR, unlike the σ value, will provide a measure of the correlation between successive residuals (Durbin & Watson, 1951), and hence is an indication of their randomness:

$$SVR = \frac{\sum_{i=n_1+1}^{n_2} [r(t_i) - r(t_{i-1})]^2}{\sum_{i=n_1}^{n_2} [r(t_i)]^2} \times \frac{(n_2 - n_1)}{(n_2 - n_1 - 1)} \qquad (2.14)$$

A good statistical fit of the data corresponds to SVR values between 1.7 and 2.0 (McKinnon et al., 1977). Typically, SVR values of 1.8 to 2.0 were obtained for this work.

A subjective analysis of the weighted residual plots, in combination with the σ and SVR values, provides a stringent method of evaluating the quality of fit. When the physical model is a sum of exponentials terms satisfying such statistical criteria, it is accepted. The addition of another exponential term shows no significant improvement in the statistical fit

and, in fact, is evidence that the data has been "over-fit" (Szabo, 1988). This criteria is essential when fitting exponential decay curves, due to the nature of the analysis: as more exponential terms are added, the statistical fitting parameters will improve marginally with each successive addition.

2.3.2.b Simultaneous Analysis

A simultaneous (global) analysis of multiple fluorescence decay curves serves to increase the accuracy of the time-resolved fluorescence parameters for any given sample (Knutson et al., 1983). A number of decay curves can be generated by exciting the sample at one wavelength and measuring the emission at a series of wavelengths (typically 10-14) spanning the fluorescence spectrum. Provided that the lifetimes remain consistent across all wavelengths, these values can be linked for global analysis effectively decreasing the degrees of freedom and over-determining the fluorescence parameters. As a result, the testing sensitivity of the physical model is increased dramatically. This method proves to be superior to single curve analysis when resolving lifetime values close in magnitude (within a factor of 2) and in estimating the value of small preexponential terms (Knutson et al., 1983). The fractional contribution of each decay component at individual wavelengths can be used to construct a decay associated spectra (section 1.2.2.3) for the individual fluorescent components (Knutson et al., 1982).

2.3.3 Advantages of the TCSPC Instrumentation/Method

The method of single photon detection results in extremely high sensitivity. There are several advantages to the instrumental arrangement described in section 2.3.1. The mode-locked synchronously pumped, cavity dumped dye laser provides an excitation source with high intensity, and high and variable (80 - 4000 kHz) repetition rates (Szabo, 1988) which allow for rapid data collection and measurement of low quantum yield or low optical density samples (Ware et al., 1983). The extremely narrow (10 ps) pulse widths of the excitation source result in pulse stability, optimizing the precision of the measured lifetime values, which are dependent upon both the pulse stability and PMT transit time (O'Connor & Phillips, 1984). The MCP-PMT allows for high precision due to its rapid transit time and negligible wavelength dependent IRFs. The proximity type MCP-PMT is also wavelength-independent, eliminating distortions which could arise from time shifts between the instrument response function and the sample decay curve. The stability of the pulse also eliminates rising edge distortions in the decay curves, and in combination with the wavelength-independent pulse shape (instrument response), allows for the routine analysis of the complete decay curve. The excitation source is completely polarized allowing for the measurement of anisotropy parameters and its wavelength is tunable (275 - 350 nm), providing a suitable range for the excitation of aromatic amino acids, amino acid analogues and other applications. The low (10 Hz) dark count rate of the MCP-PMT produces excellent signal-to-noise ratios.

Experimental Methods

This chapter describes in detail the methods and materials required for protein purification, identification, modification and crystallization. The design and implementation of a novel apparatus for the measurement of time-resolved fluorescence parameters from crystalline proteins will be presented.

3.1 Protein Isolation & Identification

Time-resolved fluorescence has proven to be a highly sensitive method for monitoring spectroscopic parameters in proteins. *In vivo* concentrations in the nM - μM range are often more than sufficient for an adequate fluorescence signal. However, this also means that even trace amounts of fluorescent contaminants will contribute to a spectrum or decay curve. For this reason, high performance liquid chromatography (HPLC, Gilson, Mandel Scientific Co., Rockwood, ON) was the ultimate purification step utilized for all proteins studied. In order to assure that the collected fraction was homogeneous, a small sample of the pooled HPLC fractions was reanalyzed by HPLC. The purity and identity of the protein was subsequently evaluated by nebulization-assisted electro-spray ionization (ESI) mass spectrometry (API III quadrupole. Sciex, Mississauga, ON) using protein (approximately 0.5 mg/mL) in acetic acid/water (10% V/V).

3.1.1 The Neurotoxins

The crude venoms of *Lacticauda semifasciata, Naja naja kouathia* and *Bungarus multicinctus* (Sigma Chemical Co., St. Louis, MO, USA) were treated by batch separation using Whatman pre-swollen CM-52 carboxymethyl (CM) cellulose cation exchange resin (Mandel Scientific Co., Rockwood, ON) which had been pre-equilibrated with NaAc (10 mM; pH 6.5; BDH Chemicals Ltd., Toronto, ON). The CM-cellulose was stirred for one hour at 4°C with a mixture of the crude venom dissolved in NaAc (10 mM , pH 6.5). The resin was filtered *in vacuo* and the adsorbed material was extracted from the resin using NaCl (190 mM), in NaAc (10 mM ; pH 6.5). The mixture was lyophilized to near dryness and dialysed against NaAc (10 mM; pH 6.5) in preparation for HPLC separation. All three toxins were purified by HPLC on a TSK CM-5PW column (Supelco Canada, Oakville, ON) using NaAc (10 mM ; pH 6.5) with a salt gradient. α-Bungarotoxin (Figure 3.1), α-cobratoxin (Figure 3.2) and erabutoxin b (Figure 3.3) eluted at 0.06 M, 0.16 M and 0.02 M concentrations of NaCl (BDH Chemicals Ltd., Toronto, ON), respectively. Only a portion of the HPLC peak, corresponding to the highest absorbance, was collected in order to ensure the highest purity. ESI mass spectrometry was used to confirm protein purity and identity.

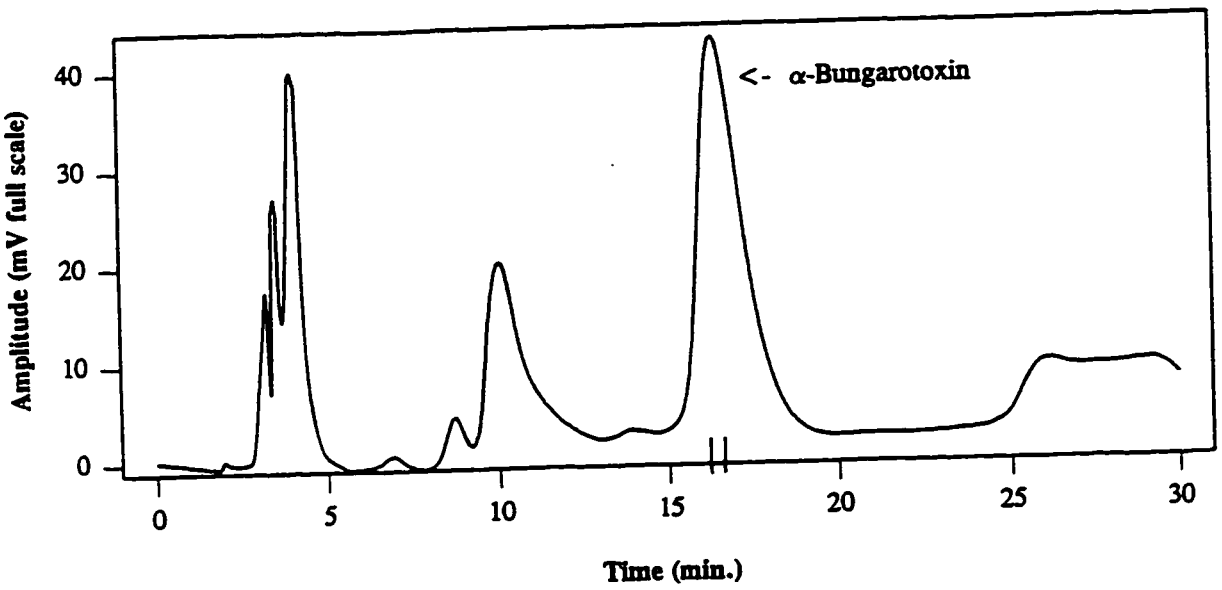

Figure 3.1 HPLC profile of CM batch-treated venom from *Bungarus multicinctus*. The collected fraction is indicated by the arrow, label and vertical boundary lines. Buffer A: 10 mM NaAc pH 6.5; Buffer B: Buffer A + 0.1 M NaCl; Gradient: 0 - 2 min (55 % B) 2 - 20 min (55 - 100 % B) 20 - 25 min (100 % B)
λ_{max} = 280 nm

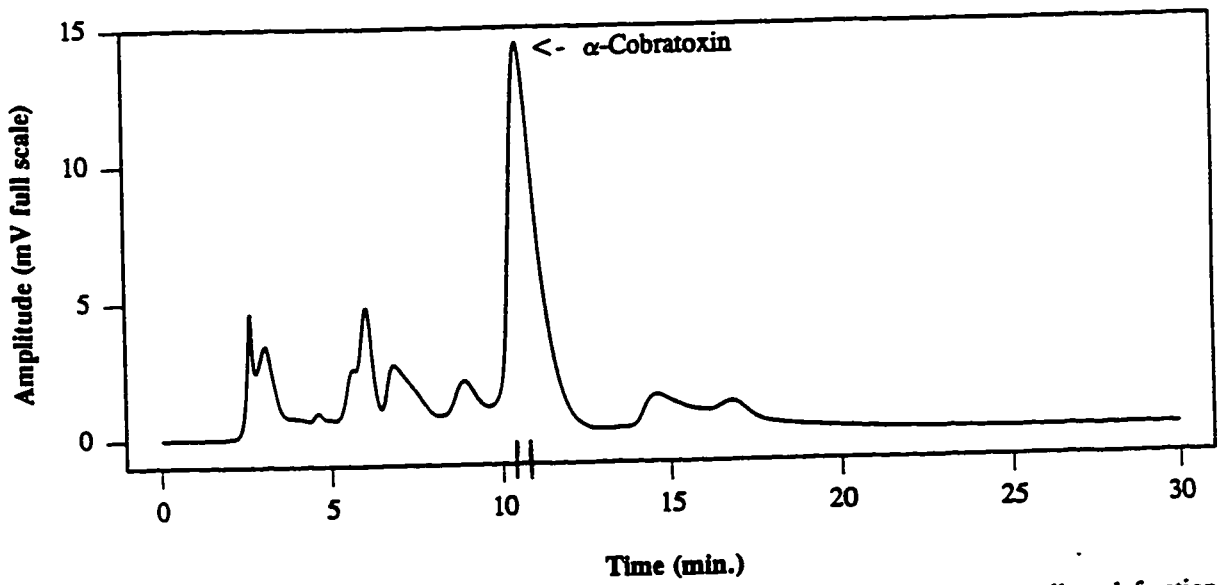

Figure 3.2 HPLC profile of CM batch-treated venom from *Naja naja siamensis*. The collected fraction is indicated by the arrow, label and vertical boundary lines. Buffer A: 10 mM NaAc pH 6.5; Buffer B: Buffer A + 0.19 M NaCl; Gradient: 0 - 2 min (50 % B) 2 - 20 min (50 - 80 % B) 20 - 25 min (80 - 100 % B)
λ_{max}=280 nm

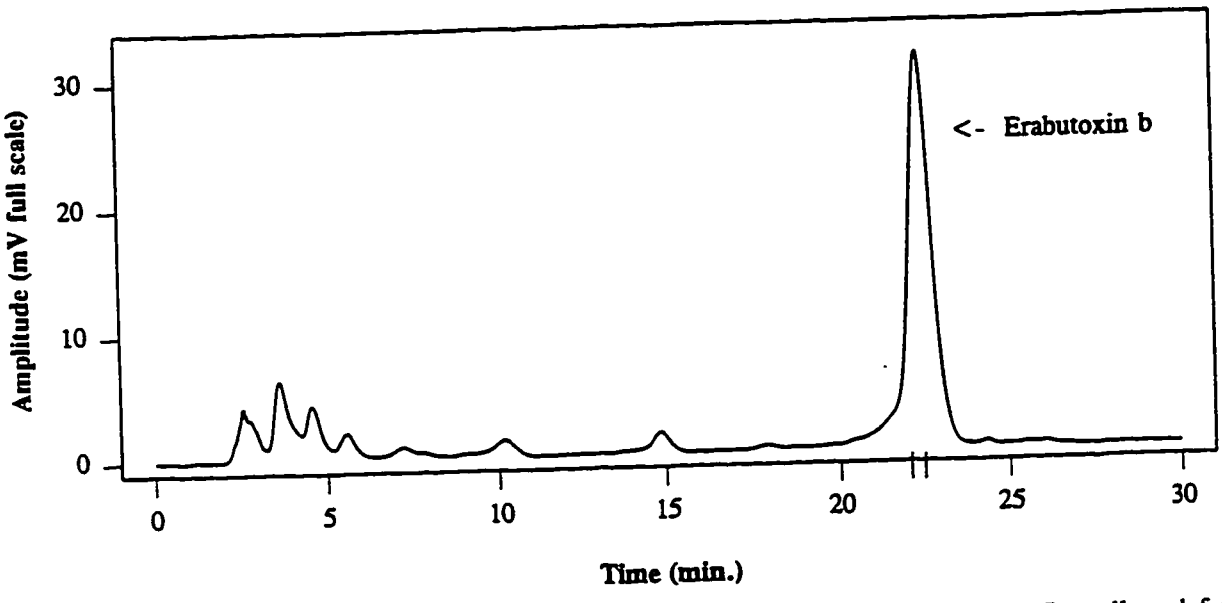

Figure 3.3 HPLC profile of CM batch-treated venom from *Lacticauda semifasciata*. The collected fraction is indicated by the arrow, label and vertical boundary lines. Buffer A: 10 mM NaAc pH 6.5; Buffer B: Buffer A + 0.19 M NaCl; Gradient: 0 - 2 min (0 % B) 2 - 20 min (0 - 15 % B) 20 - 25 min (15 - 100 % B) λ_{max}=280 nm

3.1.2 Enoyl-CoA Hydratase (Crotonase)

In order to produce adequate amounts of protein required for crystallization trials, crotonase from rat liver mitochondria was cloned and overexpressed in *E. coli*.

3.1.2.a Cloning & Overexpression

A cDNA plasmid for rat mitochondrial enoyl-Coenzyme A (CoA) hydratase (EC 4.2.1.17) was a kind gift from Prof. Osumi (HIT, Hyogo, Japan). The clone was PCR primed and ligated into pET20b(+) plasmid (Tonge, personal communication). The gene

was overexpressed in E. coli using Inositol phosphate triglyceride (IPTG; Sigma Chemical Co., St. Louis, MO) as the inducer. Growth plates were prepared by adding ampicillin (AMP; Sigma Chemical Co., St. Louis, MO) to an autoclaved mixture of Luria-Bertani (LB) broth and agarose (Gibco, BRL, Mississauga, ON) and pouring this mixture into sterile petri dishes. A one litre (L) solution of LB broth consists of bacto yeast extract (5 g; Gibco, BRL), bactotryptone (10 g; Gibco, BRL, Mississauga, ON), and NaCl (10 g), at pH 7. A sterile toothpick was used to scrape the top of a glycerol stab gel and streak the plates. The plates were left to grow overnight at 37 °C. An isolated colony of *E. coli* was chosen from one of the plates using a sterile toothpick and was added to a sterile culture tube containing LB/AMP (5 mL). The culture tube was left to shake overnight at 37 °C. The OD_{600} was monitored as an indication of bacterial growth and was found to be optimally > 2.0 at this stage. The bacterial broth (5 mL) was added to LB/AMP (1 L) in a baffle flask (4 L) and was left to shake for four hours at 37 °C. Although an OD_{600} of 0.7 is generally indicative of mid-log phase, the best yields were obtained from solutions which reached an OD_{600} > 2.0. The cells were centrifuged at 3000 r.p.m. for ten minutes and the supernatent discarded. Fresh LB/AMP (100 mL) was used to resuspend the pellet and this mixture was added back to the baffle flask. IPTG (10 mL; 0.1 M) was added to the flask to induce crotonase expression, and the mixture was left to shake for 3 hours at 37 °C. The cells were centrifuged at 6000 r.p.m. for 20 minutes and the supernatent discarded. Following centrifugation, the cells were resuspended in potassium phosphate (10 mL; 20 mM; BDH Chemicals Ltd., Toronto, ON), ethylene diamine tetraacetic acid (EDTA; 3 mM; BDH

Chemicals Ltd., Toronto, ON) pH 7.4 (buffer A). The cells were disrupted using a french press, and the cell debris pelleted by centrifuging the resultant mixture at 17000 r.p.m. for 1/2 hour (5 °C). The supernatent was subsequently dialysed overnight against buffer A with 1 mM dithiothreitol (DTT; Sigma Chemical Co., St. Louis, MO). A sepharose-CoA affinity column was prepared by conjugating CoA (Sigma Chemical Co., St. Louis, MO) onto a sepharose gel: a slurry of epoxyactivated sepharose 6B (Pharmacia Canada Ltd., Dorval, PQ) was reacted with a 2-fold excess of CoA. The dialysate was passed over the sepharose-CoA affinity column, which had been pre-equilibrated with buffer A, and the crotonase subsequently eluted with buffer A containing 0.2M KCl (BDH Chemicals Ltd., Toronto, ON). Each column fraction was assayed for activity. The enzyme was crystallized using ethanol (Steinman & Hill, 1975; Stern et al., 1956) and stored as a precipitate at -20 °C.

3.1.2.b Ultrapurification and Identification

Protein purity was evaluated by HPLC using a DEAE-5PW column (Supelco Canada, Oakville, ON). A single peak appeared when the protein was eluted with buffer A and a 0 - 0.2 M KCl gradient (Figure 3.4). The enzyme was identified by gene sequencing, N-terminal sequencing and ESI mass spectrometry (Tonge et al., in preparation).

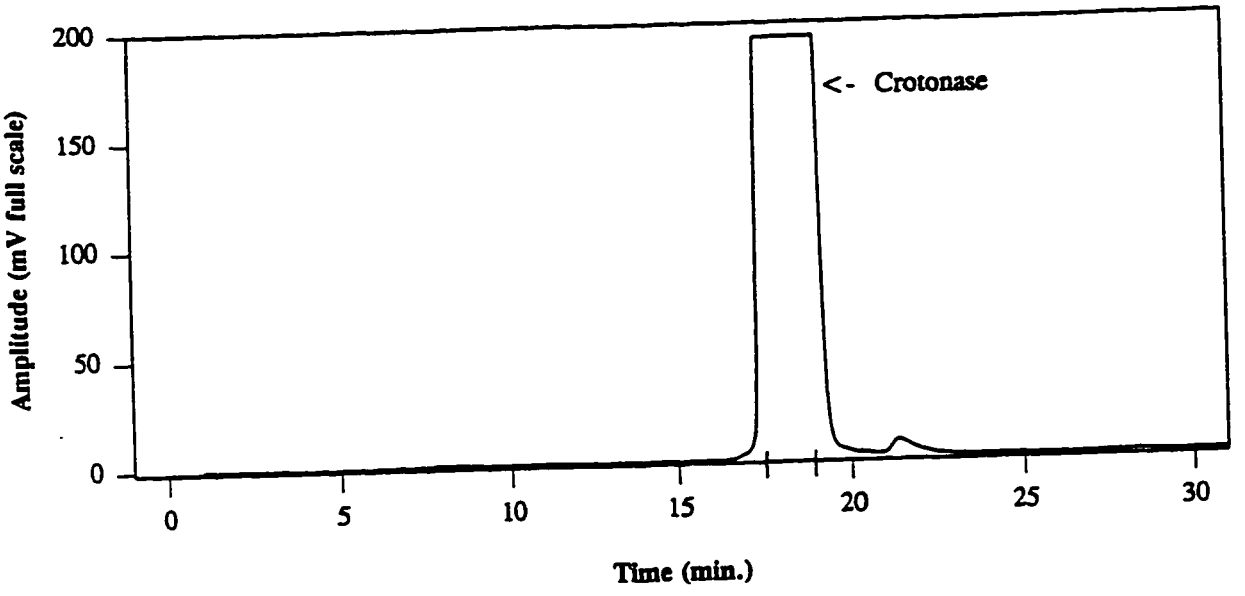

Figure 3.4 HPLC profile of affinity-treated expressed crotonase from *E. coli*. The collected fraction is indicated by the arrow, label and vertical boundary lines. Buffer A: 10 mM KH_2PO_4 pH 6.0; Buffer B: Buffer A + 0.5 M KCl; Gradient: 0 - 10 min (0 % B) 10 - 25 min (0 - 100 % B) 25 - 30 min (100 % B) λ_{max}=280 nm

3.1.2.c Enzyme Activity Assay

The direct spectrophotometric method (280 nm) was used to quantitatively assay crotonase (Steinman & Hill, 1975; Stern et al., 1956), omitting ovalbumin from the assay mixture. This method is based on the characteristic UV absorption of enoyl-CoA hydratase coenzyme A (crotonyl CoA; A) which is abolished upon the hydration of the α,β-unsaturated system:

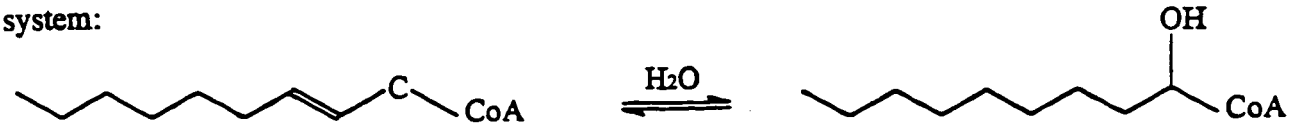

A B

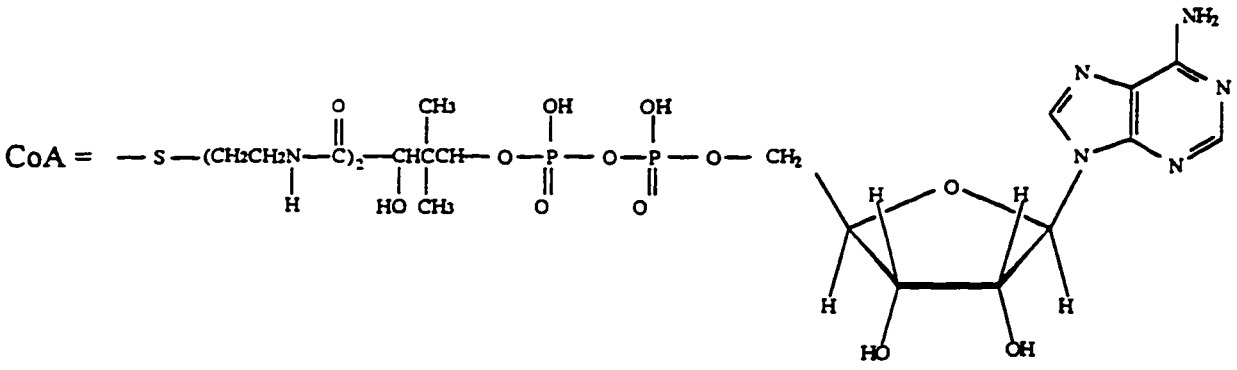

Typically, the spectrophotometer was zeroed using a cuvette with buffer A (950 μL). To the cuvette, crotonyl-CoA (25 μL) was added followed by column eluate (25 μL; diluted if necessary) with fast mixing. The OD_{280} was monitored over time and a slope calculated to give a reading in min^{-1}. The reading was then corrected for any dilution factors to give crotonase activity.

3.1.3 Azurin

Holoazurin was purified from acetone-dried cells of *Pseudomonas fluorescens* (*Pfl*; ATCC 13525) according to previous reports (Ambler & Wynn, 1973; Hutnik & Szabo, 1989a). Ammonium acetate and ammonium sulphate were purchased from BDH Chemicals Ltd., Toronto, ON. TRIS Acetate (Tris[hydroxymethyl] aminomethane acetate) was acquired from SIGMA Chemical Co. (St. Louis, MO), and Centricon-10 (10 000 MW cut off) microconcentrators were acquired from Amicon Inc. (Beverly, MA). The modified purification procedure described by Hutnik and Szabo (1989a) was generally followed, excluding the ammonium sulphate precipitation, gel filtration and CM-52 concentrating step.

A CM-5PW HPLC method, based on the original CM chromatographic step 7 was developed (Figure 3.5). Each HPLC fraction was analyzed by ESI mass spectrometry.

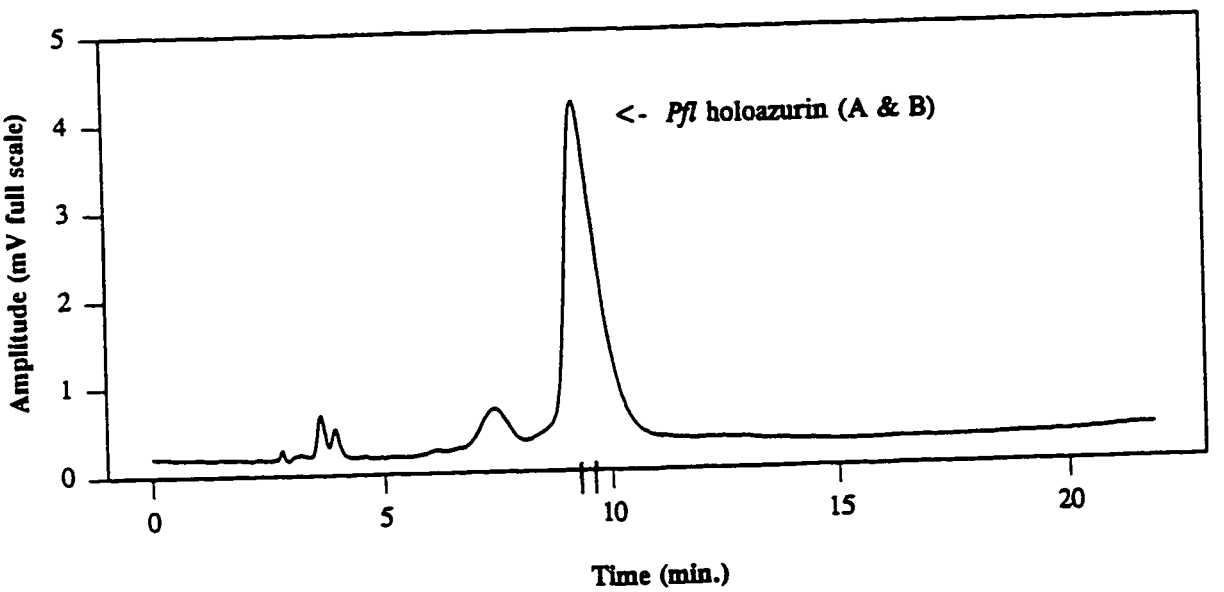

Figure 3.5 HPLC profile of CM-treated extract from *Pseudomonas fluorescens*. The collected fraction is indicated by the arrow, label and vertical boundary lines. Buffer A: 10 mM NaAc pH 4.0; Buffer B: Buffer A + 0.19 M NaCl; Gradient: 0 - 2 min (30 % B) 2 - 20 min (30 - 45 % B) 20 - 25 min (45 % B) λ_{max}=280 nm

Copper-free (apo) protein was obtained using the modified KCN dialysis method as described elsewhere (Hutnik & Szabo, 1989a). The complete absence of an absorption band, which peaked at approximately 625 nm, was used to verify successful removal of the Cu^{2+}. The preparation of apoazurin was carried out in a fume hood (as a safety precaution) due to the production of HCN.

3.2 Protein Modification

Several methods were employed to facilitate protein denaturation for the structural investigations presented in Chapter 4. The neurotoxins were denatured using either guanidinium hydrochloride (GuHCl) or by cleavage of the disulphide bonds via reduction and (amido)carboxymethylation (CM or ACM). The identity of the CM and ACM modified toxins was determined by ESI mass spectrometry as previously described.

3.2.1 GuHCl Denaturation

Solid GuHCl (Sequinal grade; Pierce Chemical Co.,) was added to HPLC pure blank solutions and those containing neurotoxin. The final volume of solution was measured and GuHCl concentration calculated.

3.2.2 Reduction & Carboxymethylation

Carboxymethylated (CM) material was prepared by dissolving 1 mg of toxin in 1 mL of 8 M urea (BDH Chemicals Ltd., Toronto, ON), 1 mM TRIS pH 9.3 (Buffer A). The vessel was flushed with N_2 and the reaction was left to stir for one hour. To this solution,

0.25 mL of 100 mM 2,3-dihydroxy-1,4-dithiobutane (dithioerythritol; Sigma Chemical Co., St. Louis, MO) in buffer A was added. Again the vessel was flushed with N_2 and the reaction left to stir. After three hours, a three fold excess (with respect to the number of SH groups) of iodoacetic acid (Sigma Chemical Co., St. Louis, MO) in Buffer A was added, the vessel was flushed with N_2 and the reaction stirred for ten minutes in the dark. Absence of free SH was detected using 5,5'-dithiobis[2-nitrobenzoic acid] (DTNB; BDH Chemicals Ltd., Toronto, ON) as indicated by a colourmetric reaction. The mixtures were dialysed against MQ water, lyophilized and repurified by DEAE-5PW HPLC (isocratic elution: 10 mM NaAc pH 6.5 with 99 mM NaCl).

3.2.3 Reduction and Amidocarboxymethylation

The amidocarboxymethylated (ACM) material was prepared, as above, by substituting iodoacetamide (Sigma Chemical Co., St. Louis, MO) for iodoacetic acid. Since the pI of the protein is not altered by amidocarboxymethylation, the modified toxins could be purified in the same manner as the native toxins (see section 3.1.1).

3.3 Protein Crystallization

All proteins were crystallized by vapour diffusion using the hanging droplet method. A small droplet (2 - 6 μL) of precipitant is added to the same volume of concentrated

protein, in an appropriate buffer system on a siliconized microscope slide (Prosil-28, microscope slides (glass and plastic); Hampton Research, Riverside, CA). The microscope slide is inverted and sealed with silicon grease over one well of a Lindbro crystallization plate (Hampton Research, Riverside, CA) containing precipitant. The droplets are left to sit at an appropriate temperature until crystallization occurs.

3.3.1 Erabutoxin b

Crystals of erabutoxin b were grown (at RT) from aqueous protein (~ 26 mg/mL) pH ~ 5 mixed 1:1 with ammonium sulphate (1.4 - 1.48 M), similar to published procedures (Tsernoglou & Petsko, 1976).

3.3.2 Crotonase

Crotonase crystals were grown overnight by vapour diffusion with equal volumes (5 μL) of crotonase (5.9 mg/mL) and EtOH (15-22% V/V) in sodium potassium phosphate (0.1M; pH 7.5) as the reservoir solution.

3.3.3 Azurins

Pfl holoazurin crystals were grown by the hanging droplet method using equal volumes of HPLC peak # 2 (Figure 3.5) with ammonium sulphate (2.9 - 3.0 M) in Tris buffer (200 mM; pH 7.5), according to published procedures (Zhu et al., 1994). A higher protein concentration (8.2 mg/mL) was required to grow crystals from the HPLC-pure material compared to crystals prepared without this final step.

Apoazurin crystals (0.1 mm × 0.03 mm × 0.03 mm) were grown under identical vapour diffusion conditions as the holo protein using a protein concentration of 9.2 - 10.0 mg/mL.

3.4 Solution Studies

In order to establish a relationship between protein secondary structure and fluorescence parameters, proteins were measured in dilute solution by CD and fluorescence. The results of these experiments are presented in Chapter 4.

3.4.1 Circular Dichroism

CD measurements were taken from solutions in quartz spectropolarimeter cells (0.1

mm ; circular) at 20°C. The instrument was calibrated with aqueous d-10-camphorsulfonic acid. In order to eliminate absorbance from acetate at lower wavelengths, both the HPLC pure protein and HPLC blank (collected from a blank HPLC run at the time in the gradient when protein would be expected to elute) were desalted on a Sephadex G-25 gel filtration column (Mandel Scientific Co., Rockwood, Ontario, Canada; void volume = 0.8 mL) using sodium potassium phosphate (1 mM; pH 6.5) as eluent. Protein concentration was determined from the absorbance at 280 nm using an extinction coefficient of 7953 M^{-1} cm^{-1} for α-bungarotoxin and 6766 $M^{-1}cm^{-1}$ for α-cobratoxin and erabutoxin.

3.4.2 Fluorescence Spectroscopy

Steady-state and time-resolved fluorescence measurements were made using the same samples in 1 mM PBS pH 6.5 which had been measured by CD. The CD and fluorescence data for a single sample was collected during the same day in order to ensure experimental consistency. The fluorescence measurements of protein samples in solution reported in Chapter 5 were collected from protein samples directly eluted from the HPLC. An HPLC fraction from a blank run (described above) was used as the fluorescence blank.

3.5 Crystal Studies

The measurement of protein crystals by fluorescence involved special considerations due to the small size and fragile nature of the crystalline material. Since the crystals contain such a small amount of buffer solution, there was no need to measure a buffer blank.

3.5.1 Steady State Fluorescence

The large rectangular shaped crystals of the myoglobins used in previous studies (Willis et al., 1991) allowed for steady state fluorescence measurements to be made in the SLM 8000 fluorometer. This was accomplished by aligning several crystals side by side in a front-face cell (Eisinger & Flores, 1979). The crystals used in this study were either too small and fragile for such a manipulation or alignment was not possible due to the crystal's shape.

The steady-state fluorescence of the protein crystals used in this study was measured using the time-resolved instrument in the following manner: the fluorescence intensity, at a series of emission wavelengths, was determined by integration of the fluorescence decay curve over a fixed time period. The intensity was subsequently corrected for instrument response using N-acetyl tryptophan amide as a fluorescence standard measured both on the time-resolved instrument and the SLM 8000 (corrected).

3.5.2 Time-Resolved Fluorescence Spectroscopy

Single crystals, washed with protein-free mother liquor, were placed centrally on the inside front face of a long-necked round CD cell (width = 2 mm, diameter = 2 cm) containing protein-free mother liquor (50 μl), providing solvent humidity. Any liquid directly in contact with the crystal was removed using thin absorbent strips. The cell was sealed with parafilm and mounted on a device consisting of a goniometer attached to an x, y, z translation stage (Figure 3.7), where the front face of the cell was perpendicular to the goniometer rotational axis. The apparatus was designed such that the crystal, when placed in the centre of the cell, would be in the axis of rotation of the goniometer. The cell clamp with plastic screw ensured that the crystal position could be maintained during cell removal and subsequent replacement. The rod attached to the cell clamp was made of sufficient length to assure that both the goniometer and goniometer rod would not interfere with either the excitation beam or subsequent crystal fluorescence, which would produce unwanted scattered light during data collection.

The crystal was first aligned with the laser beam by eye using the x, y, z translations until a spot of fluorescent marker, placed on the outside of the cell directly above the crystal, was illuminated. The fluorescent marker was carefully washed from the outside of the cell using spectral grade methanol (3×). The signal was subsequently optimized by monitoring the total fluorescent counts per second while adjusting the crystal position in the x, y, and z direction.

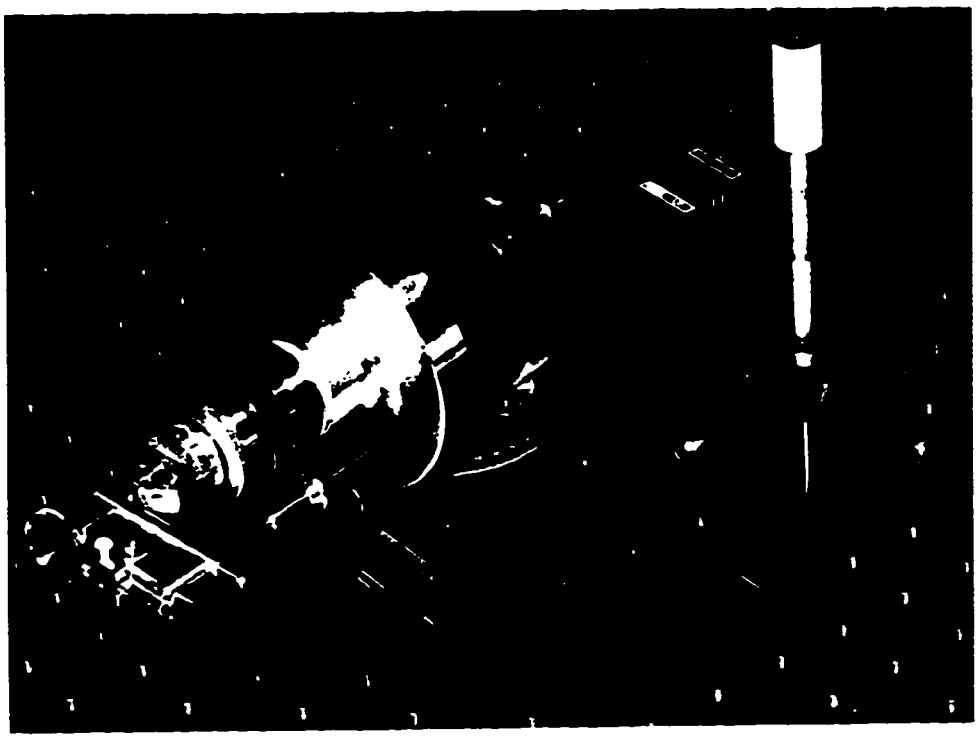

Figure 3.6 Photograph of the apparatus utilized for time-resolved fluorescence measurements of single protein crystals. A 1 mm CD cell is mounted on a device consisting of a goniometer head attached to an x, y, z translation stage.

The excitation beam was incident on the cell at an angle of 35° to the normal of the cell face, in order to prevent specularly reflected light from entering the detection optics.

3.5.3 Orientation Experiments

Orientation experiments were performed by rotating the crystal with respect to the plane of excitation polarization, and the fluorescence decay behaviour was measured at 10° rotation intervals. After several data sets were collected for the same crystal, the sample was returned to the original orientation and the fluorescence decay parameters were remeasured in order to assess crystal photodamage. If the parameters were different from those originally measured, then the data sets which were obtained between the previous reproducible data set and the non-reproducible data set were discarded.

3.5.4 Phosphorescence

Steady-state measurements were collected according to section 3.5.1 with the following exception: since the steady-state phosphorescence data was to be analyzed and assessed in a qualitative capacity, no corrections were made to the curves.

PART III: Secondary Structure & Fluorescence

Probing Local Secondary Structure of Proteins

This chapter explores the relationship between the relative concentration ("c") values, derived from the fluorescence pre-exponential terms, and protein secondary structural features. Such a study enables the evaluation of the predictive capabilities for this fluorescence parameter.

4.1 Introduction

Following denaturation many proteins are able to refold to their original structure or other organized structures under suitable conditions, implying that the amino acid sequence provides the necessary information which determines the protein's secondary and tertiary structure. The relationship between the amino acid sequence and protein folding must be understood for the rational design of novel proteins. One problem in protein folding is the determination whether local areas of a protein have the propensity to act as initiators of global folding. The ability to monitor structural changes at a local site on a protein is often desirable when studying protein folding/unfolding. NMR and CD have been used routinely to determine the structure of peptide fragments which represent local areas of a protein, however, these methods can be challenged by the low levels of structure. Furthermore, the ability to measure the structural details at a specific site of a protein (in solution) is not

possible by CD, since this spectroscopic method only provides a global average of the protein secondary structure. NMR using the main NOE parameters can give localized structural information, but such determinations are difficult. The time-resolved fluorescence decay parameters of Trp offer the potential to directly report structural information from a local site (where the Trp residue is located) in a protein at *in vivo* concentrations.

Although Trp fluorescence has the potential to probe the structure of its surrounding environment, data to support this relationship has not been clearly established. This has lead to an effort to correlate protein structural features with measurable fluorescence parameters. Time-resolved fluorescence studies of PTH had suggested that there was a relationship between fluorescent Trp "c" values and local secondary structure (Willis & Szabo, 1992). This idea was further explored by Willis et al. (1994) using single Trp model peptides known to exhibit helical character. Recall from Chapter 1, that often single Trp proteins display triple exponential decay kinetics in solution and it has been proposed that these three lifetime values originate from three distinct conformations of the Trp side chain. Both the fluorescence parameters and CD values were recorded with varying degrees of peptide denaturation facilitated by subsequent additions of GuHCl. These studies showed the relative contributions of the three decay time components were directly proportional to the α-helix content. It was proposed that the decay time values were associated with different ground-state χ_1 rotamers of the Trp side chain and the observed changes in the relative proportions of the decay time components were the result of main chain conformational constraints on the χ_1 rotamer populations.

The three neurotoxins, erabutoxin b, α-cobratoxin and α-bungarotoxin are composed primarily of β-sheet, β-turn and random coil secondary structure as determined by CD, NMR and X-ray crystallography (Low et al., 1976; Tsernoglou and Petsko, 1976; Bernstein et al., 1977; Inagaki et al., 1980; Ménez et al., 1980; Walkinshaw et al., 1980; Hider et al., 1982; Inagaki et al., 1985; Love and Stroud, 1986; LeGoas et al., 1992). Erabutoxin b is classified as a short chain neurotoxin and displays a higher β-sheet content than the two "long chain" neurotoxins (α-cobratoxin and α-bungarotoxin). There is significant homology between the tertiary structures of the short and long chain neurotoxins. The additional amino acids found in the long chain neurotoxins are located in the N-terminal random coil tail. The invariant Trp residue, which has been found necessary for interactions with the acetylcholine receptor, is located in the centre of an antiparallel β-sheet in all three neurotoxins. These neurotoxins are defined by a simple β-sheet secondary structure which is maintained through a minimum of four disulphide linkages located at one end of the molecule (Figure 1a, 1b). The Trp can be considered completely solvent exposed.

A preliminary study of these neurotoxins had revealed that the relative proportions for the fluorescence decay times were distinct from those observed for Trp in an α-helix and random coil (Dahms et al., 1992). Since by definition these neurotoxins exhibit no true tertiary structure (Figure 1a, 1b; Bernstein et al., 1977; Smith et al., 1988), it was suggested that the "c" parameters (obtained by fluorescence) were indicative of Trp within a solvent exposed β-sheet secondary structure. If this were the case, the denatured neurotoxins should display relative decay time proportions similar to those observed for Trp in a random coil.

Model β-sheet peptides have been designed, but none contain a Trp residue and production of such peptides require considerable resources and synthetic peptide strategies. The commercial availability of the snake venoms and the ease of toxin isolation made these proteins excellent candidates for fluorescence studies on β-sheet structures. The complete results on the structural correlation for these three neurotoxins are presented. The effect of unfolding experiments (GuHCl) and disulphide modification on the fluorescence parameters of a Trp residue located within the β-sheet of erabutoxin b, α-cobratoxin and α-bungarotoxin will be discussed.

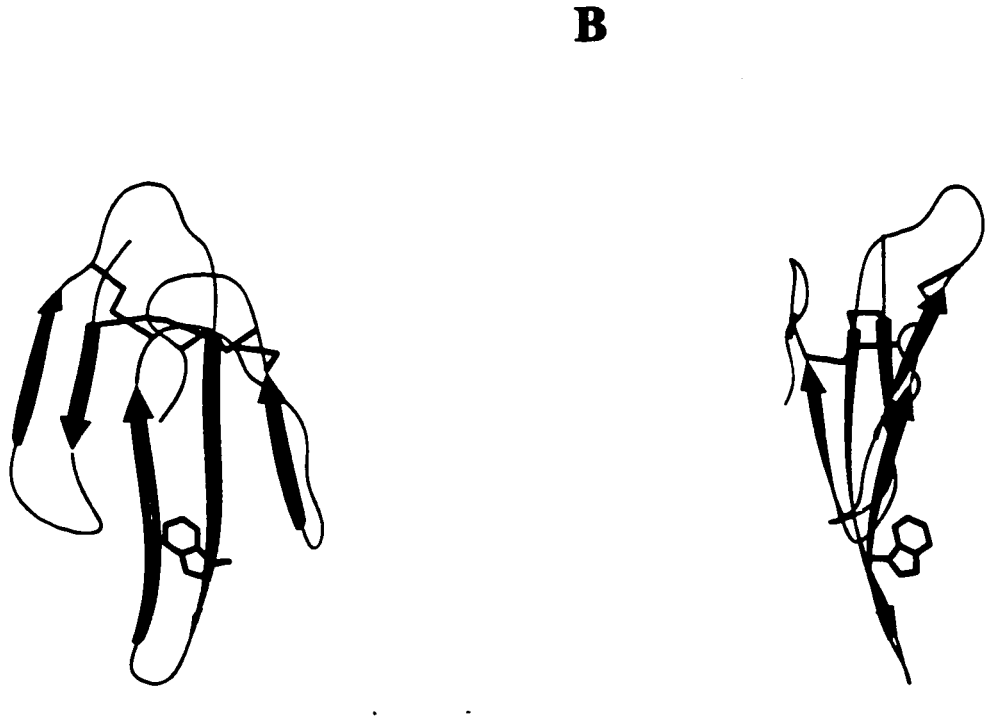

Figure 4.1 Setor representation of erabutoxin b (3ebx.pdb; Bernstein et al., 1977). A) "Front face" view B) "Side" view. (backbone = gold; disulphides = yellow; trp = purple; ribbon = β-sheet; rope = random coil)

4.2 The Neurotoxins

4.2.1 Evaluation of Protein Identity and Purity

Reanalysis of the pooled HPLC fractions (see Chapter 3) of each neurotoxin showed a single peak by HPLC indicating >99.9% purity (data not shown). ESI mass spectrometry was used to establish both the identity and purity of the native and modified toxins. The observed molecular weights for the HPLC-purified toxins were in good agreement ($\leq$ 0.03 % difference ($\pm$ 1.5 g/mol)) with the calculated molecular weights (Table 4.1), as determined by the protein sequence.

Table 4.1 ESI mass spectral analysis of HPLC purified toxins and carboxymethylated toxins.

ID	Calculated$_{MM}$§ (g/mol)	ESIMS$_{MM}$ (Daltons)	Standard Deviation	% Difference
Ebtx b‡	6860.8	6860.1	0.2	0.01
α-CoTx‡	7821.1	7821.0	0.8	0.001
α-BuTx‡	7984.3	7984.9	0.1	0.007
Ebtx b CM*	7334.9	7333.6	0.3	0.02
α-CoTx CM*	8413.7	8412.4	1.0	0.02
α-BuTx CM*	8576.9	8575.0	1.0	0.02
Ebtx b ACM†	7325.0	7323.1	0.7	0.02
α-CoTx ACM†	8402.6	8400.1	1.2	0.03
α-BuTx ACM†	8564.2	8562.3	0.8	0.02

‡Native toxins: erabutoxin b (Ebtx b), α-cobratoxin (α-CoTx), α-bungarotoxin (α-Butx). *Toxins treated by reduction and carboxymethylation. †Toxins treated by reduction and amidocarboxymethylation. §Isotope average calculated molecular mass.

Each ESI mass spectrum (see Figure 4.2) represented only one species providing further evidence that the proteins were homogeneous.

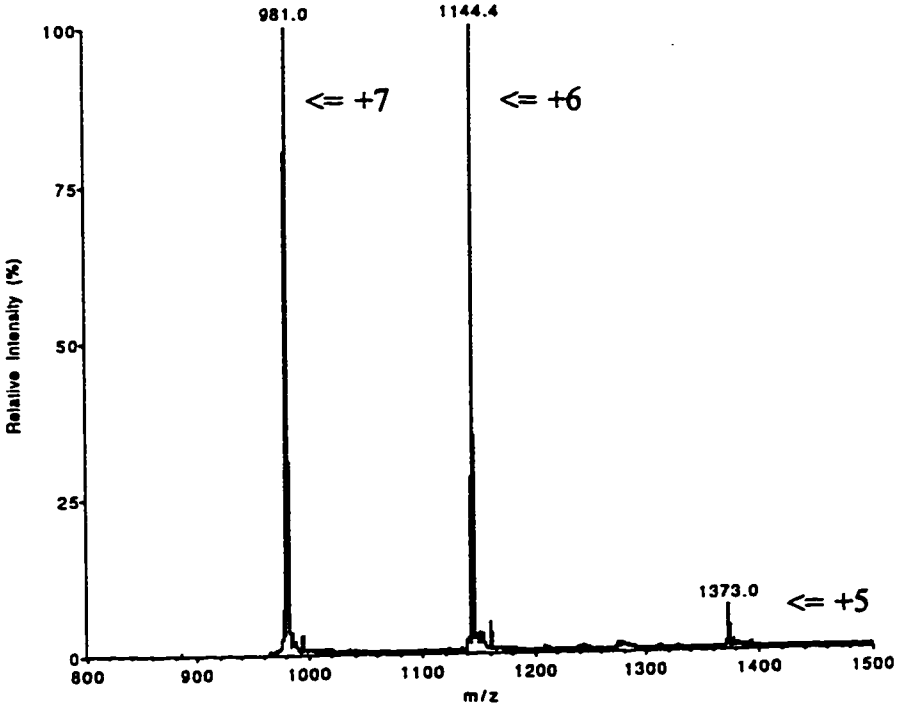

Figure 4.2 ESI mass spectral analysis of HPLC purified erabutoxin b. The spectral trace is indicative of the data obtained for all the proteins cited in this work.

4.2.2 Circular Dichroism

The CD spectra of each neurotoxin at μM concentrations indicated a high β-sheet content (represented in Figure 4.3 dash-dot-dash line). Erabutoxin b displayed the greatest

amount of β-sheet spectral characteristics, as predicted from the crystal structures (Walkinshaw et al., 1980; Love and Stroud, 1986; Basus et al., 1988). The native toxins treated with 6 M GuHCl (Figure 4.3 solid line), and the CM or ACM toxins, displayed CD spectral features consistent with random coil secondary structure. The β-sheet CD spectral features were fully recovered upon dialysis of the GuHCl- treated native toxins, indicating complete refolding of the proteins (Figure 4.3 dash-dot-dash line). The CD spectral maxima at 202 nm and 228 nm (Figure 4.3) are indicative of β-sheet secondary structure. The spectral maxima at 228.6 nm was chosen as a measurement of β-sheet content as the larger maxima at 200 nm was obscured by the absorption of GuHCl.

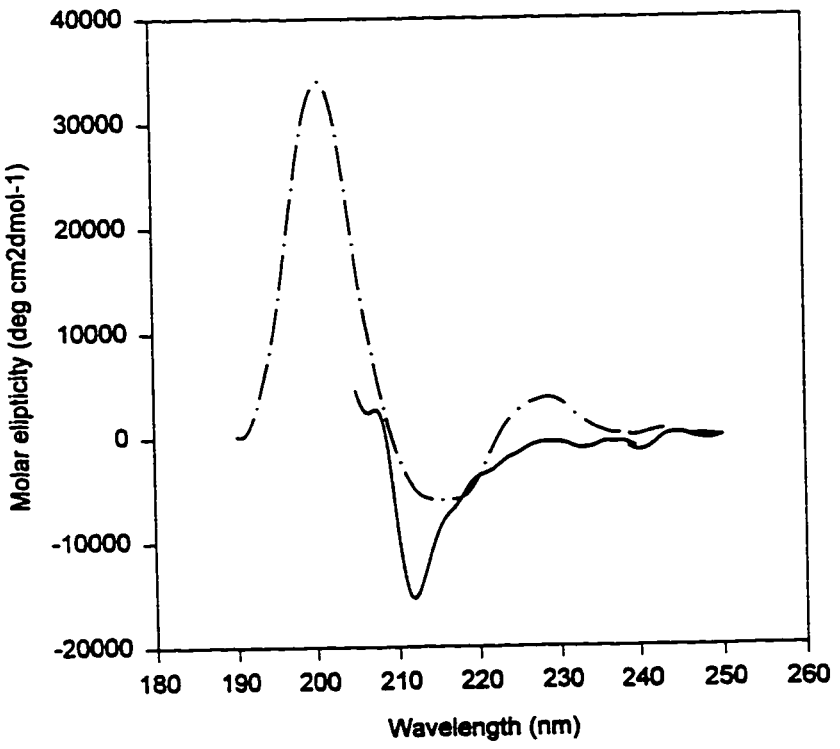

Figure 4.3 Far-uv CD spectrum of native or refolded erabutoxin b (1mM phosphate pH 6.5) —— · —— and denatured erabutoxin b (1mM phosphate pH 6.5 with 6M GuHCl) ———— ·

Several different methods were used to denature the toxins. GuHCl was initially used to titrate the protein with different molar concentrations of the denaturant. Previous studies (Willis and Szabo, 1992) have shown that GuHCl has a negligible effect on the fluorescence parameters of the model compound NATA. Since the toxins are small proteins, the four (erabutoxin b) or five disulphide linkages seem to be very important in maintaining structural integrity. Therefore, two other methods of denaturation were examined: reduction and (amido)carboxymethylation of the disulphide linkages. Carboxymethylation has the advantage of adding only a small group to the protein but results in the addition of eight (or ten) negative charges. For this reason reduction/amidocarboxymethylation was also utilized, allowing the protein to maintain its native pI.

4.2.3 Fluorescence & the Trp Environment

Steady-state and time-resolved fluorescence values for erabutoxin b, α-cobratoxin and α-bungarotoxin are summarized in Tables 4.2, 4.3, and 4.4, respectively. The steady state λ_{max} for each of the neurotoxins becomes progressively longer with successive additions of GuHCl and is furthest red-shifted for the CM and ACM toxins. This trend is consistent with an increasingly solvent exposed Trp and is expected with loss of secondary structure.

As discussed in Chapter 1, it is possible to obtain a decay-associated spectra (DAS) by combining the steady state and time-resolved fluorescence data (Figure 4.4). Assuming 1) that the decay kinetics arise from ground-state conformational heterogeneity and 2) that the

ground-state conformers of the Trp residue have very similar extinction coefficients and radiative lifetimes, then the relative proportions of the three conformers in the ground state ("c") can be determined (Willis and Szabo, 1992). Each "c" value is calculated by integrating the area under each spectral curve which is associated with a particular decay time (DAS). The integrated value is then divided by the respective decay time (τ_i) and normalized giving a relative "concentration" value for each rotamer.

Time-resolved fluorescence decay measurements of native erabutoxin b and α-cobratoxin in buffered solution at 12 individual emission wavelengths (305-420 nm) displayed three exponential decay components, whereas α-bungarotoxin was best described by four decay times. In all three cases, the decay times were similar at each wavelength justifying the global analysis of these data sets.

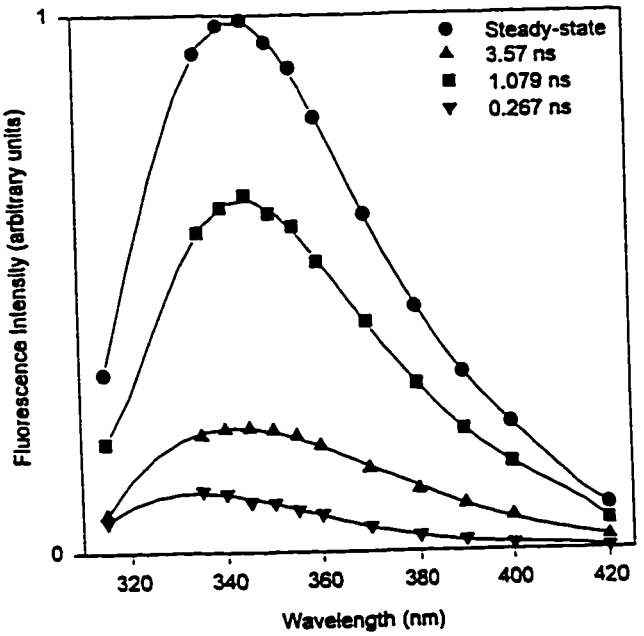

Figure 4.4 Decay-associated spectra of α-cobratoxin determined from the global analysis of data collected for 12 emission wavelengths (305 nm - 420 nm) using 295 nm excitation at 20°C.

In the case of erabutoxin b and α-cobratoxin, the statistical fits for three discrete exponential decay times (τ_i) were good under all conditions ($1.05 \leq \chi^2 \leq 1.11$ and $1.8 \leq$ SVR ≤ 1.9). The three fluorescence decay times of erabutoxin b are very comparable to that of α-cobratoxin, under all conditions, indicating a similar environment for the Trp residue (Tables 4.2 & 4.3).

Table 4.2 Time-resolved fluorescence parameters for erabutoxin b determined from the DAS (λ_{ex}= 295 nm, λ_{em} = 12 wavelengths) at different denaturant (GuHCl) concentrations.

ID	τ_1 (ns)	τ_2 (ns)	τ_3 (ns)	c_1	c_2	c_3	λ_{max}	SVR	σ
Native	3.85 ±0.02	1.180 ±0.002	0.258 ±0.003	0.04	0.86	0.10	340	1.80	1.10
2M GuHCl	3.30 ±0.02	1.264 ±0.003	0.263 ±0.004	0.08	0.79	0.13	340	1.85	1.07
3.7 M GuHCl	3.26 ±0.01	1.408 ±0.005	0.306 ±0.005	0.14	0.70	0.16	343	1.92	1.06
5.2 M GuHCl	3.437 ±0.007	1.45 ±0.01	0.277 ±0.004	0.36	0.40	0.24	350	1.83	1.08
CM	3.676 ±0.009	1.58 ±0.01	0.354 ±0.006	0.33	0.43	0.24	350	1.93	1.04
ACM	2.916 ±0.008	1.264 ±0.009	0.290 ±0.004	0.29	0.43	0.28	348	1.92	1.05

Subtle differences in the decay time values reflect small differences in the local Trp environment due to the surrounding amino acid side chains within a 7Å radius of the indole ring (Figure 4.5). The two toxins display nearly identical fluorescence decay times for the CM and ACM treated material. In each case, shorter fluorescence decay times are observed for ACM as compared to the CM treated protein. Assuming that the CM and ACM groups are close to the Trp, this observation is in accordance with previous studies in which amide groups were found to be more efficient quenchers of Trp than carboxylate (Cowgill, 1976).

Table 4.3 Time-resolved fluorescence parameters for α-cobratoxin were determined from the DAS (λ_{ex} = 295 nm, λ_{em} = 12 wavelengths) at different denaturant (GuHCl) concentrations.

ID	τ_1 (ns)	τ_2 (ns)	τ_3 (ns)	c_1	c_2	c_3	λ_{max}	SVR	σ
Native	3.57 ±0.01	1.079 ±0.003	0.267 ±0.003	0.07	0.68	0.25	343	1.77	1.11
2M GuHCl	3.21 ±0.01	1.067 ±0.003	0.285 ±0.002	0.09	0.67	0.24	344	1.85	1.07
3.7 M GuHCl	2.99 ±0.01	1.097 ±0.002	0.300 ±0.003	0.12	0.68	0.20	347	1.77	1.09
6.6 M GuHCl	3.263 ±0.007	1.202 ±0.006	0.280 ±0.007	0.24	0.53	0.23	346	1.83	1.07
CM	3.692 ±0.008	1.49 ±0.01	0.350 ±0.004	0.30	0.40	0.30	347	1.92	1.05
ACM	2.937 ±0.005	1.080 ±0.006	0.251 ±0.003	0.26	0.41	0.33	348	1.86	1.05

Figure 4.5 Setor representation of the local Trp environment for erabutoxin b (3ebx.pdb, Bernstein et al., 1977). (Backbone = gold; Trp = purple; Ile = beige; Asp = red; Glu = red; Lys = royal blue)

One would expect the structure of the ACM-denatured toxin is different from that of the CM-denatured toxin due to the negative charges added by the carboxylate group in the latter case. An alternate explanation of the data is one in which Trp is not quenched by the ACM amide, but by another moiety.

The native bungarotoxin showed a poor fit to four exponential decay times (χ^2 = 1.18 and SVR = 1.64). The fluorescence decay kinetics of α-bungarotoxin are more complex than those observed for the other two toxins. The fluorescence decay curve of α-bungarotoxin can not be fit to three exponentials and the statistical criteria indicate that four decay time values provide an unacceptable fit (Table 4.4, Figure 4.6).

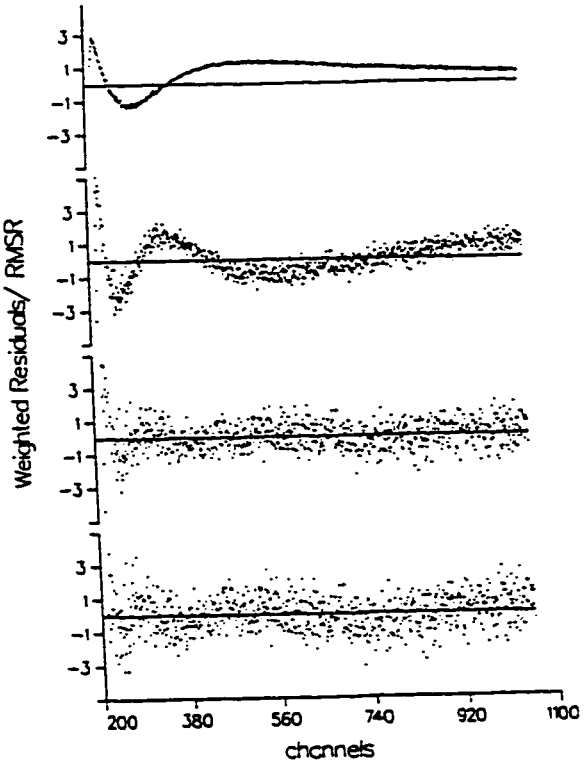

Figure 4.6 Weighted residual plots from the fitting of the bungarotoxin fluorescence decay curve to single, double, triple and quadruple exponential decay kinetics (from top to bottom).

The structure of α-bungarotoxin determined by X-ray crystallography (Love and Stroud, 1986) is distinct from that determined by NMR (Inagaki et al., 1985; Basus et al., 1988). The NMR structure places the conserved Trp residue in a position similar to that of all other postsynaptically acting neurotoxins, whereas the crystal structure reports less β-sheet and an unusual orientation of the invariant Trp. The difference in the two structures has been attributed to crystal packing (Basus et al., 1988), where there are two low energy conformations with different backbone geometry. Since the crystal packing forces are

sufficient to bring about this conformational change, it was concluded that there must be a relatively low barrier to interconversion. It is reasonable to propose that the high sensitivity of fluorescence spectroscopy allows for the detection of Trp in this alternate backbone conformer. Hence, the Trp residue might be expected to display different decay times for each backbone conformation. This would potentially lead to six decay time components. It is difficult or impossible to resolve decay times of similar value (ie. within a factor of 1.5), much less five or six discrete decay time values (McKinnon et al., 1977; Szabo et al., unpublished results). The added complexity of this system is explained by the presence of two low energy conformations (alternate backbone geometry) for α-bungarotoxin in solution (Walkinshaw et al., 1980). Thus, as well as the Trp side chain rotamers, two added Trp environments would be contributed by backbone heterogeneity.

The fluorescence decay times for all three toxins did vary ($\leq$ 25%) with denaturation (Tables 4.2, 4.3 & 4.4), reflecting a change in the Trp environment .

The relative contributions of the three decay times observed for erabutoxin b and α-cobratoxin varied with [GuHCl] and were dramatically altered by disruption of the disulphide bonds (CM/ACM toxins). Transition from the β-sheet to random coil state in erabutoxin b (GuHCl) resulted in approximately a 9 fold increase, 2 fold decrease and 2 fold increase for the relative proportions ("c" values) of the long, intermediate and short decay time, respectively. A change of similar magnitude was observed for the "c" values with CM, ACM and GuHCl treated erabutoxin b.

Table 4.4 Time-resolved fluorescence parameters for α-bungarotoxin were determined from the DAS (λex= 295 nm, λem = 12 wavelengths) at different denaturant (GuHCl) concentrations.

ID	τ_1 (ns)	τ_2 (ns)	τ_3 (ns)	τ_4 (ns)	c_1	c_2	c_3	c_4	λ_{max}	SVR	σ
Native	2.52 ±0.02	0.551 ±0.007	0.201 ±0.002	0.057 ±0.001	0.01	0.10	0.54	0.34	339	1.64	1.18
2M GuHCl	2.92 ±0.02	0.656 ±0.009	0.274 ±0.003	0.080 ±0.001	0.03	0.22	0.65	0.10	341	1.69	1.17
3.7 M GuHCl	3.15 ±0.01	0.99 ±0.02	0.373 ±0.004	0.115 ±0.002	0.06	0.16	0.66	0.12	341	1.88	1.07
5.2 M GuHCl	3.051 ±0.006	0.995 ±0.007	0.281 ±0.003	0.058 ±0.003	0.18	0.31	0.41	0.10	347	1.82	1.09
5.2 M GuHCl	2.987 ±0.004	0.875 ±0.005	0.231 ±0.002	— —	0.21	0.42	0.36	—	347	1.59	1.16
CM	4.05 ±0.02	1.94 ±0.01	0.445 ±0.004	— —	0.20	0.47	0.33	—	350	1.85	1.05
ACM	3.05 ±0.01	1.405 ±0.007	0.251 ±0.002	— —	0.25	0.43	0.32	—	343	1.82	1.08

CM and ACM modification of α-cobratoxin effected a 4 fold increase, 1.7 fold decrease and 1.2 fold increase in the "c" values of the long, intermediate and short decay times, respectively. Remarkably, at 6.6 M GuHCl the α-cobratoxin did not display "complete random coil" fluorescence "c" values even though the CD spectra was indicative of random coil. The progression of β-sheet to random coil in bungarotoxin is complicated by a shift in the number of decay time components, therefore the change in decay time relative proportion can not be quantified. Both the decay times and their relative proportions were restored to

native toxins values upon the removal of GuHCl by dialysis (data not shown). For all three toxins, the CM and ACM treated material was best described by triple exponential decay kinetics.

4.2.4 More on the Trp Environment...

In order to further assess the Trp environment, quantum yields of the three toxins were measured under various conditions. The quantum yield data supports the previous statement that the Trp environments in native erabutoxin (Φ = 0.075) and α-cobratoxin (Φ = 0.065) are comparable, whereas the bungarotoxin Trp is highly quenched (Φ = 0.013). In the case of bungarotoxin, the disulphide of the β-turn is within a 7Å radius of the indole ring (2abx.pdb; Bernstein et al., 1977).

With increasing concentrations of GuHCl, the erabutoxin quantum yield did not vary significantly (0.075 - 0.077), supporting the conclusion that GuHCl has a negligible effect on the fluorescence parameters of Trp (Willis and Szabo, 1992) and that the Trp is solvent exposed in the protein's native state. Denaturation of the toxins by reduction and carboxymethylation resulted in larger quantum yield values: erabutoxin-CM (Φ = 0.086); α-cobratoxin-CM (Φ = 0.088); bungarotoxin-CM (Φ = 0.066). Such a trend indicates that in the native toxin, the Trp fluorescence is quenched by charged groups (or a disulphide group in the case of bungarotoxin) within a 7Å radius of the indole ring, and these groups are removed from the local area of the Trp in the CM-denatured toxins.

4.2.5 Rotamer Populations and Secondary Structure

As outlined in Chapter 1, Trp multiexponential fluorescence decay behaviour has been rationalized in terms of alternate conformational states of the Trp side chain due to rotation about the C_α-C_β (χ_1 rotamer) and/or C_β-C_γ (χ_2 rotamer) bonds (Donzel et al., 1974; Szabo and Rayner, 1980). Several methods have provided direct evidence for this model (Philips et al., 1988; Colucci et al., 1990; Tilstra et al., 1990; Ross et al., 1992) and most recently, time-resolved fluorescence spectroscopy has been used to demonstrate the existence of Trp side chain rotamers in erabutoxin b protein crystals (Dahms et al., 1995; see Chapter 5). Significant correlations have been established between side chain dihedral angle probabilities and backbone ϕ,ψ values (Janin et al., 1978; McGregor et al., 1987; Piela et al., 1987; Dunbrack and Karplus, 1993; Schrauber et al., 1993) which define protein secondary structure. If the distribution of amino acid side chain conformers is dependent upon the local protein backbone ϕ,ψ angles, then rotameric populations would provide a sensitive probe of local secondary structure.

Using this model, the fluorescence decay time values (τ_i) would be associated with the different Trp rotamers and the normalized pre-exponential amplitudes (α_i) or fractional concentrations (c_i, in the case of data from a DAS experiment) would reflect the relative proportion of each rotamer. Therefore the "c" values should vary as a function of local secondary structure.

Based on this reasoning, the relationship between Trp fluorescence parameters and

protein secondary structure was investigated (Willis and Szabo, 1992; Willis et al., 1994). The most recent study utilized α-helical model peptides in which a Trp residue had been placed at the centre of the helix. In one case, the peptide monomer was non-helical whereas the peptide dimer displayed an α-helical structure. By altering the peptide concentration, it was possible to monitor the change in fluorescence parameters with a change in local secondary structure. The other model peptide was α-helical as a monomer and loss of structure was conferred by titration with GuHCl. TFE was utilized to induce further helical character in both cases. These studies showed that the relative contribution of each fluorescence decay time was correlated with α-helix content.

The "c" values for native erabutoxin b and α-cobratoxin are distinct from those observed for Trp in a random coil or α-helix (Tables 4.2 & 4.3 versus Willis and Szabo, 1992; Willis et al., 1994) and the Trp residue of each toxin is found on a β-sheet (NMR and X-ray crystallographic data). It was not our intention to provide kinetics of the folding or unfolding of the proteins nor to provide a detailed structural titration curve with denaturant. Rather, the goal was to establish whether or not the "c" values observed for the toxins were indicative of a Trp local β-sheet secondary structure, and if those values would change upon denaturation with GuHCl or by elimination of the structurally important disulphide bonds.

The "c" values of erabutoxin b and α-cobratoxin are dominated by the intermediate decay component (0.86/0.68) with relatively small contributions from the long and short decay components (Tables 4.2 & 4.3). Likewise, the combined contribution from the

intermediate two decay times of α-bungarotoxin dominate its fluorescence. These results are similar to those observed for melanocyte-stimulating hormone in acidic lipids, and in this case the hormone is thought to exist in a β-turn type structure (Ito et al., 1993). This is in contrast to the helical dimer (HD, α-helical structure), which displays relative contributions of 0.43, 0.38 and 0.19 for the long, intermediate and short decay times, respectively (Willis et al., 1994). In its complete monomeric form (non-helical), the "c" values become 0.28, 0.45 and 0.27, respectively. In contrast, the "c" values observed for PTH in the presence of 35% TFE (α-helical) were 0.33, 0.53 and 0.14. Native PTH displayed "c" values of 0.36, 0.44 and 0.20 and in the presence of 6M GuHCl the values observed were 0.48, 0.39 and 0.13.

4.2.4.a Structural Correlation

For all three toxins, disruption of the disulphide bonds by either method resulted in total loss of secondary structure by CD (data not shown). The fluorescence of each toxin is best described by three decay times with "c" values (Tables 4.2, 4.3 & 4.4) comparable to those found for the (non-helical) "helical monomer peptide" (Willis et al., 1994). Since the interaction of neighbouring residues with Trp will affect the fluorescence decay time values, the characteristic relative proportion ("c") may not always be associated with the same lifetime for all proteins. The "c" values which were reported for denatured PTH, PTH fragments (Willis and Szabo, 1992) and nuclease A (Eftink and Wasylewski, 1992) are

different from those of both the helical monomer and the denatured toxins. This implies that there is not a unique set of "c" values representing the denatured state for all proteins. However, these values may still be used to monitor protein unfolding for a given protein.

If we assume that the "c" values of these toxins reflect the secondary structural features for the protein backbone in the vicinity of the Trp residue, we can monitor unfolding at a very specific site. Since the CM and ACM toxins show only random coil structure by CD (data not shown), the "c" values observed under these conditions are used as the values expected for the completely denatured toxins. The CD spectral maximum (228.6 nm) was plotted versus the time-resolved fluorescence "c" values with progressive denaturation by GuHCl (Figures 4.7, 4.8 & 4.9) for each toxin. The relationship between the loss of global β-sheet structure as detected by CD and time-resolved fluorescence was not linear.

Figure 4.7 shows the denaturation of erabutoxin b with increasing concentrations of GuHCl. The "c" values change only slightly between the native state and 3.7 M GuHCl even though the CD shows marked loss of β-sheet. However, when molar ellipticity$_{228\ nm}$ values are plotted versus [GuHCl] (data not shown), a linear relationship was observed. Although there was global unfolding in the protein in this [GuHCl] range, the local structure surrounding the Trp residue was maintained. This implies that there is an equilibrium intermediate at 3.7 M GuHCl with very little secondary structure other than that which is in direct contact the Trp residue. These results are in agreement with recent studies of barnase which showed the centre of a β-sheet was the first to fold and the last to unfold (Fersht, 1993). In these toxins, the Trp residue is located near the centre of the β-sheet.

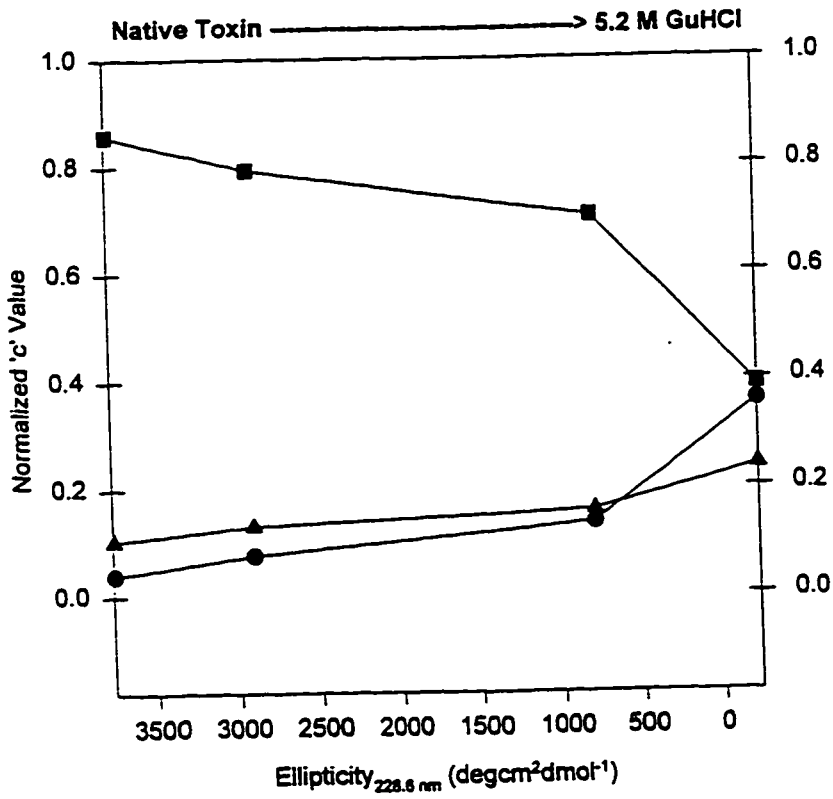

Figure 4.7 Relationship between CD (228.6 nm) and "c" values for erabutoxin b with varied GuHCl concentrations (0 M, 2 M, 3.7 M & 6 M). ● C_1 ■ C_2 ▲ C_3

A similar phenomenon is observed for α-cobratoxin (Figure 4.8) and α-bungarotoxin (Figure 4.9), but the effect is more dramatic in these two cases. With GuHCl treatment the α-cobratoxin Trp "c" values begin to converge towards those observed for the modified toxins (random coil), however total loss of secondary structure does not occur even at 6.6 M GuHCl. The global analysis of the α-bungarotoxin fluorescence at 5.2 M GuHCl was best

fit to four exponential decay times (SVR = 1.82, χ^2 = 1.09) as compared to triple exponential decay kinetics (SVR = 1.59, χ^2 = 1.16), indicating that the local area surrounding the Trp residue was not yet completely denatured and backbone heterogeneity is still observed. [CM and ACM treated α-bungarotoxin displayed triple exponential decay kinetics with "c" values similar to CM and ACM treated erabutoxin b and α-cobratoxin].

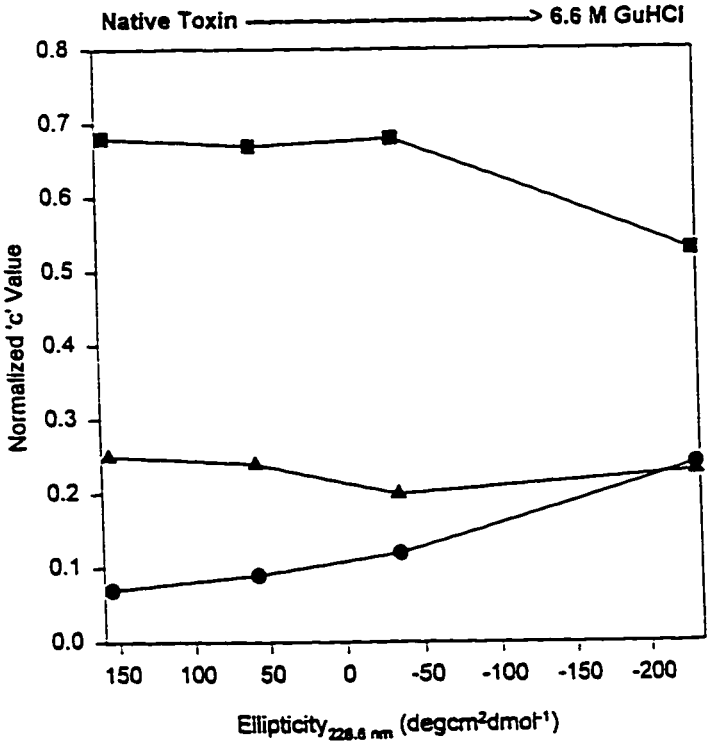

Figure 4.8 Relationship between CD (228.6 nm) and "c" values for α-cobratoxin with varied GuHCl concentrations (0 M, 2 M, 3.7 M & 6.6 M). ● C_1 ■ C_2 ▲ C_3

Structural data shows both the α-cobratoxin (Figure 4.10) and α-bungarotoxin (Figure 4.11) have an added disulphide bridge, located at the β-turn between the third and fourth β-strand, whereas the erabutoxin does not (Figure 4.1 A). It seems that the close proximity of

the disulphide to the Trp residue preserves some of the local backbone conformation, even in the presence of high GuHCl concentrations. Protein stability, granted by the disulphide linkages, was also observed by the recovery of the CD and fluorescence values (refolding) for each protein (data not shown) upon elimination of 6 M GuHCl (dialysis). The stability conferred by the disulphide linkage, in the case of α-bungarotoxin and α-cobratoxin, is observed in combination with the effect from the Trp residue being at the centre of the β-sheet.

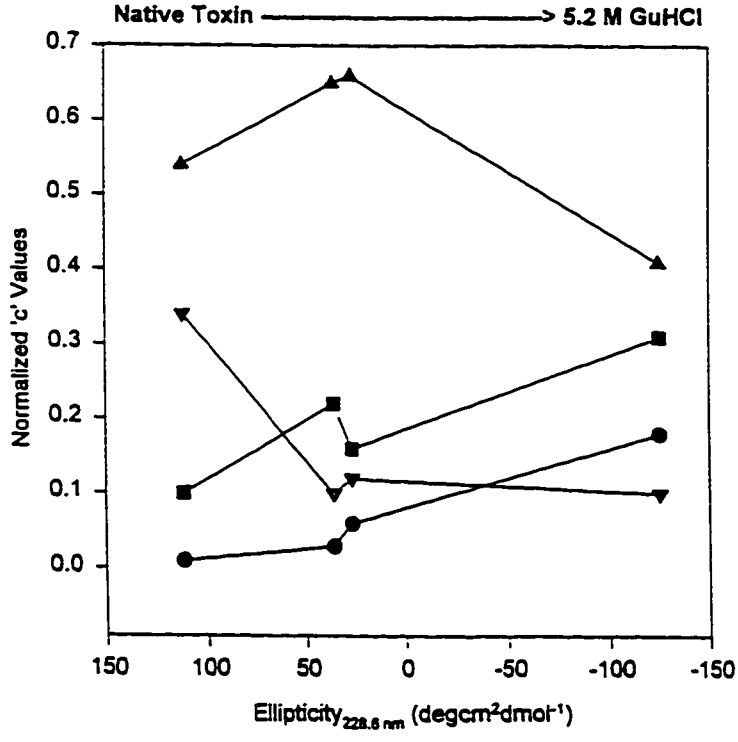

Figure 4.9 Relationship between CD (228.6 nm) and "c" values for α-bungarotoxin with varied GuHCl concentrations (0 M, 2 M, 3.7 M & 5.2 M). ● C_1 ■ C_2 ▲ C_3 ▼ C_4

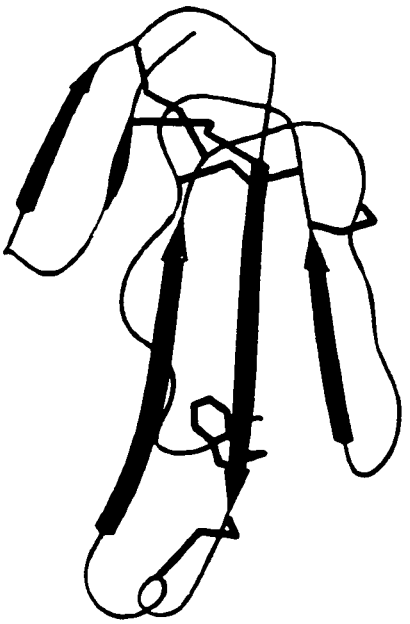

Figure 4.10 Setor representation of α-cobratoxin (1ctx.pdb; Bernstein et al., 1977). (backbone = gold; disulphides = yellow; trp = purple; ribbon = β-sheet; rope = random coil)

Figure 4.11 Setor representation of α-bungarotoxin (2abx.pdb; Bernstein et al., 1977).(backbone = gold; disulphides = yellow; trp = purple; ribbon = β-sheet; rope = random coil)

4.3 Conclusions

It is evident that care should be exercised in the use of fluorescence "c" values (rotamer relative proportions) as a structural predictive tool, in the absolute sense. The evidence presented in this chapter strongly suggests that the "c" values for Trp in a β-sheet are dramatically different from those observed for Trp in an α-helical or random coil type structure. This study confirms the laboratory's earlier proposal, that there is a connection between the secondary structure of protein segments containing a Trp residue and the "c" values characteristic of that Trp's fluorescence. Not surprisingly, the relationship appears to be more complex than first assumed, likely due to subtle effects caused by the interactions of the Trp side chain with alternate neighbouring residues. This added interaction of the Trp side chain could be studied using single Trp model peptides in which the residues directly next to the Trp residue are varied.

It is clear that the dependence of the fluorescence decay relative proportions on secondary structure can be used to monitor very localized structural changes in a protein at *in vivo* concentrations. This technique has the potential to be a powerful tool for helping to unravel the rules which govern protein folding.

PART III: Conformational Heterogeneity & Fluorescence

Conformational Heterogeneity in Crystalline Proteins

Time-resolved fluorescence studies of single Trp proteins in solution and in the crystalline state can provide unique comparisons between the "dynamic" state and "static" state: a means of correlating time-resolved fluorescence measurements with structural data obtained by X-ray crystallography. Herein is a summary of the spectrophotometric information collected for four different proteins in the aqueous and crystalline form.

5.1 Introduction

For protein crystals, the electron density of the tryptophan side chain (when compared with other residues) is considered to be well-defined by crystallographic criteria and is almost exclusively modelled as a single conformer (See Brookhaven Data Bank protein structures; Bernstein et al., 1977). Therefore, one might expect that single-exponential decay kinetics would be observed for an individual tryptophan residue in a crystalline protein. In this case, measuring the fluorescence parameters of single protein crystals could provide a direct comparison between a particular fluorescence lifetime and local structural features of the Trp environment (defined by the X-ray crystal structure). This would provide a better understanding of the factors governing Trp fluorescence in solution and allow for increased interpretation of protein fluorescence parameters.

Table 5.1 Local secondary structure of single Trp/Tyr proteins.

Protein Name (single-Trp)	Local Secondary Structure of Trp†
Azurin	Random coil
Rubredoxin	Centre of random coil turn
Melletin	Within α-helix
Ribonuclease T1	Within α-helix
Staphylococcal Nuclease	Within α-helix
Subtilisin Carlsberg	Within α-helix
Tryptophan Synthase $\alpha_2\beta_2$	Within α-helix
Elongation Factor Tu	Last loop of an α-helix
Glucagon	Last loop of an α-helix
Phosphofructokinase	Last loop of an α-helix
Phospholipase A2	End of an α-helix
α-Amylase Inhibitor	Turn of antiparallel ß-sheet
α-Bungarotoxin	Antiparallel ß-sheet
α-Cobratoxin	Antiparallel ß-sheet
erabutoxin b	Antiparallel ß-sheet
Monellin	Antiparallel ß-sheet (N-terminus)
Subtilisin Inhibitor	Antiparallel ß-sheet
Variant 3 Scorpion	Neurotoxin Antiparallel ß-sheet
Cyclophilin	Structure not yet released
Cystatin	Structure not yet released
Protein Name (single-Tyr)	**Local Secondary Structure of Tyr**
Calbindin D9K	Last loop of an α-helix (next to Ca^{2+} binding loop)
Parvalbumin	Within α-helix (next to Ca^{2+} binding loop)
Murine Urinary Protein	Structure not yet released
Soybean Hydrophobic Protein	Structure not yet released

† Structure defined by atomic co-ordinates (Brookhaven Data Bank; Bernstein et al., 1977).

Time-resolved fluorescence studies of the crystalline heme protein myoglobin (Willis et al., 1991) have demonstrated the feasibility of accurately measuring Trp fluorescence decay parameters from protein crystals. In the case of myoglobin, the fluorescence decay times of the Trp residues were primarily determined by the rate of energy transfer from the

Trp to the heme group. Since this rate of deactivation greatly exceeds that of all other competing processes, information on local structural details of the protein from tryptophan fluorescence was not observable. When selecting the proteins for this particular project, an attempt was made to eliminate contributions from non-proteinaceaous fluorescent moieties (ie. heme groups, vitamins, cofactors & metals) which produced an initial list of twenty-two candidates (Table 5.1).

5.2 Erabutoxin b

Erabutoxin b (also see Chapter 4) was the first non-heme single protein crystal to be studied by Trp fluorescence (Dahms et al, 1995). The crystal structure of erabutoxin b has been determined by two groups (Tsernoglou & Petsko, 1976; Low et al., 1976) and reported almost simultaneously. The structure was later refined to 1.4 Å resolution (Smith et al., 1988) with the Trp residue modelled in a single conformation (χ_1 = 72.8, χ_2= -88.7; 3ebx.pdb; Bernstein et al., 1977).

5.2.1 Evaluation of Protein Purity & Identity

The crystals of erabutoxin b were treated in much the same way as erabutoxin in solution (Section 4.2.1) with respect to purity and identity. The protein was sometimes crystallized from SIGMA-purified toxin without further purification, therefore it was

necessary to evaluate the purity of the protein crystals. Erabutoxin b produced rod-shaped crystals (Figure 5.1) that were > 99 % pure by HPLC (refer to Figure 3.3). The molecular weight of the crystalline material was identical to that found for the HPLC pure material (Table 4.1). The crystals produced a diffraction pattern, however, determination of all three crystallographic cell parameters was impeded by the small crystal size (0.2 mm x 0.05 mm).

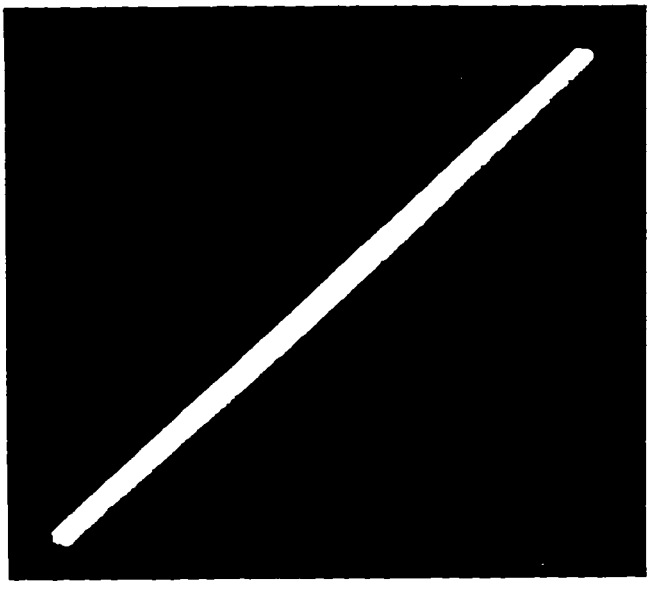

Figure 5.1 Microphotograph of erabutoxin b single crystals (longest dimension = 0.2 mm).

5.2.2 The Singlet Excited State & Heterogeneity

Excitation of Trp 29 from single erabutoxin b crystals, with 295 nm light from the laser system, produced a significant fluorescence signal. The photon count rate was dependent upon crystal size and orientation. When there was a decrease in count rate of greater than 15% during the experiment, a scatter element was detected in the data and

consequently in the decay parameters. This fluorescence behaviour was indicative of crystal photodamage and could be observed as cracking of the crystal and loss of birefringence (viewed under a microscope with polarizers).

The steady state spectrum of the erabutoxin b crystals was identical to that in aqueous buffer, having an emission maximum at 340 nm (Figure 5.2), revealing that the Trp 29 residue within the protein crystal remains in a very polar environment. This phenomena can be accounted for by the many water molecules modelled into the crystal lattice of erabutoxin b. The Trp of this protein is very solvent exposed (as compared with Trp in other proteins) due to the flat structure arising from the ß-sheet structural motif (see Figure 4.1 a & b) in which the Trp is located.

Time resolved fluorescence decay measurements of erabutoxin b in buffered solution at 12 individual emission wavelengths (305-400 nm) displayed three exponential decay components whose decay times were similar at each wavelength. This justified the global analysis of these data sets to provide the decay times displayed in Table 5.2. The DAS were constructed by combining the steady state and time-resolved fluorescence data (Figure 5.2a).

The intermediate decay component (1.17 ns) makes the largest relative contribution (85%) to the fluorescence spectra, whereas, the longest (3.64 ns) and shortest (0.28 ns) decay component each made a small relative contribution (4% and 12 %, respectively). The spectral maxima of the long and intermediate decay components is similar to that of the steady state spectrum, whereas, the spectral maxima of the shortest decay time appears to be shifted to a lower wavelength (Figure 5.2b).

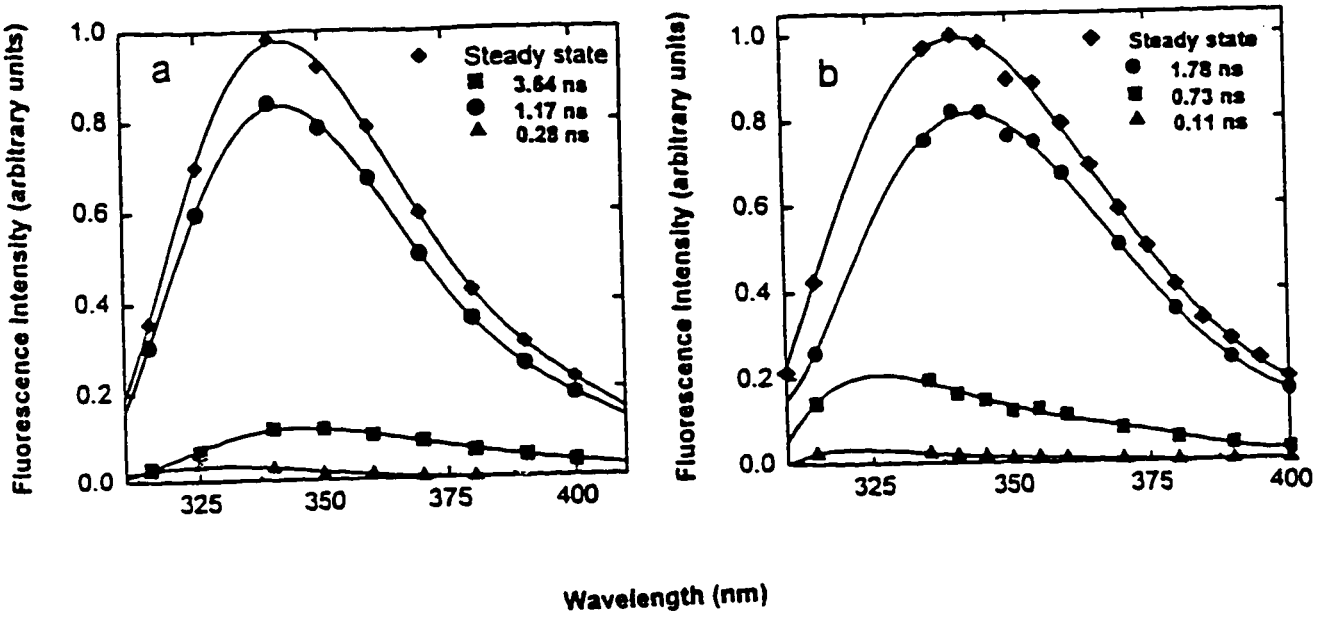

Figure 5.2 DAS of erabutoxin b in solution (a) and in the crystalline state (b). The standard errors and statistics as specified in Table 5.2 apply. The DAS of erabutoxin b in the crystalline state was measured at one protein crystal orientation. The shape and relative proportions of each curve is affected by the crystal alignment with respect to the polarized excitation source.

Contrary to expectations, the Trp fluorescence of erabutoxin b single crystals also required three decay times to model the fluorescence decay kinetics (Table 5.2). Ten crystals were examined, each producing similar fluorescence decay parameters and statistics allowing for the global analysis of these data. However, there is a limit to the total number of data sets which can be simultaneously analyzed, precluding the global analysis of more than twenty sets of data. Global analysis combining several fluorescence decay data sets for three individual crystals produced acceptable statistics, confirming the consistency of the data

measured from different crystals. The fluorescence decay times were also obtained from the global analysis of a combination of 20 data sets from measurements made at 10 different emission wavelengths (305-400 nm) and ten angular orientations of a single crystal. The values and statistics obtained from this type of analysis was consistent with those originally determined (Table 5.1). The longest decay component (1.78 ns) displayed a spectral maxima similar to the steady state spectrum, whereas the spectral maxima of the two shorter decay components (0.73 ns and 0.11 ns) were shifted to lower wavelengths (Figure 5.2b).

Table 5.2 Time resolved Trp fluorescence of erabutoxin b in solution and in the crystalline state: Fluorescence decay-times from the global analysis of multiple emission wavelengths (295 nm excitation, 20°C, pH 7) as compared with literature values.

Erabutoxin b	$^{\dagger}\tau_1$ (ns)	τ_2 (ns)	τ_3 (ns)	$<\tau>$	SVR	χ^2 (σ)
Solution	3.64	1.171	0.276	1.17	1.81	1.09
Crystal	1.78	0.734	0.113	---	1.71	1.12
Tanaka et al.[‡]	4.30	1.11	---	1.80	---	3.36

[†] The fluorescence lifetime values of erabutoxin b in solution were generated by the global analysis of a multiple wavelength experiment (12 data sets). The fluorescence lifetimes of the erabutoxin b crystal were determined by the global analysis of combined data from a multiple (10 data sets) wavelength and a multiple orientation (10 data sets) experiment. Typical errors associated with τ_1, τ_2, τ_3 were $\pm$ 0.02, 0.002, and 0.004 for erabutoxin b in solution and $\pm$ 0.002, 0.004, and 0.002 for erabutoxin b in the crystalline state.
[‡] Erabutoxin in solution (Tanaka et al., 1987).

The fluorescence of Trp 29 in erabutoxin b is best described by triple exponential decay kinetics, both in solution and in the crystalline state. The three fluorescence decay times exhibited by the erabutoxin b crystals are much shorter than those observed in solution (Table 5.1). Quenching of the Trp fluorescence in the crystal likely results from local intermolecular interactions in the crystalline state, which are not present in solution. The most likely candidate for fluorescence quenching is a disulphide moiety located close to the Trp residue. Examination of the crystal structure (3ebx.pdb; Bernstein et al., 1977) showed that the distance from the nearest intramolecular disulphide residue to Trp 29 is 13-14 Å. However, the erabutoxin b molecules are packed together in the crystal such that the intermolecular distance from the disulphide of one protein molecule and Trp 29 of an adjacent molecule is considerably closer (6.9 Å; Figure 5.3). Model studies with synthetic cyclic tripeptides which examined the distance dependence of Trp fluorescence quenching by disulphide groups showed that the critical quenching distance is 7 Å (Cowgill, 1970). The mechanism of quenching was not apparent from this earlier study, however, several common pathways were rejected and it was proposed that a vibrational dissipation of the excitation energy was facilitated by an extremely short-range interaction between the aromatic ring and the sulphur atoms. The average lifetime ($<\tau>$) value of erabutoxin b in solution (1.17 ns) was considerably lower than that measured by Tanaka *et al.*, (1987; 1.80 ns), and the individual fluorescence decay times did not agree with those previously measured (Table 5.2). This discrepancy might have arisen from the difficulty the earlier study had in adequately resolving the short decay time, which is evidenced by the large χ^2 value (3.36).

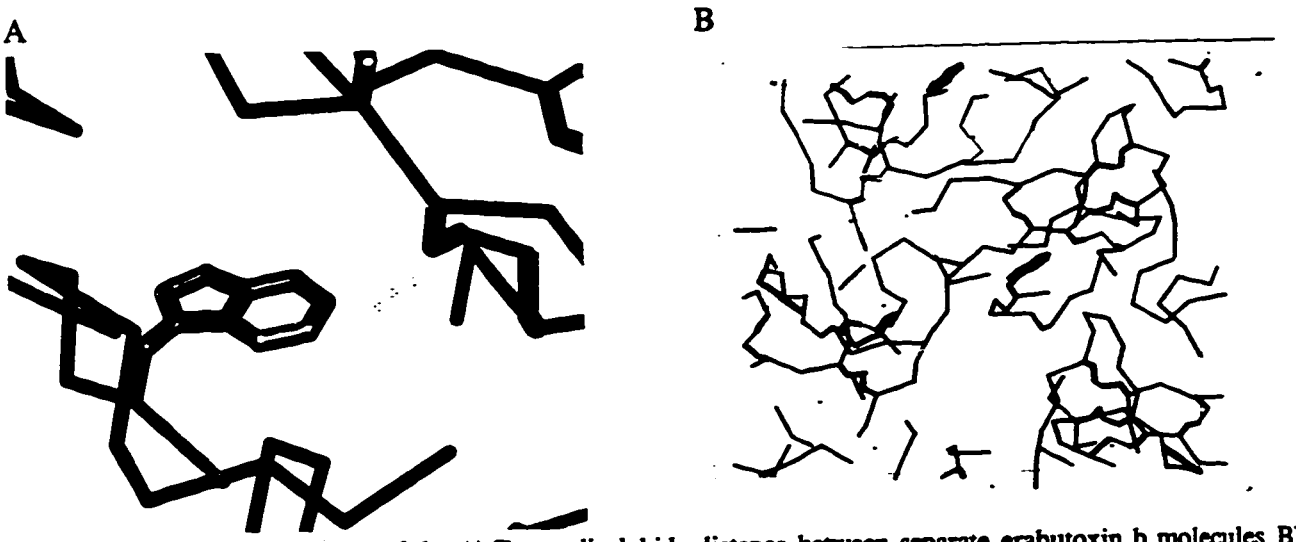

Figure 5.3 Setor representation of the A) Trp to disulphide distance between separate erabutoxin b molecules B) in the crystallographic unit cell. (Backbone = blue; Trp = purple; disulphide = yellow; distance = blue dots)

The DAS of erabutoxin b in solution (Figure 5.1a) revealed the shortest decay component to have a "blue-shifted" spectra, indicating that this emitting species experiences a more hydrophobic environment than the other two rotamers. In the case of the erabutoxin b crystal, both of the two shorter decay components exhibited a maxima at a lower wavelength which is consistent with emission from a highly quenched tryptophan in a non-polar environment.

Time-resolved data for erabutoxin b in solution at 300-nm excitation was consistent with that measured at 295-nm (data not shown) with acceptable statistical fits. Therefore, there is no evidence of any significant Tyr 25 fluorescence contribution at 295-nm excitation which might otherwise account for a blue shifted spectrum.

The observation of three exponential decay components for the erabutoxin b crystals

is the most significant aspect of this work. There are two possible explanations for this result. The first model consists of the Trp side chain in a single conformation with the surrounding amino acid side chains in heterogeneous conformations. Several fluorescence lifetimes would arise due to different quenching mechanisms of at least three distinct local Trp environments conferred by alternate protein or surrounding side chain conformations. The second model proposes conformational heterogeneity of the Trp side chain, with only one of the conformers being detected by X-ray crystallography. In the latter model, the individual Trp residue of each protein molecule within the crystal could adopt at least three distinct conformations. The interaction of the Trp side chain with different structural elements (protein backbone or other side chains) would lead to different fluorescence decay times. There would be no possibility of conformer exchange on the time scale of the fluorescence measurement. Recall that the latter interpretation is the basis for the rotamer model of Trp fluorescence decay behaviour in protein solutions.

5.2.3 The Orientation Experiment

In order to test these two models, orientation experiments were designed based on the following reasoning: the absorption of the Trp residue is dependent upon the angular orientation of the excited state transition moment with respect to the polarization direction of the excitation beam. Maximum absorption will occur when the transition dipole is aligned with the excitation plane of polarization. At 295 nm the L_a transition of Trp (Figure 1.12) is

likely the dominant one in aqueous buffer, with the L_b transition making only a minor contribution to the absorbance (Valeur & Weber, 1977). Therefore, the fluorescence should be primarily from the L_a singlet state. Since the fluorescence intensity is proportional to the square of the absorption transition probability, the fluorescence intensity of a fluorophore should vary with an angular dependence of the fluorophore's dipole with respect to the polarization direction (vertical) of the excitation source. In this case, there are effectively three fluorophores (one for each rotamer) and the relative intensity of each will be reflected in the normalized pre-exponential terms (globally determined α values) derived from the fluorescence decay curve. An orientational dependence of the normalized pre-exponential terms of the fluorescence decay should be expected if the rotamer hypothesis were correct, since each rotamer (and therefore each dipole) would be aligned differently in the crystal. If the three fluorescence decay times were the result of three distinct Trp conformers in separate molecules of the crystal, then the relative proportions (normalized pre-exponential terms) of the decay components should vary with crystal orientation but the decay time values should not. If the data were to be explained by the first model where the Trp is in a single conformation with alternate local environments, then no variation of the normalized pre-exponential terms should be observed during the orientation experiments.

The fluorescence decay times remained constant at all orientation angles, but it was found that the normalized pre-exponential terms varied. The orientational dependence of the normalized pre-exponential terms of each decay component for three different crystals is displayed in Figure 5.4 (a-c). Full 360° rotation experiments were precluded by eventual

crystal photodamage. Orientation experiments were performed on several individual crystals and each produced three distinct functions for the normalized pre-exponential terms. In two of the three orientation experiments illustrated, there was a significant orientational dependence of these terms (Figure 5.4(a,b)). Two of the erabutoxin b crystals measured exhibited only limited variation of the pre-exponential terms (represented in Figure 5.4c). It was possible to combine twenty data sets, 10 each from two different crystals, in order to confirm the consistency of the lifetime values. When this analysis was performed in all three possible combinations with the lifetime values fixed to the mean values from the global analysis of the three individual crystal data sets (Table 1.), satisfactory statistical parameters were obtained (SVR = 1.73 and χ^2 = 1.11).

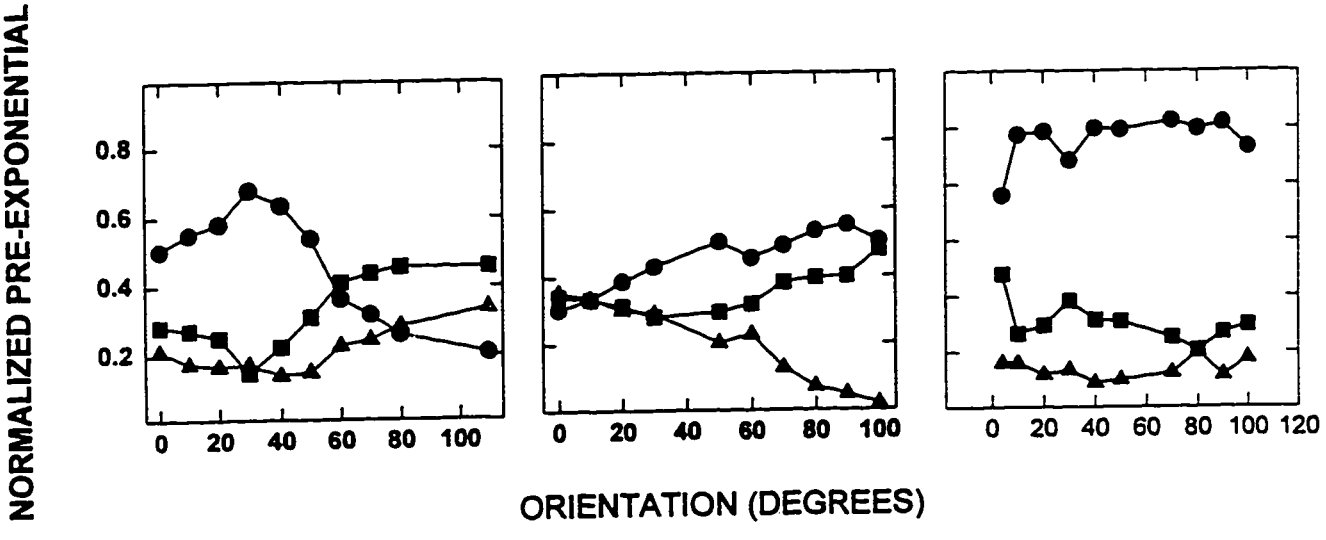

Figure 5.4 Dependence of the relative fluorescence decay-time component proportion on crystal orientation with respect to the polarization of the excitation beam. A, B, and C represent data acquired from individual erabutoxin b protein crystals. ● 1.78 ns, ■ 0.73 ns, ▲ 0.11 ns.

Significantly, the normalized pre-exponential terms (which correspond to the relative contributions of each decay component) were dependent upon the crystal orientation. This provides direct evidence for at least three Trp side chain rotamer conformations (contained in separate protein molecules) within the crystals.

5.2.4 Simulations & Calculations

It was possible to simulate the pattern for the orientational dependence of the normalized pre-exponential terms. These calculations took into account the exact experimental geometry (Figure 5.5): the four erabutoxin b molecules in the crystallographic unit cell (Figure 5.3), different possible populations of each Trp conformer within the protein crystal, and alternate starting positions of the erabutoxin b crystal in the sample cell (with respect to flat crystal surfaces).

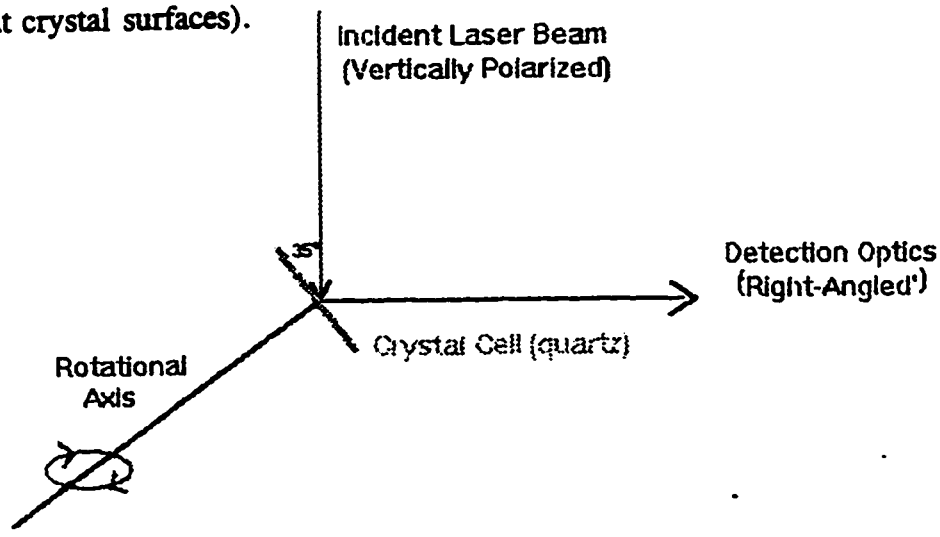

Figure 5.5 Experimental geometry of the crystal apparatus used for fluorescence measurements as viewed from above.

A Sigma Plot macro-programme (Appendix A) was written to calculate the theoretical dependence of the relative decay-time proportions on protein crystal orientation: the other two tryptophan side chain rotamers, not found by X-ray crystallography, (simulated using QUANTA software) were included, and the initial population of each rotamer could be varied. Since the two alternate Trp orientations were unknown, the conformations originally chosen for the simulations were modelled with a χ_1 rotation of exactly 120° from the crystallographically determined rotamer (g+, g- and t Trp rotamers). We recognized that this simple approach may not be realistic given the interactions of the Trp side chain with the rest of the protein molecule. Therefore, the sub-programme "Conformational Search" (QUANTA software, employing CHARMM energy calculations) was employed to sample alternate Trp low energy conformations for erabutoxin b. Since weak electron density originating from alternate Trp rotamers could have been modelled as water molecules, the search was performed in the absence of the water molecules. The two low energy conformers which were closest to the originally modelled χ_1/χ_2 angles were chosen. A χ_1 rotation was used to represent rotation of the Trp about the peptide backbone and a χ_2 rotation of 180° was used to represent an indole ring flip (Figure 5.6). These rotamers were not resolved by X-ray crystallographic data (3ebx.pdb; Bernstein et al., 1977) and were modelled as additional Trp low energy conformations. The alternate Trp side chain rotamers were modelled into the structure (QUANTA software) using the following χ_1/χ_2 angles from low energy models found in the conformational search: conformer 2 = -168.94°/-94.7°, conformer 3 = -36.62°/-88.92°.

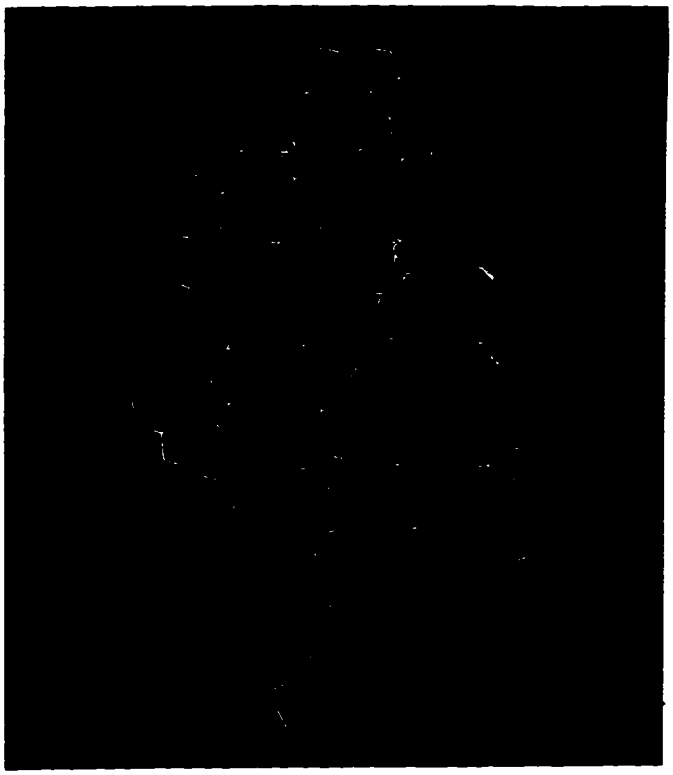

Figure 5.6 Setor representation of Trp rotameric configurations for a χ_1 and χ_2 rotation. (Trp = purple, beige and pink; Backbone: C = white; N = blue; O = red).

The Trp L_a transition dipole was approximated by subtracting the spatial coordinates of NE1 and CE3 (indole nitrogen and carbon 4).

In practice, the crystal lay on its long axis (Figure 5.1) on the side of the sample cell. Therefore, the theoretical position of the crystal in the sample cell was assumed to be the long axis of the unit cell. This was simulated by subjecting the initial tryptophan dipole coordinates to a rotation matrix (Diamond, 1988), such that the directional cosines ((l,m,n) = (0,0,1) and $\theta_1 = 45°$) were defined by the crystal axes. The values produced by the

initial manipulation were then rotated through a second matrix (at intervals of 10° for θ_2) in which l,m,n were defined by the exact experimental geometry. Final values were squared (since the fluorescence is proportional to the square of the absorbance) and the relative proportion of each theoretical fluorophore calculated. Due to the predominant flat face of the crystal's long axis (Figure 5.1), the crystals could be consistently positioned along the length of the rod. However, the initial angular position of the crystals with respect to the vertically polarized laser beam could not be achieved with any precision. The protein crystals could not be repositioned due to their fragile nature. The latter affects the experimental observations such that different portions (up to 100°) of the total orientational variations (360°) were sampled with each crystal.

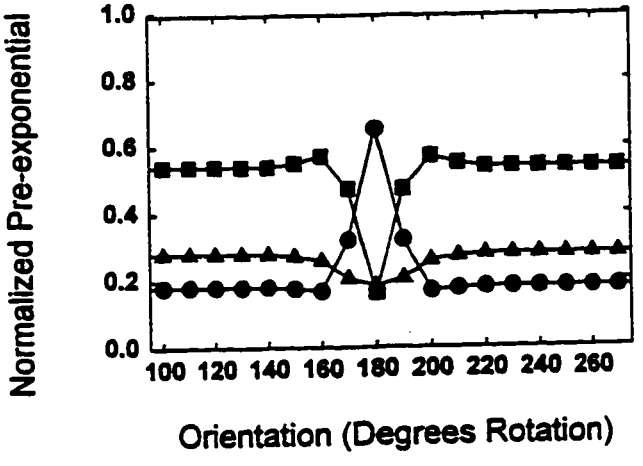

Figure 5.7 Theoretical orientational dependence (180°) of the relative fluorescence decay-time proportions for erabutoxin b protein crystals. Simulated data where; Trp χ_1 = 72.8°, χ_2= -88.7°/ χ_1 = -168.94°, χ_2= -94.7°/ χ_1 = -36.62°, χ_2= -88.9° (g^{+-}, g^{-}, and t, respectively) with 0.7, 0.1 and 0.2 as the relative proportions of the three rotamers and excitation polarization perpendicular to the z-axis of the crystal unit cell.

A change in the relative population of each Trp side chain rotamer was found to alter the shape and amplitude of the orientation dependence curves (data not shown). The most predominant rotamer could not be absolutely determined from the crystal fluorescence data. The simulation curve, produced by assuming the relative proportions of the three rotamer populations to be 0.1, 0.2, and 0.7 (values similar to those determined by solution fluorescence), is shown in Figure 5.7. There are some remarkable similarities between the experimental curves (Figure 5.4) and portions of the simulated curve (Figure 5.7). Part of this simulation (165°-195°) shows the same dramatic variation of the rotamer proportions as the experimental results shown in Figures 5.4a and b. The orientation experiment illustrated in Figure 5.4c (representative of data from two different crystals) showed only a limited variation of the pre-exponential values and was similar to another portion (140°-165°, 195°-240°) of the simulation pattern shown in Figure 5.7. Since it was possible to sample only a 100° portion of a total 360° (180° considering periodicity) rotation, it would seem that the portions of the entire curve were sampled randomly. The starting point of the curve would be associated with the initial orientation of the crystal, producing subsets of the entire curve. It could be argued that the minimal orientational dependence shown in Figure 5.4c is representative of Trp in a single conformation, but with alternate environments conferred by other heterogeneous side chains within a critical distance of the Trp (first hypothesis). In this case, the crystal would surely exhibit different fluorescence decay times than the other two crystals, and this is not the case. An alternate explanation for the minimal variation observed in Figure 5.4c, would be different proportions of the three rotamers in each crystal.

However, altering the initial set of rotamer proportions for the simulations produced an entirely distinct set of orientation curves (data not shown). During the simulations, altering the initial orientation of the crystal (x,y or z axis) upon the sample cell face also produced a distinct set of curves, however the curves generated using the long axis of the crystal unit cell gave results most representative of the experimental results. This is in agreement with the experimental case in which the crystal lays on the face of the long z axis.

When the two alternate rotamers were modelled with similar χ_2 angles, effectively only changing χ_1 by approximately 120°, the periodicity (~ 180°) was similar to that found experimentally. On the other hand, when one of the three χ_1 rotamers was modelled with the χ_2 angle 180° from the other two rotamers (Trp ring flip), the periodicity was significantly reduced to less than 60°. This was markedly different from that observed for all the experimental measurements, and provides some evidence that the actual Trp rotamers are similar to those modelled in this simulation (no indole ring flip).

Several recent studies (Ponders & Richards, 1987; Dunbrack and Karplus, 1993; Schrauber et al., 1993) have examined side chain rotamer populations in various X-ray crystal structures of proteins (resolution $\leq$ 2.0 Å). These studies show that the mean positions for χ_1 = 60°, 180°, and -60° (g^+, t, and g^-), based on secondary structural features (Janin et al., 1978) are not necessarily accurate representations of many side chain rotamers, but can serve as a starting position for predicting side chain conformations in proteins. Factors which appear to affect the "rotamericity" of side chains include backbone torsions of the residue under consideration, as well as tertiary packing constraints (Dunbrack and

Karplus, 1993; Schrauber et al., 1993). The designations of g^{+-}, g^{-} and t used herein are the same as those defined by Ponder and Richards (1987), whose rotamer library is a compilation of non-secondary structure specific rotamer frequencies for all amino acids, based on 19 well-determined crystal structures. The rotamer frequencies found by Ponder and Richards for the rotamers modelled in this study are 20.7% (g^{+-}), 6.9% (g^{-}) and 13.8% (t), with only the g^{-} χ_1 value differing significantly from the value used in this study. When normalized, the values are 0.50 (g^{+-}), 0.17 (g^{-}) and 0.33 (t), showing a trend which was similar to the relative proportions used in our simulations, namely 0.70 (g^{+-}), 0.10 (g^{-}) and 0.20 (t). Based on the ϕ, ψ angles (-161.3° and 171.8°, respectively) defined for Trp 29 in the erabutoxin b structure, the rotamer library constructed by Schrauber and coworkers (1993) would predict a significant population of g^{+-} (21%), g^{-} (4%), and t (9%). The normalized values of these three rotamers can be calculated as 0.62, 0.12 and 0.26, respectively, and is in good agreement with the 0.70, 0.10 and 0.20 used for our simulation. This rotamer library included a large sample (85 Trp side chains) in the ß-strand classification, which is advantageous, however, the ϕ, ψ range was large (-240° to 0° and 60° to 230°, respectively). Data from the updated rotamer library constructed by Dunbrack and Karplus (1993) has been sorted into all possible combinations of 20° ϕ, ψ angle increments. Only four Trp residues are found in the ϕ, ψ range defined by the erabutoxin b crystal structure and these are populated as g^{++} (50%), g^{+-} (25%) and t (25%) rotamers. The prediction of three predominant rotamers by the aforementioned studies is consistent with the three rotamers detected in this study. There are significant discrepancies between

our simulations and the predictions from two of the three rotamer libraries (Dunbrack and Karplus, 1993; Schrauber et al., 1993), and none of the libraries predicts three χ_1 rotamers with similar χ_2 angles ($\sim$ -90°) as being the most frequent.

It should be noted that for this study the Trp rotamers are proposed to exist in separate molecules within the same protein crystal. Conversely, the Trp rotamer libraries are based on side chain conformations arising from proteins with slightly different ϕ, ψ angles, with the exception of gramicidin (1GMA; Langs, 1988) and relaxin (6RLX; Eigenbrot et al., 1991), which each have one or more Trp side chains modelled with one alternate rotamer (Bernstein et al., 1977). The frequency of side chain rotamers from the rotamer libraries may yet reflect different rotamer populations within one protein crystal, especially in the case where all possible combinations of 20° ϕ, ψ angle increments were used (Dunbrack and Karplus, 1993; Dunbrack, personal communication). It has been suggested that the detection of alternate rotamers (when less than 33% at 1.4 Å resolution) are beyond the detection limits of current x-ray crystallographic techniques (Smith et al., 1986), hence the data base used for the rotamer libraries may be considered to be a first approximation.

5.2.5 Anisotropy of Crystals?

One might expect an r value of unity for a protein crystal, since the system is rigid and any Trp vibrations would likely occur on a sub-picosecond time scale. From the anisotropy decay, there appears to be minimal steady state anisotropy in the crystal.

However, the results are inconclusive, which is not surprising, if one considers the system: The principle of anisotropy in solution is dependent upon having a system with an isotropic orientation of the absorption transitions and following excitation, the anisotropy of those excited molecules is monitored. Assuming the rotamer model, there would be three anisotropic rotamers in the crystal each having a different alignment with the polarized excitation beam and with the vertical and horizontal detection optics. Each rotameric species will contribute to the fluorescence signal, therefore interpretation of the anisotropy becomes highly complicated.

5.3 Crotonase

Crotonase (enoyl-CoA hydratase, EC 4.2.1.17) catalyses the reversible syn addition of water across the carbon double bond of trans-2,3-unsaturated fatty acid acyl-CoA thiolesters. Although the X-ray crystallographic structure of crotonase is yet to be determined (in progress), this protein contains a single Trp residue and was easily crystallized, providing a suitable candidate for this project. Biochemical (Stern et al., 1956; Steinman and Hill, 1975) and preliminary crystallographic data (Tonge et al, 1994) suggest crotonase exists as a dimer of hexamers in solution and in the crystalline state (six identical subunits). Crotonyl CoA (non-fluorescent) was used as the substrate of crotonase for these investigations.

5.3.1 Evaluation of Protein Purity & Identity

Following the ethanol precipitation step, the expressed enzyme was > 99.9% pure by HPLC (Figure 3.4) and the measured molecular mass (28290 Da) was within 0.01% of the calculated isotope average mass (28287 Da). Both sequencing of the gene and N-terminal amino acid analysis confirmed the correct sequence of the enzyme. The enzyme was homogeneous by activity assay with crotonyl Co-A (Steinman & Hill, 1975).

Crotonase crystals (Figure 5.8a; 0.6 mm x 0.6 mm x 0.2 mm) in the presence and absence of substrate (crotonyl-CoA), were grown by the vapour diffusion method and diffracted to approximately 2.8Å. The unit cell parameters of the recombinant crotonase are: a = b = 68.0 Å, and c = 214.2 Å, with two molecules (hexamers) in the crystallographic unit cell. The space group is $P6_222$ with one molecule in the asymmetric unit. A cartoon of the packing model for crotonase is shown in Figure 5.8b. Simple circular shapes are used for convenience to represent each protein monomeric unit.

a

b

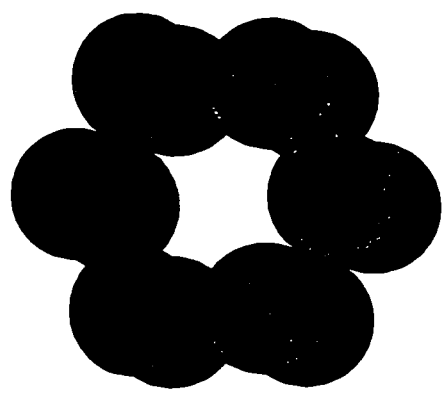

Figure 5.8 a) Microphotograph of crotonase crystals (largest dimension = 0.6 mm). b) Cartoon representation of the crotonase packing model. Each circle (yellow = front; blue = back) represents a monomeric subunit and the purple lines represent the hypothetical orientations of one Trp dipole.

5.3.2 The Singlet State & Heterogeneity

The emission maximum (Table 5.3) of the native protein in solution suggests a relatively buried (hydrophobic) Trp. In the presence of crotonyl-CoA (in solution), the average lifetime (2.1 ns) is quenched by 29% compared to crotonase in solution (τ_{ave}= 2.9 ns). The change in the pre-exponential terms and lifetimes may indicate a large conformational change upon binding of the substrate to the enzyme. On the other hand, the single Trp residue could be within the active site or in close proximity, such that each Trp conformer is quenched by the crotonyl-CoA to a different extent. Based on the degree of quenching, the latter explanation is likely. This hypothesis will be confirmed once the crystal structure has been determined.

The fluorescence of crystalline crotonase is best described by triple exponential decay kinetics, suggesting that three different Trp rotamers exist within different molecules of crotonase in the crystal.

The "c" values for the crystalline crotonase are within 7% of crotonase in solution. This result was expected based on the crotonase packing model (Figure 5.8b) in which there are a large possible number of Trp dipole orientations. Although the power to predict local secondary structure for a single Trp protein using the fluorescence "c" value cannot be generally applied, it is still valid for a given protein. Nonetheless, it is worthwhile to note the trend of the three "c" values and the data suggest the Trp is located within a β-sheet secondary structural segment of the protein (compare Tables 4.2 & 4.3 with Table 5.3).

Table 5.3 Time-resolved fluorescence decay parameters for crotonase in the presence and absence of crotonyl-CoA and in the crystalline state.

ID	†τ_1 (ns)	τ_2 (ns)	τ_3 (ns)	‡c_1 (α_1)	c_2 (α_2)	c_3 (α_3)	λ_{max} (nm)	SVR	σ
1	5.57	2.06	0.51	0.18	0.68	0.14	325	1.8	1.09
2	5.65	2.25	0.80	0.11	0.57	0.31	—	1.9	1.09
3	4.73	1.39	0.10	0.14	0.21	0.66	—	1.7	1.10
4	4.92	2.55	0.63	0.22	0.61	0.17	325	1.9	1.07

1) Results from decay-associated spectra (DAS, 12 wavelengths) of crotonase in solution (Buffer A).
2) Results from 350 nm emission of crotonase in solution (Buffer A).
3) Results from 350 nm emission of crotonase (Buffer A) in the presence of excess crotonyl-CoA.
4) Results from DAS (11 wavelengths) of crotonase crystal.
† Typical errors associated with τ_1, τ_2, and τ_3 were ± 0.02, 0.007 and 0.006 ns.
‡ In the case of the DAS results, the "c" values represent the relative proportion of each decay-time component over the entire spectrum, whereas, for single emission wavelengths, the α values are the normalized pre-exponential terms representing the relative proportion of each decay-time at a single wavelength.

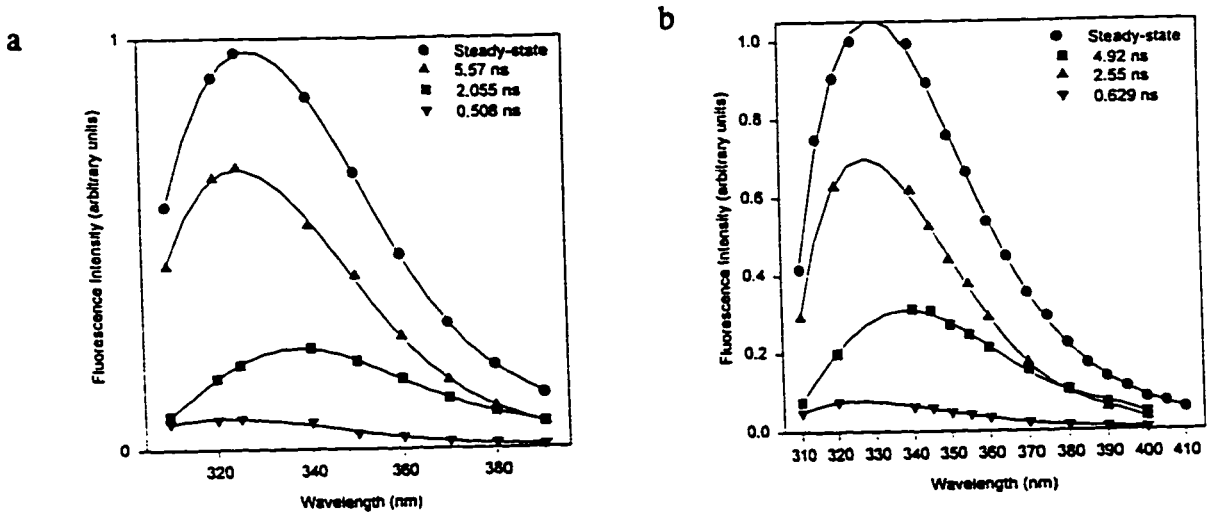

Figure 5.9 DAS of crotonase in solution (a) and in the crystalline state (b). The standard errors and statistics as specified in Table 5.3 apply. The DAS of crotonase in the crystalline state was measured at one protein crystal orientation.

Each lifetime value is slightly different between the solution and crystalline state with τ_1 becoming 12% shorter in the crystalline state, whereas, τ_2 and τ_3 become 24% longer in the crystal. The Trp average lifetime is 11% longer in the crystalline state (solution: τ_{ave} = 2.47 ns; crystal: τ_{ave} = 2.74 ns), implying the Trp is slightly shielded from local (within 7Å) side chain quenchers in the crystal (as compared to solution). The 2.055 ns and 0.508 ns components share a λmax of 325 nm, while the longer lifetime (5.57 ns) has a λmax between 325-340 nm (Figure 5.9). This intimates that the shorter two lifetimes arise from buried Trp conformers while the long lifetime arises from a conformation in a more polar environment.

5.3.3 The Orientation Experiment

This crotonase crystals provide an interesting crystallographic system for fluorescence study in light of the erabutoxin experiments, due to the large number of molecules in the crystallographic unit cell (twelve). If there are three different orientations of the indole ring in crotonase (predicted from the solution fluorescence decay kinetics), as well as twelve molecules in each crystallographic unit (Figure 5.8), then there would be a minimum of 36 (3 x 12) possible orientations for the Trp dipole in one crotonase crystal. This is essentially an isotropic arrangement of Trp transition dipoles and should effectively simulate crotonase in solution. Therefore, one would expect the orientation experiment to display little or no variation in the pre-exponential terms, since the crystal is rotated with respect to the vertically polarized laser beam.

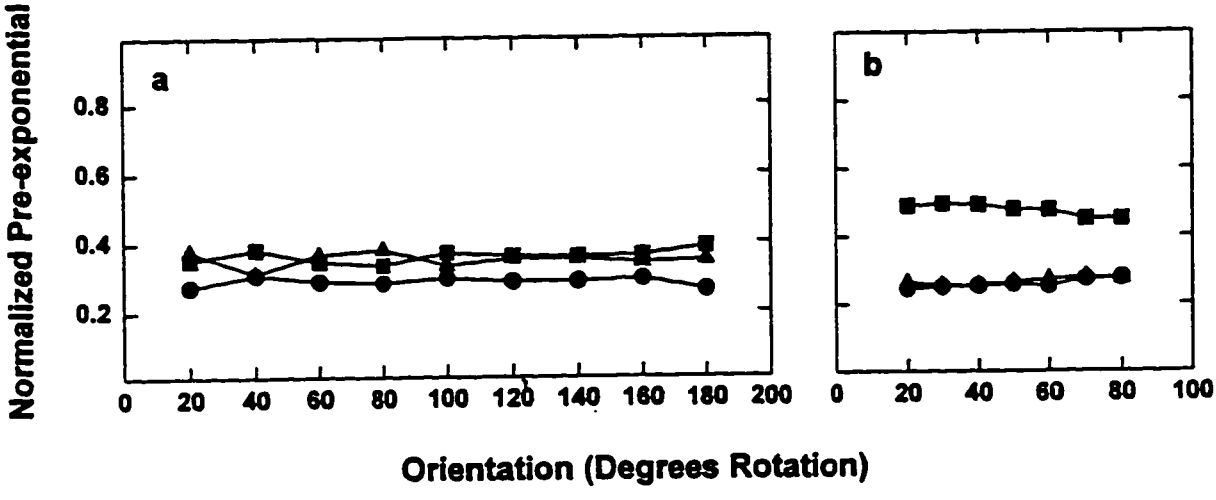

Figure 5.10 Dependence of the relative fluorescence decay-time component proportion on crystal orientation with respect to the polarization of the excitation beam. The curve is representative of measurements from individual crotonase crystals. ● 4.92 ns, ■ 2.55 ns, ▲ 0.629 ns.

As predicted, there was no significant variation of the normalized pre-exponential terms with crystal orientation (Figure 5.10; >180° rotation) in the several crystals measured. This lends further support to the interpretation of the normalized pre-exponential orientational variation found for crystalline erabutoxin b in terms of C^{α}-C^{β} Trp side chain rotamers (Dahms et al., 1995). Furthermore, the results show it is unlikely that the variation found for erabutoxin was the result of unusual light scatter from the crystal faces or other experimental artifacts characteristic of measuring crystals by time-resolved fluorescence.

3.4 Azurin

The bacterial azurins constitute a homologous class of metalloenzymes (Ambler & Brown, 1967; Ryden & Lundgren, 1976), which function as redox partners in bacterial electron transfer (Canters et al., 1990 & Van de Kamp et al., 1990). *Pseudomonas fluorescens* (*Pfl*, ATCC 13525) azurin is classified as a type I copper protein due to its characteristic blue absorption band; λ_{max}= 625 nm. The elucidation of the Cu^{2+} ligand site and the mechanism of the redox reaction have been the objective for most spectroscopic and structural studies of the various azurins.

Pfl holoazurin contains only one Trp residue at position 48, which provides a suitable intrinsic probe for fluorescence studies of its internal structural features. Several studies from this laboratory have focused on the metal binding properties and conformational heterogeneity of *Pfl* holoazurin (Szabo et al., 1983, Hutnik & Szabo, 1989a,b). Apoazurin was shown to display single exponential decay kinetics in solution, whereas, in the presence of either copper, cobalt or nickel, triple exponential decay kinetics were observed. These data imply that the presence of a metal centre imparts conformational heterogeneity upon the protein. It was proposed that this conformational change may be important in the mediation of the electron-transfer process. The long fluorescence decay time component (4 - 5 ns) observed for both *Pseudomonas aeruginosa* (*Pae*) and *Pfl* azurin in solution, was attributed to an apoazurin-like protein conformation, in which the Trp 48 is further from the Cu^{2+} binding site (Hutnik & Szabo, 1989a,b).

5.4.1 Evaluation of Protein Identity & Purity

In a previous report from this laboratory (Hutnik & Szabo, 1989a), which employed a similar purification procedure (excluding HPLC), atomic absorption and amino acid analysis revealed a 1:1 copper-protein complex for *Pfl* holoazurin with a spectral ratio of 0.50 or greater. The spectral ratio (620 nm/280 nm) of the protein is used as a criterion with which to establish purity of the holo form. The highest spectral ratio previously reported for *Pfl* holoazurin (Hutnik & Szabo, 1989a) was 0.55, which was considered homogeneous.

The HPLC CM-5PW holoazurin chromatogram (Figure 3.5) displays two major peaks which both have absorbance maxima at approximately 280 nm and 620 nm with no evidence of a Soret band (420 nm; absorption from contaminating cytochromes). The ratios of the two HPLC peaks seemed to vary dramatically (1:9 -> 7:3) between different batches of the *Pseudomonas fluorescens* bacteria. The subtle difference in the two apparent isoforms is evidenced in the HPLC separation (Figure 3.5). The concentrations of eluting Na^{2+} ions for each azurin species are only 4 mM apart in the salt gradient. The spectral ratio calculated for both the HPLC purified holoazurins was between 0.57 and 0.60. The apoazurin material was completely lacking an absorption band at 620 nm, indicating the complete absence of Cu^{2+}.

The holoazurin amino acid sequence has been determined in conjunction with this work (Figure 5.11; Lee et al., in press) and the isoelectric point determined to be 6.7. This is in accordance with the value approximated by isoelectric focussing (Hutnik & Szabo,

1989a). The original batch contained a larger proportion of HPLC peak A, therefore this material was used for protein sequencing and mass spectral analysis. The mass spectral data for this peak (13627.6 Da) is in excellent agreement with the isotope average mass calculated from the sequence (13625.6 Da). The sequence of HPLC peak A has been reported elsewhere (Lee et al., in press). The 2 mass unit difference is expected since the protein used for mass spectral analysis had been reduced, and the native protein has one disulphide linkage giving a difference of 2.016 Da. Addition of the hydrogen mass gives an observed mass of 13625.6 Da which is in exact agreement with the sequence data. The molecular weight was determined for both HPLC peaks and there was no difference within the accuracy of the ESI mass spectral method. The high resolution of the CM-5PW HPLC separation method may be separating two different conformers of the copper-bound protein, each having a slightly different net surface charge.

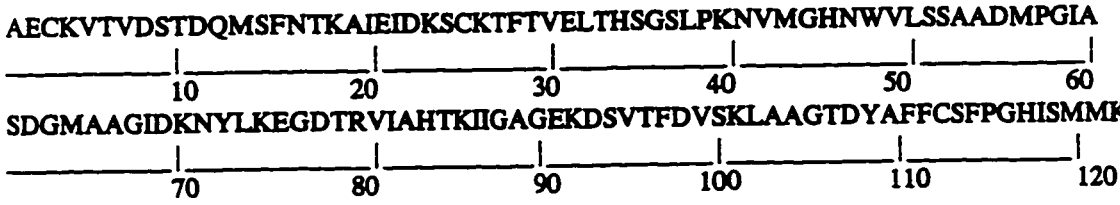

Figure 5.11 Primary sequence of Pseudomonas fluorescens azurin. The sequence was determined according to Lee et al. (in press).

Large crystals were obtained for both the holo (0.6 mm x 0.6 mm x 0.2 mm) and apo protein (0.2 mm x 0.2 mm x 0.07 mm) after sitting at room temperature for 10 days (Figure 5.12). The holoazurin crystals appear dark blue whereas the apoazurin crystals are clear and both can be described as chunky bipyramids. The cell parameters have been measured for both the holo (a = 31.95 = , b = 43.78 , c = 78.81) and apo protein (a = 31.91, b = 43.85 , c = 79.19) and can be considered identical. The larger holoazurin crystals diffracted to 2.05 Å, whereas the smaller apoazurin crystals diffracted to 2.4 Å.

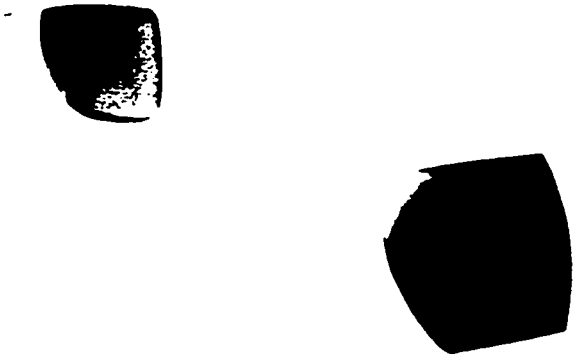

Figure 5.12 Microphotograph of *Pfl* holoazurin crystals (largest dimension = 0.6 mm). The apoazurin crystals were identical in shape to the holoazurin crystals, but were colourless due to the absence of Cu^{2+} and smaller (largest dimension = 0.2 mm).

5.4.2 The Singlet State & Heterogeneity

The steady-state fluorescence spectra of the apo and holoazurin give identical emission maxima (308 nm) in accordance with previous studies (Szabo et al., 1983). The blue-shifted spectral maxima (308 nm) observed for both the holo and apoazurin in solution was consistent with previous studies (Szabo et al., 1983) and is indicative of Trp in a very hydrophobic environment. These results are in agreement with the crystal structure (Lee et al., in press), which shows Trp to be contained within the hydrophobic interior of the protein (Figure 5.13).

Figure 5.13 Setor representation of *Pfl* holoazurin (Lee et al., in press). (Backbone random coil = green; β-sheet = yellow; α-helix = royal blue; Trp = beige & blue; Cu^{2+} = orange)

In the absence of copper, quenching of the Trp is dramatically reduced and only the long decay time is observed in agreement with previous studies (Hutnik & Szabo, 1989a). The single fluorescence decay time (Table 5.4) observed for the HPLC pure apoazurin material at pH 7.5 (4.683 ns ± 0.005 ns; SVR = 1.88; σ = 1.06; λ_{ex}= 292 nm; λ_{max}= 335 nm) was shorter than that previously measured (5.10 ns ± 0.01 ns; Hutnik & Szabo, 1989a). This result was expected based on holoazurin pH studies, in which the long lifetime value becomes shorter with increasing pH. At pH 5.0 the long decay time value for holoazurin is 4.95 ns, whereas, it becomes 4.71 ns at pH 7.0 (Hutnik & Szabo, 1989a). A similar pH dependence is expected for the apoazurin.

The time-resolved fluorescence decay of *Pfl* holoazurin is best described by triple exponential decay kinetics with lifetime values similar to those previously measured (Hutnik & Szabo, 1989a). The DAS of *Pfl* holoazurin was measured in 200 mM Tris pH 7.5 buffer consistent with crystallization conditions (Table 5.4). The largest contributor to the fluorescence is the shortest lifetime component with relatively low contributions from the intermediate and long lifetimes. The lifetime values determined from the global analysis of 9 data sets (300 nm - 350 nm) measured for HPLC pure holoazurin are virtually identical to those determined at single wavelengths and similar pH (Hutnik & Szabo, 1989a). The two shortest decay-times contribute the most to the total fluorescence in all cases (0.91 - 0.94) and have been attributed to quenching effects from the Cu^{2+} ligand, whereas, the longer decay time would arise from a structure in which the Cu^{2+}-ligand complex was further away from the Trp residue.

Table 5.4 Time-resolved fluorescence decay parameters for *Pfl* holo- and apoazurin and in solution and in the crystalline state.

ID	$^{\dagger}\tau_1$ (ns)	$^{\dagger}\tau_2$ (ns)	$^{\dagger}\tau_3$ (ns)	$^{\dagger}\tau_4$ (ns)	$^{*}c_1$ (α_1)	$^{*}c_2$ (α_2)	$^{*}c_3$ (α_3)	$^{*}c_4$ (α_4)	SVR	σ
Holo solution										
1	4.91	0.52	0.105	—	0.09	0.06	0.85	—	—	—
2	4.56	0.76	0.104	—	0.05	0.03	0.92	—	1.95	1.01
3	4.49	0.46	0.101	—	0.02	0.03	0.95	—	1.91	1.02
Holo crystal										
4	2.546	0.31	0.082	—	0.06	0.08	0.86	—	1.91	1.04
5	2.769	1.36	0.167	0.0537	0.14	0.01	0.52	0.33	1.80	1.08
Apo solution	4.683	—	—	—	1	—	—	—	1.88	1.06
Apo crystal	3.786	—	—	—	1	—	—	—	1.90	1.07

1) Time-resolved fluorescence parameters for Pfl. holoazurin (λ_{em}= 310 nm) prior to HPLC purification (Hutnik & Szabo, 1989b).
2) Time-resolved fluorescence parameters for Pfl. holoazurin (λ_{em} = 310 nm) HPLC #1.
3) Time-resolved fluorescence parameters for Pfl. holoazurin (λ_{em}= 310 nm) HPLC #2.
4) Time-resolved fluorescence parameters for Pfl. holoazurin (λ_{em}= 310 nm) in the crystalline state.
5) Time-resolved fluorescence parameters from the DAS (8 wavelengths) of Pfl holoazurin in the crystalline state.

† Standard errors were on the order of ± (0.04 - 0.005), ± (0.04 - 0.01), ± (0.005 - 0.001) and ± 0.0005 for τ_1, τ_2, τ_3 and τ_4, respectively.

‡ In the case of the DAS results, the "c" values represent the relative proportion of each decay-time component whereas for single emission wavelengths, the α values are the normalized pre-exponential terms representing the relative proportion of each decay-time at a single wavelength.

Apoazurin crystals, as in solution, exhibit a spectral maximum at 308 nm and display single exponential decay kinetics (Table 5.4). Preliminary investigation of the crystalline apoazurin revealed double exponential decay kinetics with a long lifetime (2.82 ns) and an intermediate decay time value (0.86). Given the similarity between these values and those measured for the crystalline holoazurin, it was postulated that the apoazurin crystals had

leached Cu^{2+} from the siliconized microscope slides used in the vapour diffusion process. This hypothesis was tested by allowing a sample of apoazurin (solution), which displayed single exponential decay kinetics, to sit in the fridge in a glass test tube for several weeks (crystallization time). The resultant material displayed double exponential decay kinetics and exhibited a small 620 nm absorbance. When the apoazurin crystals were grown on plastic microscope slides using crystallization buffers which had been pre-treated with Chelex, this problem was avoided and single exponential decay kinetics (3.786 ns $\pm$ 0.003 ns, SVR = 1.90, σ = 1.07) were observed. The detection of such a small contaminant demonstrates the high sensitivity of this method and instrumentation. This result also provides further support for the rotamer model of Trp photophysics, since single exponential decay kinetics were predicted based on the solution fluorescence properties. Apoazurin is one of a very few proteins to display single-exponential fluorescence decay kinetics in solution. The lifetime value for crystalline apoazurin (3.786 ns) is shorter than that observed in solution (4.683 ns). In this case quenching must arise from a closer contact of amino acid side chains surrounding the Trp (within 7 Å), due to the constrained nature of the crystals. This also suggests that the shorter average lifetime observed for the crystalline holoazurin is not solely due to a closer proximity of the Cu^{2+} ligand, but also, other surrounding residues.

The apparent emission maximum of the crystalline holoazurin is longer ($\approx$ 320 nm) than in solution (308 nm). However this value is not necessarily accurate, since the raman scattering of water (323 nm emission at 292 nm excitation) did not allow for the accurate measurement of emission between 313 nm and 333 nm, and thus the maximum may be a

false product of the regression used by the plotting program.

The global analysis of holoazurin in solution at 8 wavelengths (300 nm - 350 nm) revealed that the best statistical fit was to four decay times (Table 5.4). The average lifetime value for the crystalline holoazurin is shorter than that observed in solution. This is consistent with previous studies on crystalline erabutoxin b (Dahms et al., 1995). Due to crystal packing constraints it is likely that the Trp of crystalline holoazurin is closer in proximity to the Cu^{2+} and therefore more highly quenched. Data measured at separate wavelengths could be fit very well to three decay times, however global analysis at all wavelengths revealed four decay time values. A possible explanation for the latter observation is as follows: In solution there are actually four discrete Trp side chain rotamers for which the lifetimes of two of these rotamers are very close in value. Therefore, triple exponential decay kinetics are observed. In the crystalline state, these lifetime values are resolved due to the slightly altered arrangement of one of the Trp environments.

The mechanism for the quenching of Trp by copper is a matter for speculation however in previous studies Hutnik & Szabo (1889a) proposed there was either an electron transfer from the excited state of Trp to the copper centre, or, an interaction between the charge-transfer excited state of Trp and the electronic structure of the copper-ligand complex. From the crystallographic data (Lee et al., in press), which would report on the most abundant conformer (shortest decay time), it seems there can be no direct interaction between the indole ring and the copper-ligand complex. The Trp is 8.17 Å from the copper centre and it is likely that electron transfer occurs indirectly through the ring system of a nearby

phenylalanine (Teale & Weber, 1958). The Phe15 is directly between the Cu^{2+} and Trp residue, with 5.94 Å between Phe15 and the Cu^{2+} and 4.31 Å between Phe15 and Trp48.

5.4.3 The Orientation Experiment

When single *Pfl.* holoazurin crystals were rotated with respect to the plane of polarization, variation of the pre-exponential terms was observed (Figure 5.14). It is very interesting to note the patterns in variation can be divided into two subsets which include the two longer decay times (2.769 ns & 1.36 ns) and the two shorter decay times (0.167 ns & 0.054 ns). Within each set of values, the pre-exponential terms vary inversely.

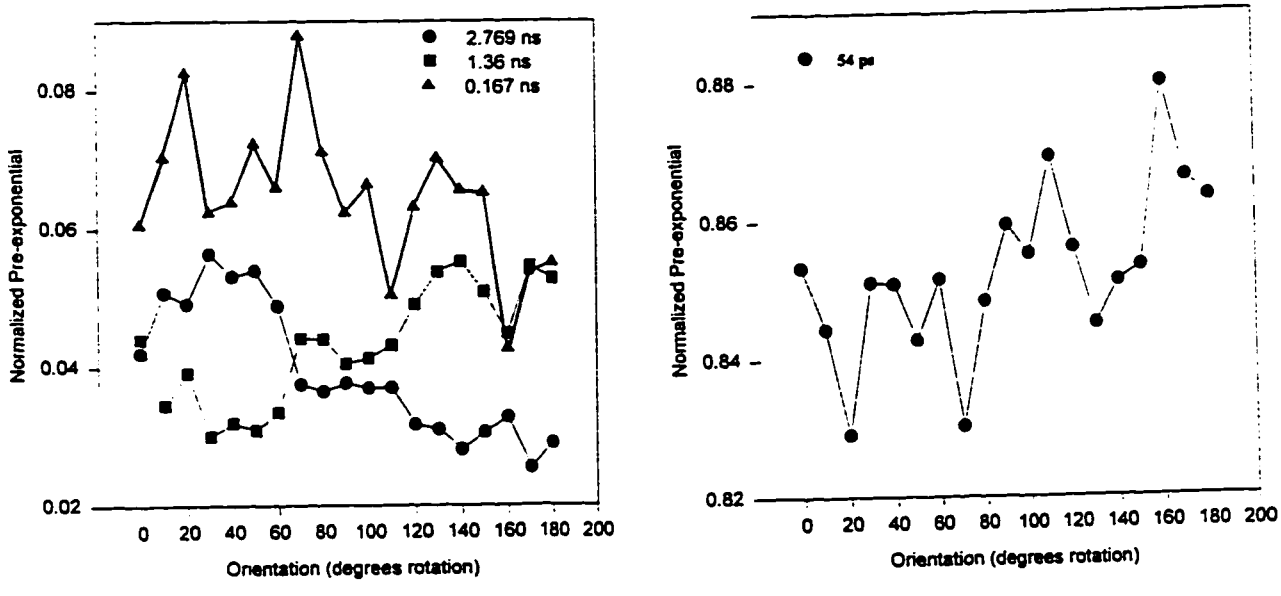

Figure 5.14 Dependence of the relative fluorescence decay-time component proportion on crystal orientation with respect to the polarization of the excitation beam. The curve is representative of measurements from individual *Pfl* holoazurin crystals. ● 2.769 ns, ■ 1.36 ns, ▲ 0.167 ns ▼ 54 ps.

This inverse relationship could easily be the result of two distinct χ_2 Trp conformers (180° ring flip) for which the L_a dipoles of the two indole rings would lie orthogonal to one other, producing the inverse variation of the pre-exponential terms (Figure 5.15). The two subsets of lifetimes may therefore arise from two different ligand complexes. A pH-induced conformational transition has been detected in *Ps. aeruginosa* oxidized azurin crystals when studied at pH 5.5 and pH 9.0 (Huber et al., 1991). Since the crystals were grown at pH 7.5, it is reasonable to assume that there may be a mixture of protein conformational states. Although two discreet protein conformations are not detected for the *Pfl.* holoazurin by X-ray crystallography, significant disorder is observed in the region of the backbone near the Trp residue. Furthermore, the EPR X-band spectra (Brill, 1978) demonstrate fluctuations in the geometry of the liganded copper complex of *Pfl.* holoazurin in solution, and the NMR spectra (Canters et al., 1990) indicate two azurin conformers with very small local structural differences. Time-resolved fluorescence is sensitive enough to detect such structural subtleties. It seems reasonable to propose that the two longer decay components arise from an azurin structure in which the copper to Phe 15 or Phe 15 to Trp 48 distance is longer, resulting in less quenching from the copper. The two shorter decay components would arise from a conformer where the copper ligand complex is closer to Trp 48 as observed in the crystal structure. The crystallographic structure can only represent the most abundant protein conformation, which would contribute the most to fluorescence and that corresponds to the shortest decay components.

Figure 5.15 Theoretical orientation of Trp χ_2 rotamers in *Pfl* holoazurin (backbone = blue, Trp = purple, beige.)

5.4.4 The Triplet State

During the original experiments with erabutoxin b crystals, a faint blue luminescence was observed when the crystal position had been adjusted for optimal excitation. This blue emission was proposed to be room temperature phosphorescence and was observed for all protein crystals studied. The observation of room temperature phosphorescence from a crystal in an oxygen-saturated environment was somewhat unexpected. The relative steady-state phosphorescence spectra was measured according to the procedure outlined for fluorescence in Chapter 3, however the values were not corrected using a standard. The

integrated decay curve values were plotted against wavelength to yield an uncorrected steady-state spectrum for holoazurin (Figure 5.16). The phosphorescence curve is characteristic of that observed for Trp in a protein (aqueous solution) at low temperature (Saviotti & Galley, 1974). This result demonstrates the possibility of measuring room temperature phosphorescence for proteins when in the crystalline state, and this technique may have future applications.

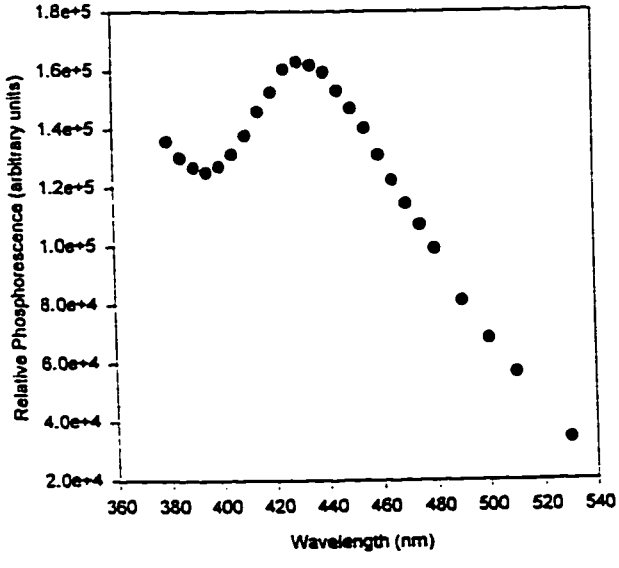

Figure 5.16 Steady-state, room temperature phosphorescence of *Pfl* holoazurin crystals (uncorrected spectrum).

5.5 Conclusions

The orientation dependent fluorescence decay experiments for single protein crystals, combined with the simulations of the orientation dependence of the pre-exponential terms,

provides strong evidence to support the rotamer model for the interpretation of time-resolved fluorescence parameters in proteins. The observation of conformational heterogeneity for Trp in a protein crystal, which was previously reported to be in a single side chain configuration, has important implications for protein X-ray crystallographic studies. It suggests that a reexamination of the X-ray data for evidence of Trp side chain rotamers is warranted. There are only two protein crystal structures in the Brookhaven data bank exhibiting two separate conformations of the Trp side chain and both these structures are highly resolved (0.86 Å for gramicidin (1gma.pdb) and 1.5 Å for relaxin (6rlx.pdb); Bernstein et al., 1977). Perhaps as more protein crystal structures are determined to higher resolution, modelling of alternate Trp side chain rotamers will become more frequent. Identification of conformational heterogeneity by very sensitive time-resolved fluorescence techniques and other methods, may provide improved levels of structural detail and lead to new insights into the structure-function relationships of proteins.

From the few protein crystals which have studied by time-resolved fluorescence, a pattern has begun to emerge: proteins which display multi-exponential fluorescence decay in solution will exhibit a similar phenomena in the crystalline state and these different decay time values can be attributed to different Trp rotamers. The only protein to be measured in the crystalline state which has single exponential decay kinetics in solution exhibits a single decay time in solution. Since most single Trp proteins display more than one decay time in solution, it follows that it is common for the Trp side chain to adopt more than one low energy conformation. On the other hand, crystallographic studies have modelled Trp almost

exclusively in a single conformation. This discrepancy can be explained by limitations in the data obtained by X-ray crystallography: unless a conformer is present as > 33% it can not be detected with an electron density map with a resolution of 1.4 Å or greater. If conformational heterogeneity is so common, then this phenomena could be very important to the function of most proteins. In the case of holoazurin, the conformational heterogeneity imparted by the copper-ligand may be key to the process of electron transfer.

Part IV: Future Directions

Suggestions for Future Work

The focus of this dissertation has been the analysis of a biophysical technique, namely fluorescence, as it applies to the study of proteins. This work has answered many questions, but in doing so, has pointed towards other interesting experiments. Therefore, it is appropriate to briefly outline some future applications of the techniques which have been developed and outlined in this dissertation.

6.1 Solutions Studies

Single Trp mutants can be manufactured for almost any protein of interest using site-directed mutagenesis. If Trp was placed in different positions of the protein, an entire set of single Trp proteins could be manufactured. Such an experimental system would allow for the systematic study of protein folding and/or unfolding, using the fluorescence "c" values and techniques outlined in Chapter 4.

6.2 Crystal Studies

Given the precise relationship between the Trp rotamer coordinates and the coordinates of the crystal faces, it should be possible to calculate the other rotamer angles. This relationship could be obtained from the crystal cell parameters and time-resolved fluorescence measurements at specific crystal orientations (with respect to the polarized excitation source). The identification of the alternate Trp rotamers may lead to the eventual rationalization of non-radiative deactivation pathways for the excited singlet state of Trp.

References

Ambler, R. P., & Brown, L. H. (1967) The amino acid sequence of *Pseudomonas fluorescens* azurin. *Biochem. J.* **104**, 784-825.

Ambler, R. P., & Wynn, M. (1973) The amino acid sequences of cytochromes c-551 from three species of *Pseudomonas*. *Biochem. J.* **131**, 485-498.

Brill, A. S. (1978) Activation of electron transfer reactions of the blue proteins. *Biophys. J.* **22**, 139-142.

Basus, V. J., Billeter, M., Love, R. A., Stroud, R. M. & Kuntz, I. D. (1988) Structural studies of α-bungarotoxin. 1. Sequence-specific ^{1}H NMR resonance assignments. *Biochemistry* **27**, 2763-2771.

Becker, R. S. (1969) Theory and Interpretation of Fluorescence and Phosphorescence, John Wiley and Sons, New York, NY, USA.

Beechem, J. M. & Brand, L. (1985). Time-resolved fluorescence of proteins. *Annu. Rev. Biochem.* **54**, 43-71.

Bernstein, F.C., Koetzle, T.F., Williams, G.J.B., Meyer, E.F., Jr, Brice, M.D., Rodgers, J.R., Kennard, O., Shimanouchi, T., & Tasumi, M. (1977). The protein data bank: A computer based archival file for macromolecular structures. *J. Mol. Biol.* **112**, 535-542.

Bhat, T. N., Sasisekharan, V. & Vijayan, M. (1979) An analysis of side-chain conformation in proteins. *Int. J. Protein Res.* **13**, 170-184.

Birch, D. J. S. & Imhof, R. E. (1991) Time Domain Fluorescence Spectroscopy Using Time-Correlated Single Photon Counting in Topics in Fluorescence Spectroscopy, v1, Plenum Press, New York, NY, USA.

Branden, C. & Tooze, J. (1991) Introduction to Protein Structure, Garland Publishing, Inc., New York, NY, USA.

Burley, S. K. & Petsko, G. A. (1986) Amino-aromatic interactions in proteins. *FEBS Lett.* **203**, 139-143.

Canonica, S. & Wild, U. P. (1985) Single photon counting with synchronously pumped dye laser excitation. *Anal. Instr.* **14**, 331-357.

Canters, G. W., Lommen, A., Van de Kamp, M. & Hoitink, C. W. G. (1990) Structure and reactivity of type-I copper sites. *Biol. Met.* **3**, 67-72.

Cantor, C. R. & Schimmel, P. R. (1980) Biophysical Chemistry, W. H. Freeman and Company, San Francisco, USA.

Chandrasekaran, R. & Ramachandran, G. N. (1970) Studies on the conformation of amino acids. XI. Analysis of the observed side group conformations in proteins. *Int. J. Protein Res.* **2**, 223-233.

Chang, M. C., Courtney, S. H., Cross, A. J., Gulotty, R. J., Petrich, J. W. & Fleming, G. R. (1985) Time-correlated single photon counting with microchannel plate detectors. *Anal. Instr.* **14**, 433-464.

Chang, M. C., Petrich, J. W., MacDonald, D. B. & Fleming, G. R. (1983) Nonexponential fluorescence decay of tryptophan, tryptophylglycine, and glycyltryptophan. *J. Am. Chem. Soc.* **105**, 3819-3832.

Colucci, W. J., Tilstra, L., Sattler, M. C., Fronczek, F. R. & Barkley, M. D. (1990) Conformational studies of a constrained tryptophan derivative: implications for the fluorescence quenching mechanism. *J. Am. Chem. Soc.* **112**, 9182-9190.

Coates, P. B. (1968) The correction for photon "pile-up" in the measurement of radiative lifetimes. *J. Phys. E.* **1**, 878-879.

Cowgill, R. W. (1976) Tyrosyl Fluorescence in Proteins and Model Peptides. *In* Biochemical Fluorescence Concepts. Chen, R. F. and Edelhoch, H., Eds, Marcel Dekker Inc., New York, NY, USA. 441-486.

Cowgill, R. W. (1970) Fluorescence and the structure of proteins. XVIII. Spatial requirements for quenching by disulphide groups. *Biochim. Biophys. Acta* **207**, 556-559.

Cowgill, R. W. (1967) Fluorescence and protein structure. X. Reappraisal of solvent and structural effects. *Biochim. Biophys. Acta* **133**, 6-18.

Cowgill, R. W. (1963) Fluorescence and the structure of proteins. I. Effects of substituents on the fluorescence of indole and phenol compounds. *Arch. Biochim. Biophys.* **100**, 36-44.

Dahms, T. E. S., Willis, K. J. & Szabo, A. G. (1992) Fluorescence Decay Kinetics of Highly Purified Neurotoxins. *Biophys. J.* **61**, A1041.

Dahms, T. E. S., Willis,K. J. & Szabo, A. G. (1995) Conformational Heterogeneity of Tryptophan in a Protein Crystal. *J. Am. Chem. Soc.* **117**, 2321-2326.

Demas, J. N. & Crosby, G. A. (1971) The measurement of photoluminescence quantum efficiencies. *J. Res. Natl. Bur. Stds - A. Phys. Chem.* **76A**, 561-577.

Donzel, B., Gauduchon, P. & Wahl, Ph. (1974) Study of the conformation in the excited state of two tryptophanyl diketopiperazines. *J. Am. Chem. Soc.* **96**, 801-808.

Dunbrack, R. L. Jr. & Karplus, M. (1993) Backbone-dependent rotamer library for proteins. Application to side-chain prediction. *J. Mol. Biol.* **230**, 543-574.

Durbin, J. & Watson, G. S. (1951) Testing for serial correlation in least squares regression. II. *Biometrika* **38**, 159-178.

Durbin, J. & G. S. Watson. 1971. Testing for serial correlation in least squares regression. III. *Biometrika* 58:1-19.

Eftink, M. R.& Wasylewski Z. (1992) Time-resolved fluorescence studies of the thermal and guanidine induced folding of nuclease A and its unstable mutant. *In* Time-Resolved Spectroscopy in Biochemistry III. *SPIE* **1640**, 579-584.

Eftink, M. R. (1990) Fluorescence Techniques for Studying Protein Structure. *In* Protein Structure Determination, Suelter, C. H., Ed., John Wiley & Sons, New York, NY, USA. **v35**, 127-205.

Eisinger, J. (1969) A variable temperature, U.V. luminescence spectrograph for small samples. *Photochem. Photobiol.* **9**, 247-258.

Eisinger, J. & Flores, J. (1979) Front-face fluorometry of liquid samples. *Anal. Biochem.* **94**, 15-21.

Evans, S. V. SETOR: Hardware-lighted three-dimensional solid model representations of macromolecules. *J. Mol. Graphics* **11**, 134-138.

Fasman, G. D., ed. (1967) Poly-α-Amino Acids, Marcel Dekker, New York, NY, USA.

Fersht, A. R. (1993) Protein folding and stability: the pathway of folding of barnase. *FEBS LETT.* **325**, 5-16.

Fiamingo, F. G., Brill, A. S., Hampton, D. A. & Thorkildsen, R. (1989) Energy distributions at the high-spin ferric sites in myoglobin crystals. *Biophys. J.* **55**, 67-77.

Freedman, R. B., Brockway, B. E. & Lambert, N. (1984) Protein disulphide-isomerase and the formation of native disulphide bonds. *Biochem. Soc. Trans.* **12**, 929-932.

Freifelder, D. M. (1982) Physical Biochemistry: Applications to Biochemistry and Molecular Biology, 2nd ed., W. H. Freeman and Company, New York, NY, USA.

Gelin, B. R. & Karplus, M. (1979) Side-chain torsional potentials: Effect of dipeptide, protein and solvent environment. *Biochemistry* **18**, 1256-1268.

Goldberg, M. E. (1985) The second translation of the genetic message: protein folding and assembly. *Trends Biochem. Sci.***10**, 388-391.

Gordon, H. L., Jarrell, H. C., Szabo, A. G., Willis, K. J. & Somorjai, R. L. (1992). Molecular dynamics simulations of the conformational dynamics of tryptophan. *J. Phys. Chem.* **96**, 1915-1921.

Grinvald, A., & Steinberg, I. Z. (1976) The fluorescence decay of tryptophan residues in native and denatured proteins. *Biochim. Biophys. Acta* **427**, 663-678.

Harris, C. M. & Selinger, B. K. (1979) Single-photon decay spectroscopy. II. The pile-up problem. *Aust. J. Chem.* **32**, 2111-2129.

Harris, D. L. & Hudson, B. S. (1990). Photophysics of tryptophan in bacteriophage T4 lysozymes. *Biochemistry* **29**, 5276-5285.

Hider, R., Drake, A., Inagaki, F., Williams, R., Endo, T. & Miyazawa, T. (1982) The molecular conformation of α-cobratoxin as studied by nuclear magnetic resonance and circular dichroism. *J. Mol. Biol.* **158**, 275-291.

Hogue, C. W. V. (1994) Fluorescence Studies of Tryptophanyl tRNA Synthetase. University of Ottawa Press, Ottawa, ON, Canada.

Hutnik, C. M. L., MacManus, J. P., Banville, D. & Szabo, A. G. (1991). Metal-induced changes in the fluorescence properties of tyrosine and tryptophan site-specific mutants of oncomodulin. *Biochemistry* **30**, 7652-7660.

Hutnik, C. M. L. (1989) The conformational heterogeneity of proteins. University of Ottawa Press, Ottawa, ON, Canada.

Hutnik, C. M., & Szabo, A. G. (1989a) Confirmation That Multiexponential Fluorescence Decay Behaviour of Holoazurin Originates from Conformational Heterogeneity. *Biochemistry* **28**, 3923-3934.

Hutnik, C. M., & Szabo, A. G. (1989b) A Time-Resolved Fluorescence Study of Azurin and Metallo Azurin Derivatives. *Biochemistry* **28**, 3935-3939.

IUPAC-IUB Commission on Biochemical Nomenclature (1970) Abbreviations and symbols for the description of the conformation of polypeptide chains. Tentative rules (1969). *Biochemistry* **9**, 3471-3479.

Inagaki, F., Tamiya, N.& Miyazawa, T. (1980) Molecular Conformation and Function of Erabutoxins as Studied by Nuclear Magnetic Resonance. *Eur. J. Biochem.* **109**, 129-138.

Inagaki, F., Hider, R. C., Hodges, S. J. & Drake, A. F. (1985) Molecular Conformation of α-bungarotoxin as studied by nuclear magnetic resonance and circular dichroism. *J. Mol. Biol.* **183**, 575-590.

Ito, A. S., Castrucci, A. M. de L., Hruby, V. J., Hadley, M. E., Krajcarski, D. T. & Szabo, A. G. (1993) Structure-Activity Correlations of Melanotropin Peptides in Model Lipids by Tryptophan Fluorescence Studies. *Biochemistry* **32**, 12264-12272.

Jablonski, A. (1935) Über den mechanismus des photolumineszenz von farbstoff-phosphoren. *Z. Phys.* **94**, 38-46.

James, M. N. G. & Sielecki, A. R. (1983) Structure and refinement of penicillopepsin at 1.8 Å resolution. *J. Mol. Biol.* **163**, 299-361.

Janin, J., Wodak, S., Levitt, M. & Maigret, B. (1978) Conformations of amino acid side-chains in proteins. *J. Mol. Biol.* **125**, 357-386.

Kilhofer, M. C., Kubina, M., Travers, F. & Haiech, J., (1992). Use of engineered proteins with internal tryptophan reporter groups and perturbation techniques to probe the mechanism of ligand-protein interactions: Investigation of the mechanism of calcium binding to calmodulin. *Biochemistry* **31**, 8098-8106.

Kirby, E. P. (1971) Fluorescence instrumentation and methodology. In: Excited States of Proteins and Nucleic Acids, R. F. Steiner & I. Winryb, Eds., Plenum Press, New York, NY, USA.

Knutson, J. R., Beechem, J. M. & Brand, L. (1983) Simultaneous analysis of multiple fluorescence decay curves: A global approach. *Chem. Phys. Lett.* **102**, 501-507.

Knutson, J. R., Walbridge, D. G. & Brand, L. (1982) Decay-associated fluorescence spectra and the heterogeneous emission of alcohol dehydrogenase. *Biochemistry* **21**, 4671-4679.

Lakowicz, J. R. (1983) Principles of Fluorescence Spectroscopy, Plenum Press, New York, NY, USA.

Le Goas, R., LaPlante, S. R., Mikou, A., Delsuc, M.-A., Guittet, E., Robin, M., Charpentier, I. & Lallemand, J.-Y. (1992) α-cobratoxin: Proton NMR assignments and solution structure. *Biochemistry* **31**, 4867-4875.

Lehninger, A. L. (1981) Biochemistry, 2nd ed., Worth Publishers Inc., New York, NY, USA.

Lin, S.-L., Stern, E. S., Kalb (Gilboa), A. J. & Zhang, Y. (1990) Evidence from X-ray absorption fine structure spectroscopy for significant differences in the structure of concanavalin A in solution and in the crystal. *Biochemistry* **29**, 3599-3603.

Love, R.A. & Stroud R. M. (1986) The crystal structure of α-bungarotoxin at 2.5 Å resolution: relation to solution structure and binding to acetylcholine receptor. *Protein Eng.* **1**, 37-46.

Low, B. W., Preston, H. S., Sato, A., Rosen, L. S., Searl, J. E., Rudko, D. & Richardson, J. S. (1976) Three dimensional structure of erabutoxin b neurotoxic protein: Inhibitor of acetylcholine receptor. *Proc. Natl. Acad. Sci. USA* **73**, 2991-2994.

Marquardt, D. W. (1963) An algorithm for least-squares estimation of nonlinear parameters. *J. Soc. Ind. Appl. Math* **11**, 431-441.

McGregor, M. J., Islam, S. A. & Sternberg, M. J. E. (1987) Analysis of the relationship between side-chain conformation and secondary structure in globular proteins. *J. Mol. Biol.* **198**, 295-310.

McKinnon, A. E., Szabo, A. G. & Miller, D. R. (1977) The deconvolution of photoluminescence data. *J. Phys. Chem.* **81**, 1564-1570.

Melhuish, W. H. (1955) The measurement of absolute quantum efficiencies of fluorescence. *New Zealand J. Sci. Technol.* **37**, 142-149.

Ménez, A., Montenay-Garestier, T., Fromageot, P. & Hélène, C. (1980) Conformation of two homologous neurotoxins. Fluorescence and Circular Dichroism Studies. *Biochemistry* **19**, 5202-5208.

Miller, J. N. (1981) Correction of excitation and emission spectra. In: Standards in Fluorescence Spectrometry, Chapman & Hall, New York, NY, USA.

O'Connor, D. V. & Phillips, D. (1984) Time-Correlated Single Photon Counting, Academic Press, London, England, UK.

Parker, C. A. (1958) Direct recording of fluorescence excitation spectra. *Nature* **182**, 1002-1004.

Pavia, D. L., Lampman, G. M. & Kriz, G. S. Jr. (1979) Introduction to Spectroscopy, Saunders College Publishing, Philadelphia, NY, USA.

Penzer, G. R. (1980) An Introduction to Spectroscopy, S. B. Brown, Ed., Academic Press, London, England, UK.

Phillips, D., Drake, R. C., O'Connor, D. V. & Christensen, R. L. (1985) Time correlated single-photon counting (TCSPC) using laser excitation. *Anal. Instr.* **14**, 267-292.

Philips, L. A., S. P. Webb, S. J. Martinez, III, G. R. Fleming, and D. H. Levy. 1988. Time-resolved spectroscopy of tryptophan conformers in a supersonic jet. *J. Am. Chem. Soc.* *110*:1352-1355.

Piela, L., G. Nemethy & Scherga, H. A. (1987) Conformational constraints of amino acid side chains in α-helices. *Biopolymers* **26**, 1273-1286.

Pilulik, L. G. & Solomakho, M. A. (1960) On the influence of temperature on the electronic spectra of complex molecules. *Opt. Spectrosc.* **8**, 176-178.

Ponder, J. W. & Richards, F. M. (1987) Tertiary templates for proteins. Use of packing criteria in the enumeration of allowed sequences for different structural classes. *J. Mol. Biol.* **193**, 775-791.

Rabek, J. F. (1982) Experimental Methods in Photochemistry and Photophysics, Part 1, John Wiley & Sons, New York, NY, USA.

Ramachandran, G. N., Ramakrishnan, C. & Sasisekharan, V. (1963) Stereochemistry of polypeptide chain configuration. *J. Mol. Biol.* **7**, 95-99.

Rayner, D. M. & Szabo, A. G. (1978) Time resolved fluorescence of aqueous tryptophan. *Can. J. Chem.* **56**, 1238-1245.

Rhodes, G. (1993) Crystallography Made Crystal Clear: A Guide for Users of Macromolecular Models, Academic Press, Inc., San Diego, CA, USA.

Richardson, J. S. (1981) The anatomy and taxonomy of protein structure. *Adv. Protein Chem.* **34**, 167-339.

Ross, J. B. A., Wyssbrod, H. R., Porter, R. A., Schwartz, G. P., Michaels, C. A. & Laws, W. R. (1992). Correlation of tryptophan fluorescence intensity decay parameters with 1H NMR-determined rotamer conformations: [Tryptophan2]-oxytocin. *Biochemistry* **31**, 1585-1594.

Rothgeb, T. M. & Oldfield, E. (1981) Nuclear magnetic resonance of heme protein crystals. *J. Biol. Chem.* **256**, 1432-1446.

Ryden, L., & Lundgren, J.-O. (1976) Homology relationships among the small blue proteins. *Nature* **261**, 344-346.

Sage, J. T., Morikis, D. & Champion, P. M. (1989) Resonance raman studies of oriented chromophores: Metmyoglobin single crystals. *J. Chem. Phys.* **90**, 3015-3032.

Saviotti, M. L. & Galley, W.C. (1974) Room temperature phosphorescence and the dynamic aspects of protein structure. *Proc. Natl. Acad. Sci. USA* **71**, 4154-4158.

Schrauber, H., Eisenhaber, F. & Argos, P. (1993) Rotamers: To be or not to be? An analysis of amino acid side-chain conformations in globular proteins. *J. Mol. Biol.* **230**, 592-612.

Smith, J. L., Corfield, P. W. R., Hendrickson, W. A. & Low, B. W. (1988) Refinement at 1.4 Å resolution of a model of erabutoxin b: Treatment of ordered solvent and discrete disorder. *Acta Crystallog.* **44(A)**, 357-368.

Smith, J. L., Hendrickson, W. A., Honzatko, R. B. & Sheriff, S. (1986) Structural heterogeneity in protein crystals. *Biochemistry* **25**, 5018-5027.

Sober, H. A. (1970) CRC Handbook of Biochemistry, 2nd ed. The Chemical Rubber Co., Cleveland, OH, USA.

Spencer, R. D. & Weber, G. (1970) Influence of brownian rotations and energy transfer upon the measurements of fluorescence lifetime. *J. Chem. Phys.* **52**, 1654-1663.

Steiner, R. F. (1991) Fluorescence Anisotropy: Theory and Applications in Topics in Fluorescence Spectroscopy, Lakowicz, J. R. Ed., v2, Plenum Press, New York, NY, USA.

Steinman, H. M. & Hill, R. L. (1975) Bovine liver crotonase (Enoyl Coenzyme A Hydratase). EC 4.2.1.17 L--3-Hydroxyacyl-CoA hydrolyase. *In Methods in Enzymol.* **v35**, 136-151.

Stern, J.R., del Campillo, A. & Raw, I. (1956) Enzymes of fatty acid metabolism. I. General introduction: Crystalline crotonase. *J. Biol. Chem.* **218**, 971-983.

Stokes, G. G. (1852) On the change of refrangibility of light. *Phil. Trans. R. Soc. London* **142**, 463-562.

Stryer, L. (1989) Molecular Design of Life, W. H. Freeman and Company, New York, NY, USA.

Sun, M. & Song, P.-S. (1977) Solvent effects on the fluorescent states of indole derivatives-dipole moments. *Photochem. and Photobiol.* **25**, 3-9.

Szabo, A. G. (1988) Laser instrumentation and data analysis in time-correlated photon counting fluorescence decay measurements in biochemical investigations. *In* Time-resolved Laser Spectroscopy in Biochemistry, J. R. Lakowicz, Ed., *SPIE Proceedings* v. 909, Los Angeles, CA, USA.

Szabo, A. G., Lynn, K. R., Krajcarski, D. T. & Rayner, D. M. (1978) Tyrosinate fluorescence maxima at 345 nm in proteins lacking tryptophan at pH 7. *FEBS Lett.* **94**, 249-252.

Szabo A. G. & Rayner, D. M. (1980) Fluorescence decay of tryptophan conformers in aqueous solution. *J. Am. Chem. Soc.* **102**, 554-563.

Szabo, A. G., Stepanik, T. M., Rayner, D. M. & Young, N. M. (1983) Conformational heterogeneity of the copper binding site in azurin. *Biophys. J.* **41**, 233-244.
118.

Takakuwa, T., Konno, T., Meguro, H. (1985) A new standard substance for calibration of circular dichroism: Ammonium d-10-camphorsulfonate. *Anal. Sci.* 1, 215-.

Tanaka, F., Kaneda, N., Mataga, N., Tamai, N., Yamazaki, I. & Hayashi, K. (1987) Analyses of nonexponential fluorescence decay functions of a single tryptophan residue in erabutoxin b. *J. Phys. Chem.* **91**, 6344-6346.

Teale, F. W. J. & Weber, G. (1957) Ultraviolet fluorescence of aromatic amino acids. *Biochem. J.* **65**, 476-482.

Tilstra, L., Sattler, M. C., Cherry,W. R. & Barkley, M. D. (1990) Fluorescence of a rotationally constrained tryptophan derivative, 3-carboxy-1,2,3,4-tetrahydro-2-carboline. *J. Am. Chem. Soc.* **112**, 9176-9182.

Tinoco, I., Sauer, K. and Wang, J. C. (1978) Physical Chemistry: Principles and Applications in Biological Sciences, 2nd ed., Prentice-Hall Canada Inc., Toronto, Ontario, Canada.

Tonge, P. J. (personal communication)

Tsernoglou, D. & Petsko, G. A. (1976) The Crystal Structure of a Post-Synaptic Neurotoxin from Sea Snake at 2.2 Å Resolution. *FEBS Lett.* **68**,1-4.

Turro, N. J. (1978) Modern Molecular Photochemistry, The Benjamin/Cummings Company, Inc., Menlo Park, CA, USA.

Van de Kamp, M., Silvestrini, M. C., Brunori, M., Van Beumen, J., Hali, F. C. & Canters, G. W. (1990) Involvement of the hydrophobic patch of azurin in the electron-transfer reactions with cytochrome c_{551} and nitrate reductase. *Eur. J. Biochem.* **194**, 109-120.

Walkinshaw, M.D., Saenger, W. & Maelicke, A. (1980) Three-dimensional structure of the "long" neurotoxin from cobra venom. *Proc. Nat. Acad. Sci. USA*, **77**,2400-2404.

Ware, W. R., Pratinidhi, M. & Bauer, R. K. (1983) Performance characteristics of a small side-window photomultiplier in laser single-photon fluorescence decay measurements. *Rev. Sci. Instr.* **54**, 1148-1156.

Weber, G. (1952) Polarization of the fluorescence of macromolecules. Theory and experimental method. *Biochem. J.* **51**,145-165.

Weber, G. & Rosenheck, K. (1964) Proton-transfer effects in the quenching of fluorescence of tyrosine copolymers. *Biopolymers Symp.* **1**, 333-344.

Willis, K. J., Neugebauer, W., Sikorska, M. & Szabo, A. G. (1994) Probing α-helical secondary structure at a specific site in model peptides via restriction of tryptophan side-chain rotamer conformation. *Biophys. J.* **66**,1623-1630.

Willis, K. J. & Szabo, A. G. (1992). Conformation of parathyroid hormone: Time-resolved fluorescence studies. *Biochemistry* **31**, 8924-8931.

Willis, K. J. & Szabo, A. G. (1991) Excited-state reaction and the origin of the biexponential fluorescence decay of tryptophan zwitterion. Chem. Phys. Lett. **182**, 614-616.

Willis, K. J., Szabo, A. G., Zuker, M., Ridgeway, J. M. & Alpert, B. (1990) Fluorescence decay kinetics of the tryptophyl residues of myoglobin: Effect of heme ligation and evidence for discrete lifetime components. *Biochemistry* **29**, 5270-5275.

Willis, K. J. & Szabo, A. G. (1989) Resolution of tyrosyl and tryptophyl fluorescence emission from subtilisins. *Biochemistry* **28**,4902-4908.

Wold, F. (1981) In vivo chemical modification of proteins (post-translational modification). *Ann. Rev. Biochem.* **50**, 783-814.

Yamamoto, Y. & Tanaka, J. (1972) Polarized absorption spectra of crystals of indole and its related compounds. *Bull. Chem. Soc. Japan* **45**, 1362-1366.

Zhu, D. W., Dahms, T., Willis, K., Szabo, A. G. & Lee, X. (1994) Crystallization and Preliminary Crystallographic Studies of the Crystals of the Azurin *Pseudomonas fluorescens*. *Arch. Biochem. Biophys.* **308**, 469-470.

APPENDIX A

```
PM=0.33
PP=0.33
PT=1-(PM+PP)
THA=45
LA=0
MA=0
NA=1
OA=cos(THA/2)
PA=sin(THA/2)*LA
QA=sin(THA/2)*MA
RA=sin(THA/2)*NA
AA=(PA*PA)-(QA*QA)-(RA*RA)+(OA*OA)
BA=2*((PA*QA)+(RA*OA))
CA=2*((PA*RA)-(QA*OA))
DA=2*((PA*QA)-(RA*OA))
EA=-(PA*PA)+(QA*QA)-(RA*RA)+(OA*OA)
FA=2*((QA*RA)+(OA*PA))
GA=2*((PA*RA)+(QA*OA))
HA=2*((QA*RA)-(PA*OA))
IA=-(PA*PA)-(QA*QA)+(RA*RA)+(OA*OA)
col(7)=col(1)-col(4)
col(8)=col(2)-col(5)
col(9)=col(3)-col(6)
col(10)=AA*col(7)+DA*col(8)+GA*col(9)
col(11)=BA*col(7)+EA*col(8)+HA*col(9)
col(12)=CA*col(7)+FA*col(8)+IA*col(9)
TH=col(20)
L=cos(145)
M=0
N=cos(125)
col(21)=cos(col(20)/2)
O=col(21)
col(22)=sin(col(20)/2)*L
P=col(22)
col(23)=sin(col(20)/2)*M
Q=col(23)
col(24)=sin(col(20)/2)*N
R=col(24)
col(25)=2*((P*Q)+(R*O))
col(26)=(-(P*P)+(Q*Q)-(R*R)+(O*O))
col(27)=2*((Q*R)-(P*O))
col(28)=col(25)*col(10,1,1)
col(29)=col(25)*col(10,2,2)
col(30)=col(25)*col(10,3,3)
col(31)=col(25)*col(10,4,4)
col(32)=col(25)*col(10,5,5)
col(33)=col(25)*col(10,6,6)
col(34)=col(25)*col(10,7,7)
col(35)=col(25)*col(10,8,8)
col(36)=col(25)*col(10,9,9)
col(37)=col(25)*col(10,10,10)
col(38)=col(25)*col(10,11,11)
col(39)=col(25)*col(10,12,12)
col(40)=col(26)*col(11,1,1)
```

```
col(41)=col(26)*col(11,2,2)
col(42)=col(26)*col(11,3,3)
col(43)=col(26)*col(11,4,4)
col(44)=col(26)*col(11,5,5)
col(45)=col(26)*col(11,6,6)
col(46)=col(26)*col(11,7,7)
col(47)=col(26)*col(11,8,8)
col(48)=col(26)*col(11,9,9)
col(49)=col(26)*col(11,10,10)
col(50)=col(26)*col(11,11,11)
col(51)=col(26)*col(11,12,12)
col(52)=col(27)*col(12,1,1)
col(53)=col(27)*col(12,2,2)
col(54)=col(27)*col(12,3,3)
col(55)=col(27)*col(12,4,4)
col(56)=col(27)*col(12,5,5)
col(57)=col(27)*col(12,6,6)
col(58)=col(27)*col(12,7,7)
col(59)=col(27)*col(12,8,8)
col(60)=col(27)*col(12,9,9)
col(61)=col(27)*col(12,10,10)
col(62)=col(27)*col(12,11,11)
col(63)=col(27)*col(12,12,12)
col(64)=abs(col(28)+col(40)+col(52))
col(65)=abs(col(29)+col(41)+col(53))
col(66)=abs(col(30)+col(42)+col(54))
col(67)=abs(col(31)+col(43)+col(55))
col(68)=abs(col(32)+col(44)+col(56))
col(69)=abs(col(33)+col(45)+col(57))
col(70)=abs(col(34)+col(46)+col(58))
col(71)=abs(col(35)+col(47)+col(59))
col(72)=abs(col(36)+col(48)+col(60))
col(73)=abs(col(37)+col(49)+col(61))
col(74)=abs(col(38)+col(50)+col(62))
col(75)=abs(col(39)+col(51)+col(63))
col(76)=col(64)+col(65)+col(66)+col(67)
col(77)=col(68)+col(69)+col(70)+col(71)
col(78)=col(72)+col(73)+col(74)+col(75)
col(14)=(col(76)*col(76))
col(15)=(col(77)*col(77))
col(16)=(col(78)*col(78))
DN=(col(14)*PP)+(col(15)*PM)+(col(16)*P
col(17)=(col(14)*PP)/(DN)
col(18)=(col(15)*PM)/(DN)
col(19)=(col(16)*PT)/(DN)
```

APPENDIX B: CURRICULUM VITAE

TANYA E. S. DAHMS

Date of Birth: April 14, 1967

Citizenship: Canadian

Work Address
M-54 Montreal Road
IBS, NRC
Ottawa, Canada K1A 0R6
Telephone: (613) 993-5304
Fax: (613) 952-0583
EMB: tanya@nrcbsa.bio.nrc.ca

Home Address
#36-2669 Southvale Crescent
Ottawa, Ontario, Canada
K1B 4V2
Telephone: (613) 738-9163

EDUCATION

1991-Present **UNIVERSITY OF OTTAWA, OTTAWA, CANADA**

- Ph.D. studies in physical biochemistry.
- Study of proteins by circular dichroism and time-resolved fluorescence spectroscopy.
- Correlation of fluorescence parameters with protein structural features.
- Elucidation of tryptophan rotamers in single protein crystals.

1985-1990 **UNIVERSITY OF WATERLOO, WATERLOO, ONTARIO**

- Honours Co-op Bachelor of Science (Applied Biology and Chemistry)
- Options in Classical Ballet & Psychology.
- Represented Waterloo Biochemistry at the Southwestern Ontario Undergraduate Conference for Chemistry.

EMPLOYMENT (ACADEMIC INSTRUCTION)

UNIVERSITY OF OTTAWA, OTTAWA, ONTARIO

Sessional Professor

09/95-12/95 • 2nd Year Physical Chemistry for the Biological Sciences

Undergraduate Laboratory Instructor

01/92-04/92 • 3rd Year Physical Biochemistry.
09/92-12/92 • 3rd Year Metabolism
09/91-12/91

UNIVERSITY OF WATERLOO, WATERLOO, ONTARIO

Undergraduate Laboratory Instructor

01/90-04/90 • 3rd Year Human Physiology.

Undergraduate Teaching Assistant

09/89-12/89 • 1st Year Chemistry for Engineers.

Employment Continued

10/95-Present **UNIVERSITY OF OTTAWA**
Research Associate
Purification, crystallization and preliminary X-ray crystallographic structure determination of Fab complexes.

05/92-05/93 **SYPHER:MÜLLER INC., OTTAWA, ONTARIO**
Junior Consultant to Environment Canada (EC)
Responsible for research of "Good Laboratory Practice" (GLP) in the UK and USA, design of a GLP EC bibliography and summary report.

01/91-05/93 **AVESTIN INC., OTTAWA, ONTARIO**
Scientific Consultant
Marketing & construction of Scientific Equipment.

05/90-05/91 **ROSEN ADVERTISING, OTTAWA, ONTARIO**
Senior Campaign Manager
Direct marketing, management of staff, and office supervision.

09/89-04/90 **UNIVERSITY OF WATERLOO, WATERLOO, ONTARIO**
Honours Student Thesis Project
Development of a semi-enzymatic synthesis of 2-acetamido-1,2-dideoxynojirimycin for studying inhibitory effects on glycohydrolytic enzymes.

04/89-08/89 **UNIVERSITY OF GUELPH, GUELPH, ONTARIO**
Research Assistant: Biochemistry
Development of a novel HPLC method for the determination of alpha-keto acids in plasma and muscle samples. Development of a novel method for the determination of ammonia in respired air.

09/88-12/88 Development of amino acid and ion flux HPLC analyses of muscle and plasma samples for the study of human and rat muscle metabolism.

01/88-04/88 **CONNAUGHT LABORATORIES, TORONTO, ONTARIO**
Technician 2
Synthesis of several photoaffinity probes for the study of antibody selected specificity using synthetic peptide conjugates.

05/87-08/87 **POLYSAR, SARNIA, ONTARIO**
Research Assistant: Organic Chemistry
Five-step synthesis of a model compound (2,2,4,8,8,-pentamethylnon-4-ene) for the study of butyl and halobutyl rubber. (GC,HPLC,NMR)

09/86-12/86 **EMR/CANMET, OTTAWA, ONTARIO**
Research Assistant: Analytical Chemistry
Development of extraction methods and evaluation of HPLC procedures for the separation of rare earth metals in steel samples and advanced materials.

01/86-04/86 Development of HPLC methods for the determination of anions in environmental control samples.

PUBLICATIONS

Dahms, T. E. S. & Szabo, A. G. (invited paper) A Review of Conformational Heterogeneity in Crystalline Proteins Detected by Novel Time-Resolved Fluorescence Techniques. *Methods in Enzymology.*

Lee, X., Dahms, T. E. S., Zhu, D. W., Lanthier, P., Yaguchi, M. & Szabo, A. G. (in press) The Crystal Structure of Holoazurin from *Pseudomonas Fluorescens* at 2.05 Å Resolution. *Cryst. Acta.*

Dahms, T. E. S. & Szabo, A. G. (1995) Probing Local Secondary Structure by Fluorescence: Time-resolved and Circular Dichroism Studies of Highly Purified Neurotoxins. *Biophys. J.*

Dahms, T. E. S., Willis, K. J., & Szabo, A. G. (1995) Conformational Heterogeneity of Tryptophan in a Protein Crystal. *JACS* 117, 2321-2326.

Zhu, D. W., Dahms, T., Willis, K., Szabo, A. G. & Lee, X. (1994) Crystallization and Preliminary Crystallographic Studies of the Crystals of the Azurin *Pseudomonas fluorescens. Arch. Biochem. Biophys.* 308, 469-470.

Barkley, D. J., Dahms, T. E. & Villeneuve, K. N. (1987) Permanently Coated Ion Exchangers for Liquid Chromatographic Determination of Anionic Species in Samples from Environmental Control Processes. *Journal of Chromatography* 395, 631-640.

ORAL PRESENTATIONS

Dahms, T. E. S., Kaminski, M. J., Biesterfeldt, J. D., Evans, S. J., Szabo, A. G. & Lee, X. (1996) Investigating the mechanism of electron transfer in small copper binding proteins: X-ray Crystallographic and Spectroscopic Studies of the Holo and Apoazurins from *Ps. fluorescens. Biophys J.* 68. 40th Annual Biophysical Society Meeting. Baltimore, MD.

Dahms, T. E. S. (1995) Probing Protein Structure and Conformational Heterogeneity by Time-Resolved Fluorescence. Harvard Medical School, Seminar Series, invited speaker.

Dahms, T. E. S. & Szabo, A. G. (1995) Conformational Heterogeneity of Crystalline Proteins Revealed by Time-Resolved Fluorescence. 3rd International Symposium on Innovative Fluorescence Methodologies in Biochemistry and Medicine. Maui, Hawaii.

Dahms, T. E. S. & Szabo, A. G. (1995) Rotamers, the Source of Tryptophan Conformational Heterogeneity: Confirmation by Time-Resolved Fluorescence of Crystalline Proteins. *Canadian Society for Chemistry Conference and Exhibition* 78th Annual Meeting, 813. Guelph, ON.

Dahms, T. E. S. & Szabo, A. G. (1994) Local Secondary Structure Prediction by Fluorescence: Time-Resolved Fluorescence and Circular Dichroism Studies of Highly Purified Neurotoxins. *Canadian Federation of Biological Sciences* 37th Annual Meeting, 136. Montreal, ON.

Dahms, T.E.S. & Honek, J. (1990) Synthesis of 2-acetamido-1,2-dideoxynojirimycin. *Southwestern Ontario Undergraduate Student Chemistry Conference.* Toronto, ON.

Barkley, D. J. & Dahms, T. E. (1987) Dynamic Ion Exchange Chromatography for the Determination of Rare Earths in Steels, Alloys and Advanced Materials. Ion Ex 87 North East Wales Institute, Wales.

ABSTRACTS/POSTER PRESENTATIONS

Dahms, T. E. S. & Szabo, A. G. (1995) Conformational Heterogeneity of Tryptophan in Crystalline Proteins: A Review of Time-Resolved Fluorescence Studies *Biophys J.* 67, A156. 39th Annual Biophysical Society Meeting. San Francisco, CA.

Dahms, T. E. S., Bruckman, A. J. & Szabo, A. G. (1995) Tryptophan Rotamers in Crystalline Ribonuclease T1 in the Presence and Absence of 2'-GMP Inhibitor: A Time-Resolved Fluorescence Study. *Biophys J.* 67, A162. 39th Annual Biophysical Society Meeting. San Francisco, CA.

Willis, K. J., Dahms, T., Neugebauer, W., Sikorska, M. & Szabo, A. G. (1994) Correlating Tryptophan Time-Resolved Fluorescence Decay Parameters with Secondary Structure. Studies of Synthetic α-Helical Peptides. Naples Workshop on Bioactive Peptides. Naples, Italy.

Szabo, A. G., Lee, X. & Dahms, T. E. S. (1994) Multiexponential Fluorescence Decay of Holoazurin in the Crystalline State. *Biophys J.* 66, A273. 38th Annual Biophysical Society Meeting. New Orleans, LA.

Lee, X., Dahms, T. E. S., Zhu, D. W., Lanthier, P., Yaguchi, M. & Szabo, A. G. (1994) The Crystal Structure of Holoazurin from *Pseudomonas Fluorescens* at 2.05 Å Resolution. *Biophys J.* 66, A273. 38th Annual Biophysical Society Meeting. New Orleans, LA.

Tonge, P. J., Dahms, T. E. S., To, R. & Szabo, A. G. (1994) Probing Crotonase-Catalyzed β-Elimination in Solution and in the Crystalline State: A Time-Resolved Fluorescence Study. *Biophys J.* 66, A263. 38th Annual Biophysical Society Meeting. New Orleans, LA.

Dahms, T. E. S. & Szabo, A. G. (1994) Fluorescence Predicts Local Secondary Structure: Time-resolved fluorescence and Circular Dichroism Studies of Highly Purified Neurotoxins. *Biophys J.* 66, A66. 38th Annual Biophysical Society Meeting. New Orleans, LA.

Dahms, T. E. S., Willis, K. J. & Szabo, A. G. (1993) Conformational Heterogeneity of Tryptophan in a Protein Crystal: A Fluorescence Decay Study. *International Biophysics Congress.* Budapest, Hungary.

Dahms, T. E. S., Willis, K. J. & Szabo, A. G. (1993) Fluorescence Decay Kinetics of a Tryptophyl Residue in a Protein Crystal. *Biophys J.* 64, A55. 37th Annual Biophysical Society Meeting. Washington, DC.

Dahms, T. E. S., Willis, K. J. & Szabo, A. G. (1993) Probing Metal-Induced Conformational Changes in Calbindin D9K: Time-Resolved Fluorescence Studies. *Biophys J.* 64, A55. 37th Annual Biophysical Society Meeting. Washington, DC.

Dahms, T. E. S., Willis, K. J. & Szabo, A. G. (1992) Fluorescence Decay Kinetics of Highly Purified Neurotoxins. *Biophys J.* 61, A1041. 36th Annual Biophysical Society Meeting. Houston, TX.

AWARDS

- National Science and Engineering Research Council Post Doctoral Fellowship (1996-1998)
- Canadian Society of Chemistry Conference Graduate Student Presentation Award (1995)
- National Science and Engineering Research Council PGS-B Scholarship (1993-1995)
- University of Ottawa Merit Scholarship (1993-1995)
- Four University of Ottawa Conference Travel Awards (1992-1995)
- American Biophysical Society Travel Award (1993)
- Ontario Scholar (1985)

SPECIAL SKILLS

- Protein Purification, Optical Spectroscopy (particularly Fluorescence), Protein Crystal Growth, HPLC, CD, GC and NMR.
- Understanding of French and German languages.
- High levels of achievement in dance, music and swimming.

EXTRACURRICULAR ACTIVITIES

- Executive member of Waterloo University Science Society.
- Professional dance training at Le Groupe de la Place Royale.
- Member of the Ottawa Rowing Club women's competitive programme.
- Skiing, cycling, and climbing.

References:

1. Professor Arthur G. Szabo, Chairman
   Department of Chemistry and Biochemistry
   University of Windsor
   451 Sunset Street
   Windsor, Ontario
   Canada N9B 3P4
   Tel. (519) 253-4232 x 3526
   EMB: szabo@server.uwindsor.ca

2. Professor Xavier Lee
   Department of Cancer Biology
   Cleveland Clinic Research Institute
   9500 Euclid Avenue
   Cleveland, Ohio
   USA 44195
   Tel. (216) 445-7270
   EMB: lee@xtal.ri.ccf.org

APPENDIX C: Publications Related to Thesis Work

1. Crystallization and Preliminary Crystallographic Studies of the Crystals of the Azurin *Pseudomonas fluorescens.*

2. Conformational Heterogeneity of Tryptophan in a Protein Crystal

3. Probing Local Secondary Structure by Fluorescence: Time-resolved and Circular Dichroism Studies of Highly Purified Neurotoxins.

4. The Crystal Structure of Holoazurin from *Pseudomonas Fluorescens* at 2.05 Å Resolution.

5. Conformational Heterogeneity in Crystalline Proteins: Revealed by Time-Resolved Fluorescence Studies.